QUANTITATIVE ANALYSIS OF MULTI-AGENT FORMATIONS: THEORY AND APPLICATIONS

A Dissertation

Submitted to the Faculty

of

Purdue University

by

Guangwei Zhu

In Partial Fulfillment of the

Requirements for the Degree

of

Doctor of Philosophy

May 2013

Purdue University

West Lafayette, Indiana

To KING OF KINGS AND LORD OF LORDS, Savior of my life

To my wife, sharer of my life

To my parents, givers of my life

ACKNOWLEDGMENTS

Words cannot adequately express my gratitude toward Professor Jianghai Hu, my major advisor, without whom this dissertation would be impossible. Through the past five years, I have received from him not only superior mentoring in research, but also generous financial support for attending international conferences. He always maintains the highest level of availability for his students, and provides extremely helpful insights very quickly. His research talent together with his gentle personality makes him not only a perfect advisor, but also a precious friend in my eyes.

I am also grateful to Professor Stanislaw Zak, Xiaojun Lin and Martin Corless, for serving on my dissertation committee and giving their insightful advice during both my preliminary and final examinations. I learned many useful optimization algorithms and techniques from Professor Zak's class, which have contributed to a major part of this dissertation. I also benefited from Professor Lin's classes on communication networks, not only because of his amazing teaching skills, but also the intriguing research topics he brought, which turned out to be closely related to my work. I also appreciate Professor Corless, for his questions and insights regarding my dissertation have led to many new directions of my research.

I am greatly indebted to Prof. Tong Zhou at Tsinghua University in Beijing, from whom I received training in rigorous scholarship and strong research interest in control theory during my undergraduate studies. I have great respect for his expertise in control theory, particularly robust control and filtering.

I would like to thank my wife Ce Wu and my parents Hongqing Zhu and Yishan Chen, for their constant support, unconditional love and inspirations. It was a wonder in my life to meet my wife here in West Lafayette during my graduate studies. She is the most precious gift that I never deserve.

Last but not least, I would like to ascribe all the achievements and honors to the LORD Almighty. He paved my path to the Purdue campus where I came to know Him, and in countless situations, He guided me personally and patiently. Despite being an infinitesimal portion of His infinite Wisdom, may this dissertation glorify His name.

TABLE OF CONTENTS

Page

Page

LIST OF TABLES

LIST OF FIGURES

SYMBOLS

$\mathbb{R}, \mathbb{R}_+$	set of real numbers and set of positive real numbers
$\|\mathbf{v}\|$	Euclidean norm of vector $\mathbf{v}$
$\|A\|_F$	Frobenius norm of matrix A
$\|A\|_2$	Largest singular value of matrix A
$A^\dagger$	Moore-Penrose pseudoinverse of matrix A
$\|\mathcal{A}\|$	cardinality (number of elements) of set $\mathcal{A}$
$\mathrm{tr}(A)$	trace (sum of diagonal entries) of square matrix A
$\mathrm{null}(A)$	null space of matrix A, i.e., $\{\mathbf{x} : A\mathbf{x} = \mathbf{0}\}$
$\mathrm{colsp}(A)$	column space of matrix A
$\mathrm{rowsp}(A)$	row space of matrix A
$\mathrm{rank}(A)$	rank of matrix A
$A \succ (\succeq)\ 0$	matrix A is positive definite (semidefinite)
$A \succ (\succeq)\ B$	matrix $A - B$ is positive definite (semidefinite)
$\mathcal{C}^\perp$	orthogonal subspace ($\mathcal{C}$ is a linear subspace)
$\mathbf{v}^\perp$ $(\mathbf{v} \in \mathbb{R}^2)$	vector $\mathbf{v}$ rotated 90° counterclockwise
$\mathbf{v}^\perp$ $(\mathbf{v} \in \mathbb{R}^{2n})$	stacked vector with each component of $\mathbf{v}$ in $\mathbb{R}^2$ rotated 90° counterclockwise
$\lambda_i(A)$	i-th smallest eigenvalue of square matrix A
$\mathbb{O}_n$	Orthogonal group of order n, i.e., set of n-by-n orthogonal matrices associated with matrix multiplication
$\mathbb{SO}_n$	Special orthogonal group of order n, i.e., set of n-by-n orthogonal matrices with positive determinants, associated with matrix multiplication

ABSTRACT

Zhu, Guangwei Ph.D., Purdue University, May 2013. Quantitative Analysis of Multi-Agent Formations: Theory and Applications. Major Professor: Jianghai Hu.

In this thesis, formations of multi-agent systems, including multi-vehicle systems and sensor networks, are studied from a quantitative perspective. First, matrix and scalar valued quantities related to multi-agent system formations are proposed. These quantities are useful in characterizing the robustness, collaborative performance and manipulability of multi-agent systems, are intuitively associated with physical analogies of formations. Their practical value in the analysis of formation control and localization systems is also demonstrated through application examples. With these quantitative characterizations of formations, several optimization problems can be formulated, which are helpful in designing efficient formations for improving the performance of multi-agent systems in various aspects. Finally, based on the concept of stiffness matrix, distributed algorithms are designed to localize agents in the network using angle-of-arrival information. The stability and performance analysis as well as optimization techniques regarding such algorithms are studied using the quantitative framework developed above.

1. INTRODUCTION

1.1 Background

Tasks arising in many applications such as underwater exploration, large area surveillance and emergency services, are often difficult or even impossible for a single robot, vehicle, sensor, *etc.*, to accomplish as a large region with much uncertainty needs to be covered or monitored. Completing these tasks may become feasible through the coordination of a group of autonomous agents, each capable of acting individually based on information available through local sensing and communication with adjacent peers. Recent advancements in robotics, mobile computing and sensor technologies have led to the applications of multi-agent systems in many engineering fields, as well as the development of corresponding theories. For example, Anderson *et al.* reported the theory and applications regarding multi-agent systems consisting of unmanned aerial vehicles [1]. Bhatta *et al.* [2] and Leonard *et al.* [3] studied the problem of coordinating single and multiple underwater sensing devices and its application in ocean sampling. Robot networks, as a specific instance of multi-agent systems, have also been widely studied, e.g. soccer robots [4], multiple coordinated quadrotors [5]. Systems composed of less intelligent, static/semi-static devices, such as wireless sensor networks, are often structurally similar to multi-agent systems, hence can be modeled and studied as multi-agent systems [6–8]. Even the collective behaviors of humans and animals have been investigated from the perspective of multi-agent systems, as in [9, 10].

For maximal coordination efficiency, it is often advantageous for the agents to maintain a certain *formation*, a combination of the agents' location information and their interconnections. As one would expect, formations play an especially important role in location-aware multi-agent systems [11, 12]. The capabilities of such multi-agent systems, including maintainability [11, 12], controllability [13] and localizability [14], are substantially

determined by the nature of their underlying formations. As a case in point, the local maintainability of distance-based multi-vehicle formation control systems depends on the *rigidity* of the formation graph, which characterizes the structural inflexibility and hence the ability to withstand exogenous perturbations. This property of formation is arguably the most important property of formations, on which many early research works have been published [15–19]. Despite being a well studied mathematical subject, the theory of graph rigidity (Laman's Theorem [20], rigidity matrix theorem [21, 22] and combinatorial rigidity criteria [23, 24]) was not long ago applied to the study of multi-agent systems control [12, 25, 26], including the design and analysis of agent dynamics such as splitting [27], merging [28] and closing ranks [29]. Graph rigidity has also found applications in network localization [14].

It is noteworthy, however, that a majority of research effort on formation rigidity has been dedicated to finding its *qualitative* criteria, whereas *quantitative* analysis of formation rigidity remains scarce. Such scarcity of quatitative research also exists in the study of other properties related to multi-agent formations, for example, a quantitative measure of formation controllability has been proposed not until recently [30, 31]. These *numerical* measures of formation properties are highly desirable as they allow not only the comparison but also the optimization of formations with respect to various performance objectives.

On the other hand, research works in generic multi-agent/networked systems has widely adopted the second smallest eigenvalue of the graph Laplacian, also known as the *algebraic connectivity*, as a primary indicator of the system's cooperative efficiency [32–34], and plenty of research has been done on its properties [35], optimization [32] and applications especially in consensus problems [33]. However, the formulation of algebraic connectivity does not involve any positional information and hence is incapable of differentiating formations with the same underlying graph but different position configurations, in which case their performance may significantly vary in formation control or network localization [36]. Other existing measures of formation-like structures proposed in subjects such as molecular biology [37] are incompatible with multi-agent control applications. Thus, a theoretical framework on the quantitative analysis of multi-agent formations needs to be developed.

1.2 Motivating Examples

Two common application examples of multi-agent systems are illustrated below to justify the need of quantitative analytic tools for multi-agent formations.

1.2.1 Multi-Agent Formation Control

Consider n agents (e.g. vehicles, aircraft, robots) indexed by $i \in \mathcal{V} = \{1, 2, \ldots, n\}$ moving on the two-dimensional plane $\mathbb{R}^2$. Let $\mathbf{q}_i \in \mathbb{R}^2$ denote the current position of agent i for $i \in \mathcal{V}$, and let $\mathbf{q} = \begin{bmatrix} \mathbf{q}_1^\top & \cdots & \mathbf{q}_n^\top \end{bmatrix}^\top \in \mathbb{R}^{2n}$ be the aggregated location (i.e. the configuration) of all the agents. Suppose the goal is to design a controller for the agents to achieve a given formation specified through a set of formation constraints on the agent distances: $\|\mathbf{q}_i - \mathbf{q}_j\| = d_{ij}^*$ for $(i, j) \in \mathcal{E}$. Here, $\mathcal{E} \subset \mathcal{V} \times \mathcal{V}$ and the constants d_{ij}^* are the desired agent separations.

Define the *formation constraint function* [38] as

$$F(\mathbf{q}) = \sum_{(i,j)\in\mathcal{E}} k_{ij} \left(\|\mathbf{q}_i - \mathbf{q}_j\| - d_{ij}^* \right)^2 \geq 0, \tag{1.1}$$

where $k_{ij} \geq 0$ for $(i, j) \in \mathcal{E}$ is a set of constants indicating the relative importance of keeping the constraints $\|\mathbf{q}_i - \mathbf{q}_j\| = d_{ij}^*$. A feedback controller for achieving the desired formation was proposed in [38] as follows,

$$\dot{\mathbf{q}} = -\nabla F(\mathbf{q}). \tag{1.2}$$

In other words, $\mathbf{q}$ evolves to seek the fastest decrease of the formation constraint function. It is easy to see that the controller (1.2) is localized in that the control for each agent depends only on the locations of itself and its immediate neighbors in the undirected graph $(\mathcal{V}, \mathcal{E})$.

Obviously, any configuration $\mathbf{p} \in \mathbb{R}^{2n}$ satisfying all the formation constraints is an equilibrium point of (1.2), and so are all the formations obtained from $\mathbf{p}$ through rigid body transformations. A natural question then is that, for agent configuration $\mathbf{q}$ close to such $\mathbf{p}$, whether the controller (1.2) will be able to steer $\mathbf{q}$ to $\mathbf{p}$ or one of its rigid body transforms, and if so, how fast the convergence can be achieved.

1.2.2 Network Localization

The network localization problem refers to the problem of determining the positions of nodes in a sensor network (up to a rigid body transformation) based on only relative distance measurements [39]. Denote by $\mathbf{p}_i$ the actual position of node i for $i \in \mathcal{V}$. For each node pair $(i,j) \in \mathcal{E} \subset \mathcal{V} \times \mathcal{V}$, assume a noisy measurement of the relative distance between nodes i and j is available: $z_{ij} = \|\mathbf{p}_i - \mathbf{p}_j\| + \varepsilon_{ij}$, where ε_{ij} is random with zero mean and variance σ_{ij}. Let k_{ij}, $(i,j) \in \mathcal{E}$, be a set of nonnegative weights. Estimates of $\mathbf{p}$ can be obtained as follows,

$$\hat{\mathcal{P}} = \arg\min_{\hat{\mathbf{p}}} \sum_{(i,j)\in\mathcal{E}} k_{ij}(\|\hat{\mathbf{p}}_i - \hat{\mathbf{p}}_j\| - z_{ij})^2. \tag{1.3}$$

Note that in general $\hat{\mathcal{P}}$ is a set since for any $\hat{\mathbf{p}} \in \hat{\mathcal{P}}$, all rigid body transformations of $\hat{\mathbf{p}}$ also belong to $\hat{\mathcal{P}}$. To assess the quality of the estimates, define the error between the estimate set $\hat{\mathcal{P}}$ and the true configuration $\mathbf{p}$ as

$$e_{\hat{\mathcal{P}}} = d(\hat{\mathcal{P}}, \mathbf{p}) = \inf_{\hat{\mathbf{p}}\in\hat{\mathcal{P}}} \|\hat{\mathbf{p}} - \mathbf{p}\|.$$

The question is then how to characterize the mean square estimation error $\mathrm{E}\,[e_{\hat{\mathcal{P}}}^2]$ for the above algorithm.

1.3 Preview of Main Contributions

This thesis mainly contributes to the theory of *quantitative* analysis of formations in multi-agent system, which provide insightful numerical results that directly relates to a wide range of practical applications of multi-agent systems and sensor networks. The theoretic framework proposed in this thesis can be regarded as a extension of the classic algebraic graph theory to the concept of formations, which is essentially graphs with weights and designated embeddings in $\mathbb{R}^2$. This framework is shown to be useful in analyzing multi-agent systems, e.g., as the motivating examples given in the previous section.

In Chapter 2, multi-agent formations are formulated as mathematical objects and studied from a quantitative perspective. The concepts of rigidity matrix and stiffness matrix

are introduced as descriptive quantities for multi-agent formations. These quantities are derived from the study of the mechanical analogies of multi-agent formations. Specifically, the concept of rigidity matrices, widely known in the field of structural mechanics, has received much attention in the study of multi-agent systems. Nevertheless, the stiffness matrices proposed in this thesis have a more compact representation, and are equivalent to rigidity matrices in terms of deriving important properties and quantities of formations. Moreover, being square matrices, the stiffness matrices enjoy plenty of interesting spectral properties that are not available for rigidity matrices.

In Chapter 3, the quantitative measures of formation rigidity, namely the worst-case and mean rigidity indexes, are proposed based on the eigenvalues of the stiffness matrix associated with the formation. The properties shared by both indexes indicate that these quantities conform well to our intuition toward the concept of formation rigidity. The connection of both rigidity indexes to the practical applications in multi-agent formation control and wireless sensor networks localization is also demonstrated. More specifically, it is shown through practical examples that the worst-case rigidity index substantially corresponds to the convergence rate of formation control and the mean rigidity index effectively indicates the level of estimation error in a network whose nodes are localized by relative distance measurements.

In Chapter 4, the manipulability indexes are formulated based on the manipulability matrix. The manipulability indexes quantify the influence of the leader agents to the followers in the formation control setting. The special case of a single-leader rigid formation is investigated with further details, and some direct formulas associated with this case are derived. Toward the end of the chapter, a computationally efficient algorithm based on dynamic programming principles is proposed for computing the manipulability indexes of a family of formations with special structures.

With the rigidity and manipulability indexes proposed, various formation optimization problems are formulated and solved. Chapter 5 discusses on formation optimization by maximizing rigidity indexes. In the first type of formation optimization, both the agent positions and the connection topology are fixed, and the allocation of link resources (i.e.,

connectivity strengths) over all link is to be optimized. Due to the favorable properties of the rigidity indexes, this problem can be formulated as a convex optimization problem and thus solved effectively and efficiently. In the second type of formation optimization, the agent positions and the connection topology are subject to change. A sub-optimal solution can be found using a hybrid configuration/topology optimization algorithm, which switches back and forth between position optimization and topology optimization in order to avoid local extrema with poor performance. Similarly, the problems of finding the optimal leader and its position are studied in Chapter 6. The usefulness and effectiveness of these optimization techniques is illustrated through several numerical examples.

Finally in Chapter 7, distributed algorithms for network localization is proposed on the basis of the quantitative tools developed in the previous chapters. It is shown that the localizability of network using the angle-of-arrival (AOA) information of incoming signals from neighbors is equivalent to the infinitesimal rigidity, under which situation the proposed algorithms are guaranteed to converge to the desired localization result. Various aspects of the algorithms, such as convergence and delay tolerance, are investigate from a quantitative perspective, and some formation optimization problems are formulated to improve the performance of these algorithms. Errors caused by inaccurate measurements in AOA localization process is analyzed toward the end of the chapter.

2. ALGEBRAIC FORMATION THEORY

In this chapter, multi-agent formations are formulated as a mathematical object extended from classic graphs. Basic concepts and quantities related to formations are proposed, followed by their properties and propositions that will come in handy for analysis in later chapters.

2.1 Formations

A multi-agent system (including sensor network) can be modeled abstractly as formations, where each agent is a vertex tagged with its positional information, and their interconnections as weighted edges. Below are the mathematical definitions of formations.

Definition 2.1.1 (Leaderless Formation) *A leaderless formation on the plane, or simply* formation*, is a triple* $(\mathcal{V}, \mathbf{p}, K)$ *consisting of the following:*

- $\mathcal{V} = \{1, 2, \ldots, n\}$ *is the index set of* n *vertices (agents, sensor nodes, etc.) on the plane;*
- $\mathbf{p} = \begin{bmatrix} \mathbf{p}_1^\top & \mathbf{p}_2^\top & \cdots & \mathbf{p}_n^\top \end{bmatrix}^\top \in \mathbb{R}^{2n}$ *is the (position)* configuration *of the* n *vertices, with* $\mathbf{p}_i \in \mathbb{R}^2$ *denoting the position of vertex* i*;*
- $K = [k_{ij}]_{i,j\in\mathcal{V}} \in \mathbb{R}^{n\times n}$ *is the* connectivity matrix*, where* k_{ij} *for vertices* $i, j \in \mathcal{V}$ *is the* connectivity coefficient *between them and satisfies* $k_{ii} = 0$*,* $k_{ij} \geq 0$*, and* $k_{ij} = k_{ji}$*. Denote by* $\mathcal{K}$ *the set of all such* K*.*

Note that the formations depends both on the agents' position $\mathbf{p}$ and connectivity matrix K.

We note two important distinctions of our definition of formation with some typical ones arising in other applications. First, vertices' locations are an integral part of the for-

mation definition due to their geographically distributed nature. Second, the graph topology as given by K is numeric rather than just binary. For instance, in the multi-agent formation control example in Section 1.2.1, k_{ij} represents the penalty for violating (or the stiffness of keeping) the formation constraint between agents i and j. In the network localization problem in Section 1.2.2, k_{ij} determines the penalty on deviating from the relative distance measurement between nodes i and j.

Definition 2.1.2 (Leader-Follower Formation) *A formation $(\mathcal{V}, \mathbf{p}, K)$ with a nonempty set of leaders $\mathcal{L} \subset \mathcal{V}$ is called a* leader-follower formation *and denoted by $(\mathcal{V}, \mathbf{p}, K, \mathcal{L})$. Vertices in $\mathcal{L}$ and $\mathcal{F} \triangleq \mathcal{V} \setminus \mathcal{L}$ are called* leaders *and* followers*, respectively.*

In precedent literature, leaders are also referred to as *anchors* or *beacons*. In the applications of network localization and formation control, leaders are usually used to model those nodes that know their absolute locations via, e.g., positioning devices.

Remark 2.1.1 *For readers familiar with the concepts of* weighted graphs *and* graph embeddings*, formation $(\mathcal{V}, \mathbf{p}, K)$ can be equivalently formalized as an undirected graph $G = (\mathcal{V}, \mathcal{E})$ associated with a mapping $w : \mathcal{E} \to [0, +\infty)$ denoting the edge weights, and an embedding $p : \mathcal{V} \to \mathbb{R}^2$. Some readers may also recognize this definition as an alias of the term* framework*, as is used in [22, 40].*

In practice, formations are often maintained by preserving the distances of *connected* agents, i.e., whose edges have strictly positive connectivity coefficients. As a result, the concept of *consistency* defined as follows serves as a meaning equivalence relation of formations.

Definition 2.1.3 (Consistency) *Two formations $(\mathcal{V}, \mathbf{p}, K)$ and $(\mathcal{V}, \mathbf{p}', K)$ with the same vertex set and connectivity matrix are called* consistent *if $\|\mathbf{p}_i - \mathbf{p}_j\| = \|\mathbf{p}'_i - \mathbf{p}'_j\|$ for all* those $i, j \in \mathcal{V}$ with $k_{ij} > 0$.
Likewise, two leader-follower formations $(\mathcal{V}, \mathbf{p}, K, \mathcal{L})$ and $(\mathcal{V}, \mathbf{p}', K, \mathcal{L}')$ are consistent *if: (i) $(\mathcal{V}, \mathbf{p}, K)$ and $(\mathcal{V}, \mathbf{p}', K)$ are consistent; (ii) $\mathcal{L} = \mathcal{L}'$; (iii) $\mathbf{p}_i = \mathbf{p}'_i$ for all $i \in \mathcal{L}$.*

As can be seen from the above definition, consistent formations must have the same relative distances between connected vertices, as well as identical leaders and leader positions for leader-follower formations.

If two formations have the same relative distances between *all* pairs of vertices, not just connected ones, then there must exist a congruent transformation $T \in \mathbb{R}^{2\times 2}$ composed of rotations, translations, and reflections that transforms the vertex positions of one to the other; thus the following definition.

Definition 2.1.4 (Congruency) *Two formations* $(\mathcal{V}, \mathbf{p}, K)$ *and* $(\mathcal{V}, \mathbf{p}', K)$ *are* congruent *if* $\|\mathbf{p}_i - \mathbf{p}_j\| = \|\mathbf{p}'_i - \mathbf{p}'_j\|$ *for all* $i, j \in \mathcal{V}$. *Two leader-follower formations* $(\mathcal{V}, \mathbf{p}, K, \mathcal{L})$ *and* $(\mathcal{V}, \mathbf{p}', K, \mathcal{L}')$ *are* congruent *if* $(\mathcal{V}, \mathbf{p}, K)$ *is congruent to* $(\mathcal{V}, \mathbf{p}', K)$ and $\mathcal{L} = \mathcal{L}'$.

Obviously, congruent formations are consistent. The converse, however, does not hold in general, except for formations possessing the following property.

Definition 2.1.5 (Global Rigidity [14]) *A formation* $(\mathcal{V}, \mathbf{p}, K)$ *is called* globally rigid *if any formation* $(\mathcal{V}, \mathbf{p}', K)$ *consistent with it must also be congruent to it.*

In essence, global rigidity characterizes the inflexibility of the shape of the formation, given that the relative distances between connected vertex pairs are kept constant. In the localization problem, exact distance-based localization is possible only for globally rigid formations [14].

2.2 Rigidity Matrix

Determining global rigidity is, however, in general difficult. An easier alternative is to analyze its infinitesimal version. For a given formation $(\mathcal{V}, \mathbf{p}, K)$, the distance constraints between connected vertices can be equivalently summarized as $k_{ij}\|\mathbf{p}_j - \mathbf{p}_i\|^2 \equiv k_{ij}d_{ij}^2$ for some constants d_{ij} for all $i < j$. Taking the differentiation at both sides with respect to some common variable (such as time) yields

$$k_{ij}(\mathbf{p}_j - \mathbf{p}_i)^\top(\dot{\mathbf{p}}_j - \dot{\mathbf{p}}_i) = 0, \quad \forall i, j \in \mathcal{V},\ i < j.$$

These equations can be put into a matrix form as

$$\Lambda_K \bar{R}\, \dot{\mathbf{p}} = 0. \tag{2.1}$$

where Λ_K is the diagonal matrix with k_{ij} as diagonal entries, and $\bar{R}$ is called the *normalized rigidity matrix* with rows

$$\big[\mathbf{0} \;\cdots\; \mathbf{0} \;\underbrace{\mathbf{e}_{ij}^\top}_{i\text{-th block}} \;\cdots\; \underbrace{\mathbf{e}_{ji}^\top}_{j\text{-th block}} \;\mathbf{0} \;\cdots\; \mathbf{0}\big] \in \mathbb{R}^{1\times 2n},$$

where $\mathbf{e}_{ij} \in \mathbb{R}^2$ is the unit vector defined by

$$\mathbf{e}_{ij} \triangleq \frac{\mathbf{p}_j - \mathbf{p}_i}{\|\mathbf{p}_j - \mathbf{p}_i\|}.$$

Note that diagonal entries of Λ_K and the rows of $\bar{R}$ are indexed by the same ordering of $\{(i,j)\,|\,i,j \in \mathcal{V}, i<j\}$, and there are $n(n-1)/2$ of them. We also define $R \triangleq \Lambda_K^{\frac{1}{2}} \bar{R}$, which is called the *rigidity matrix*. We assume by convention that all trivial rows (rows having all zeros) are already removed in rigidity matrix R, that is, a row is removed if its corresponding connectivity coefficient $k_{ij} = 0$.

Definition 2.2.1 (Infinitesimal Rigidity [22, 41]) *A formation (or leader-follower formation) is* infinitesimally rigid*, or simply* rigid*, if the rank of its corresponding rigidity matrix R is equal to $2n-3$.*

The set of all infinitesimal displacements $\dot{\mathbf{p}}$ caused by the simultaneous rigid body motions of the whole formation forms a subspace of $\mathbb{R}^{2n}$ of dimension three (two for translations and one for rotations), and is denoted by $\mathrm{iso}_n(\mathbf{p})$. If the solutions of (2.1) consist of only those rigid body motions, the formation is considered rigid infinitesimally, or locally. It is easy to see that $\mathrm{iso}_n(\mathbf{p}) \subset \mathrm{null}(R)$.

2.3 Stiffness Matrix

For the analysis of general "robustness" of a formation, a mass-spring analogy is adopted: each vertex is modeled by a point mass, and the connection between vertices i and j is

modeled by a spring with the spring constant k_{ij} and the natural length $d_{ij} = \|\mathbf{p}_i - \mathbf{p}_j\|$. Suppose now that the vertices' position is perturbed from $\mathbf{p}$ to $\mathbf{p}+\Delta\mathbf{p}$ for some small $\Delta\mathbf{p} = \begin{bmatrix}\Delta\mathbf{p}_1^\top & \Delta\mathbf{p}_2^\top & \cdots & \Delta\mathbf{p}_n^\top\end{bmatrix}^\top$. By the Hooke's Law, the spring between vertices i and j will exert a tension force on vertex i as $\mathbf{f}_{ij} = k_{ij}\left(\|(\mathbf{p}_i + \Delta\mathbf{p}_i) - (\mathbf{p}_j + \Delta\mathbf{p}_j)\| - \|\mathbf{p}_i - \mathbf{p}_j\|\right)\mathbf{e}_{ij}$, where

$$\mathbf{e}_{ij} \triangleq (\mathbf{p}_j - \mathbf{p}_i)/\|\mathbf{p}_j - \mathbf{p}_i\|$$

is the unit vector pointing from $\mathbf{p}_i$ to $\mathbf{p}_j$.

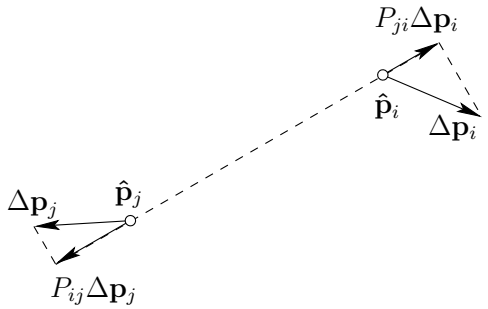

Fig. 2.1.: Determining the infinitesimal change in the length of the spring using projection

It is easy to obtain (see Fig. 2.1) that $\mathbf{f}_{ij} = -k_{ij}P_{ij}(\Delta\mathbf{p}_i - \Delta\mathbf{p}_j) + o(\Delta\mathbf{p})$, where $P_{ij} = \mathbf{e}_{ij}\mathbf{e}_{ij}^\top$ is the projection matrix onto the direction $\mathbf{e}_{ij}$. The total force exerted on vertex i is then

$$\mathbf{f}_i = \sum_{j\in\mathcal{V}\setminus\{i\}} \mathbf{f}_{ij} = -\sum_{j\in\mathcal{V}\setminus\{i\}} k_{ij}P_{ij}(\Delta\mathbf{p}_i - \Delta\mathbf{p}_j) + o(\Delta\mathbf{p}).$$

Consequently, the resulting aggregated tension force $\mathbf{f} = \begin{bmatrix}\mathbf{f}_1^\top & \mathbf{f}_2^\top & \cdots & \mathbf{f}_n^\top\end{bmatrix}^\top$ is determined by

$$\mathbf{f} = -S\,\Delta\mathbf{p} + o(\Delta\mathbf{p}), \tag{2.2}$$

or the infinitesimal version as below,

$$\dot{\mathbf{f}} = -S\dot{\mathbf{p}}, \tag{2.3}$$

Here, $S = [S_{ij}]_{i,j\in\mathcal{V}} \in \mathbb{R}^{2n\times 2n}$ is a block matrix with each block $S_{ij} \in \mathbb{R}^{2\times 2}$, $i, j \in \mathcal{V}$, given by

$$S_{ij} = \begin{cases} -k_{ij}P_{ij}, & i \neq j \\ \sum_{l\in\mathcal{V}\setminus\{i\}} k_{il}P_{il}, & i = j. \end{cases} \tag{2.4}$$

The matrix S defined above is called the *stiffness matrix* of the formation $(\mathcal{V}, \mathbf{p}, K)$. It has a structure resembling that of the Laplacian matrix [42] L of the formation, which is defined as

$$L = [l_{ij}] \quad \text{,where } l_{ij} = \begin{cases} \sum_{\ell\in\mathcal{V}\setminus\{i\}} k_{i\ell}, & \text{if } i = j \\ -k_{ij}, & \text{if } i \neq j, \end{cases} \tag{2.5}$$

with the difference that the stiffness matrix S has twice the dimension as the graph Laplacian L. See [22] for the definitions of S for general elastic structures. It was first adopted in [36] for the study of multi-agent systems.

The total elastic energy J stored in all the springs as a result of the perturbation $\Delta\mathbf{p}$ is

$$J(\Delta\mathbf{p}) = \frac{1}{2}\sum_{i,j\in\mathcal{V}} k_{ij}\|P_{ij}(\Delta\mathbf{p}_i - \Delta\mathbf{p}_j)\|^2 + o(\|\Delta\mathbf{p}\|^2) = \frac{1}{2}\Delta\mathbf{p}^\top S\Delta\mathbf{p} + o(\|\Delta\mathbf{p}\|^2). \tag{2.6}$$

In other words, S is the Hessian of the energy function J at the equilibrium position $\Delta\mathbf{p} = 0$.

We note that (2.3) and (2.6) are generalizations of the relations $f = -k\Delta p$ and $J = \frac{1}{2}k(\Delta p)^2$ in the single-spring case, with the stiffness matrix S a generalization of the spring constant k. Whenever we need to indicate the dependence of S on the vertex configuration $\mathbf{p}$ and the connectivity K, we will use the notation $S(K, \mathbf{p})$.

Remark 2.3.1 *In the special case where all entries in K are zero except k_{ij} and k_{ji} for one pair of vertices i and j, the stiffness matrix S has exactly four nonzero 2-by-2 blocks, namely, $S_{ii} = S_{jj} = k_{ij}P_{ij}, S_{ij} = S_{ji} = -k_{ij}P_{ij}$. Such an S is of rank one as $S = k_{ij}\bar{\mathbf{r}}_{ij}\bar{\mathbf{r}}_{ij}^\top$, where $\bar{\mathbf{r}}_{ij} \triangleq \begin{bmatrix}\bar{\mathbf{r}}_{ij}^{(1)\top} & \cdots & \bar{\mathbf{r}}_{ij}^{(n)\top}\end{bmatrix}^\top \in \mathbb{R}^{2n}$ is defined by, for $l \in \mathcal{V}$,*

$$\bar{\mathbf{r}}_{ij}^{(l)} = \begin{cases} \mathbf{e}_{ij}, & l = i \\ -\mathbf{e}_{ij}, & l = j \\ \mathbf{0}, & \textit{otherwise}. \end{cases} \tag{2.7}$$

Let S be the stiffness matrix defined in (2.4) for an arbitrary formation $(\mathcal{V}, K, \mathbf{p})$.

Proposition 2.3.1 *The stiffness matrix S has the following properties:*

1) *(**Linearity in** K) For any $K_1, K_2 \in \mathcal{K}$ and $\alpha, \beta \in \mathbb{R}$ such that $\alpha K_1 + \beta K_2 \in \mathcal{K}$, we have*

$$S(\alpha K_1 + \beta K_2, \mathbf{p}) = \alpha S(K_1, \mathbf{p}) + \beta S(K_2, \mathbf{p}).$$

2) *(**Scale Invariance**) $S(K, \mathbf{p}) = S(K, \gamma\mathbf{p}),\ \forall\, \gamma \in \mathbb{R}_+$.*

3) *(**Translation Invariance**) $S(K, \mathbf{p}) = S(K, \mathbf{p} \oplus \mathbf{w}),\ \forall\, \mathbf{w} \in \mathbb{R}^2$, where*

$$\mathbf{p} \oplus \mathbf{w} \triangleq \left[(\mathbf{p}_1 + \mathbf{w})^\top \ \cdots \ (\mathbf{p}_n + \mathbf{w})^\top\right]^\top.$$

4) *(**Rotation/Reflection Invariance**) For any orthogonal matrix $Q \in \mathbb{O}_2 \triangleq \{Q \in \mathbb{R}^{2\times 2} : QQ^\top = I\}$, denote $Q \odot \mathbf{p} \triangleq \left[(Q\mathbf{p}_1)^\top \ \cdots \ (Q\mathbf{p}_n)^\top\right]^\top$. Then,*

$$S(K, Q \odot \mathbf{p}) = (I_n \otimes Q) S(K, \mathbf{p}) (I_n \otimes Q)^\top,$$

where $\otimes$ denotes the Kronecker product of matrices.

Proof Property 1 follows directly from the definition of S. Properties 2 and 3 can be easily verified by noting that S depends on $\mathbf{p}$ only through the projection matrices P_{ij}, which are normalized and translation-invariant. To prove Property 4, observe that after the orthogonal transformation the new projection matrices P'_{ij} become

$$P'_{ij} = \frac{(Q\mathbf{p}_j - Q\mathbf{p}_i)(Q\mathbf{p}_j - Q\mathbf{p}_i)^\top}{\|Q\mathbf{p}_j - Q\mathbf{p}_i\|^2} = \frac{Q(\mathbf{p}_j - \mathbf{p}_i)(\mathbf{p}_j - \mathbf{p}_i)^\top Q^\top}{\|\mathbf{p}_j - \mathbf{p}_i\|^2} = QP_{ij}Q^\top.$$

As this is true for each i and j, we have $S(K, Q \odot \mathbf{p}) = (I_n \otimes Q) S(K, \mathbf{p}) (I_n \otimes Q)^\top$. Note that $I_n \otimes Q \in \mathbb{O}_{2n}$ is also an orthogonal matrix corresponding to the simultaneous rotation and/or reflection of all the vertices by Q. ■

Two configurations $\mathbf{p}, \mathbf{p}' \in \mathbb{R}^{2n}$ are called *similar* (denoted by $\mathbf{p} \sim \mathbf{p}'$) if one can be obtained from the other by a rigid body motion and a scaling, i.e., if $\gamma\mathbf{p}' = (Q \odot \mathbf{p}) \oplus \mathbf{w}$ for some $\gamma \in \mathbb{R}_+$, $Q \in \mathbb{O}_2$, and $\mathbf{w} \in \mathbb{R}^2$. Obviously, $\sim$ is an equivalence relation. The

equivalence class containing $\mathbf{p}$ is denoted by $[\mathbf{p}]_\sim$. The proof of Proposition 2.3.1 shows that the stiffness matrices of similar configurations are similar matrices and as a result have the same set of eigenvalues. Thus, the spectrum $\sigma(S(K,[\mathbf{p}]_\sim))$ is well defined within each equivalence class.

Proposition 2.3.2 (Nonnegative Definiteness) $S \succeq 0$.

Proof Note that $K = \sum\sum_{i,j\in\mathcal{V},i<j} K^{(ij)}$ where $K^{(ij)} \in \mathcal{K}$ is obtained by setting all entries in K to zero except k_{ij} and k_{ji}, and that each $S(K^{(ij)},\mathbf{p}) = k_{ij}\mathbf{q}_{ij}\mathbf{q}_{ij}^\top \succeq 0$ where $\mathbf{q}_{ij}$ is defined in (2.7). Thus, $S(K,\mathbf{p}) = \sum\sum_{i,j\in\mathcal{V},i<j} S(K^{(ij)},\mathbf{p}) \succeq 0$ by the linearity property. ■

The above conclusion can also be obtained by noting that the stiffness matrix is the Hessian matrix of the nonnegative total elastic energy function $J(\delta\mathbf{p})$ defined in (2.6) at $\delta\mathbf{p} = 0$.

Proposition 2.3.3 $\operatorname{tr}(S(K,\mathbf{p})) = \sum\sum_{i,j\in\mathcal{V}} k_{ij}$.

Proof This follows since $\operatorname{tr}(S(K,\mathbf{p})) = \sum_{i\in\mathcal{V}} \operatorname{tr}(S_{ii}) = \sum_{i\in\mathcal{V}} \operatorname{tr}\left(\sum_{j\in\mathcal{V}\setminus\{i\}} k_{ij}P_{ij}\right) = \sum\sum_{i,j\in\mathcal{V}} k_{ij}$, where the last equality follows from $\operatorname{tr}(P_{ij}) = 1$ and $k_{ii} = 0$. ■

The stiffness matrix and the (normalized) rigidity matrix are related by the following expression:

$$S = R^\top R = \bar{R}^\top \Lambda_K \bar{R}, \tag{2.8}$$

where Λ_K is the diagonal matrix whose entries are k_{ij} in proper order.

Proposition 2.3.4 *The stiffness matrix S and the rigidity matrix R share the same null space.*

Proof This is evident from (2.8). ■

Corollary 2.3.1 *A formation is rigid if and only if its stiffness matrix S has rank $2n-3$.*

Proof This is directly from Proposition 2.3.4 and Definition 2.2.1. ■

The stiffness matrix S has at least three zero eigenvalues whose corresponding eigenspace is $\mathrm{iso}_n(\mathbf{p})$. The other $2n-3$ eigenvalues are nonnegative as S is nonnegative definite.

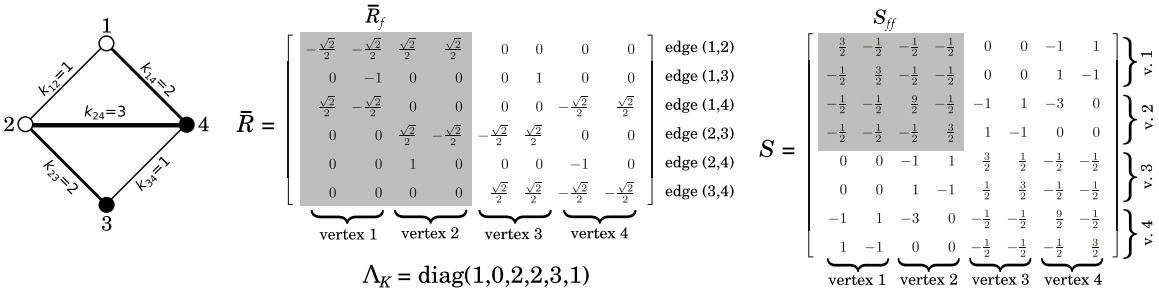

Fig. 2.2.: Examples of normalized rigidity matrix and stiffness matrix

2.4 Fixability of Leader-follower Formations

For leader-follower formations, a property corresponding to infinitesimal rigidity can also be defined. Recall that the vertex set $\mathcal{V}$ is partitioned into followers $\mathcal{F}$ and leaders $\mathcal{L}$. Correspondingly, the rigidity matrix R can be rearranged (if necessary) and partitioned as $R = \begin{bmatrix} R_f & R_\ell \end{bmatrix}$, where R_f and R_ℓ consist of the block columns of R for followers and leaders, respectively. The same partitioning applies to the normalized rigidity matrix $\bar{R}$. Consequently, the stiffness matrix S can be partitioned as

$$S = \begin{bmatrix} R_f^\top \\ R_\ell^\top \end{bmatrix} \begin{bmatrix} R_f & R_\ell \end{bmatrix} = \begin{bmatrix} \bar{R}_f^\top \\ \bar{R}_\ell^\top \end{bmatrix} \Lambda_K \begin{bmatrix} \bar{R}_f & \bar{R}_\ell \end{bmatrix} = \begin{bmatrix} S_{ff} & S_{f\ell} \\ S_{f\ell}^\top & S_{\ell\ell} \end{bmatrix}. \tag{2.9}$$

See Fig. 2.2 for an example where S_{ff} is highlighted by the shaded region. Denote by $\mathbf{p}_f$ and $\mathbf{p}_\ell$ the stacked vector of $\mathbf{p}_i$, $i \in \mathcal{V}$, for i in $\mathcal{F}$ and in $\mathcal{L}$, respectively.

Definition 2.4.1 (Fixability) *A leader-follower formation $(\mathcal{V}, \mathbf{p}, K, \mathcal{L})$ is called* fixable*, if $R_f\dot{\mathbf{p}}_f + R_\ell\dot{\mathbf{p}}_\ell = \mathbf{0}$ and $\dot{\mathbf{p}}_\ell = \mathbf{0}$ necessarily imply $\dot{\mathbf{p}}_f = \mathbf{0}$.*

For a fixable leader-follower formation, there is no infinitesimal movement of the followers that can satisfy all the distance constraints while keeping the leaders fixed. In the context of network localization, knowing the positions of the leaders together with the relative distances between vertex pairs (i, j) with $k_{ij} > 0$ enables one to uniquely determine (at least locally) the positions of all the followers. If the choice of a set of vertices as leaders makes the resulting leader-follower formation fixable, then such a set is called a *fixing set*.

Proposition 2.4.1 *The following statements are equivalent:*

1) $(\mathcal{V}, \mathbf{p}, K, \mathcal{L})$ *is fixable;*

2) R_f *has full column rank;*

3) S_{ff} *is nonsingular.*

The proof is trivial and hence omitted.

Theorem 2.4.1 *If* $(\mathcal{V}, \mathbf{p}, K)$ *is infinitesimally rigid, then any* $(\mathcal{V}, \mathbf{p}, K, \mathcal{L})$ *with* $|\mathcal{L}| \geq 2$ *is fixable.*

Proof Suppose $\mathbf{u} = \begin{bmatrix} \mathbf{u}_f^\top & \mathbf{u}_\ell^\top \end{bmatrix}^\top$ with $\mathbf{u}_\ell = \mathbf{0}$ satisfies $S\mathbf{u} = \mathbf{0}$, which implies $S_{ff}\mathbf{u}_f = \mathbf{0}$. Since $(\mathcal{V}, \mathbf{p}, K)$ is infinitesimally rigid, the nullity of S is 3. Specifically,

$$\begin{bmatrix} \mathbf{u}_f \\ \mathbf{0} \end{bmatrix} \in \text{null}(S) = \text{span}\left\{ \begin{bmatrix} \mathbf{x}_f \\ \mathbf{x}_\ell \end{bmatrix}, \begin{bmatrix} \mathbf{y}_f \\ \mathbf{y}_\ell \end{bmatrix}, \begin{bmatrix} \mathbf{p}_f^\perp \\ \mathbf{p}_\ell^\perp \end{bmatrix} \right\},$$

where $\mathbf{x}, \mathbf{y}, \mathbf{p}^\perp$ denote the simultaneous translations along x, y directions and the rotation around the origin. We claim that $\left\{\mathbf{x}_\ell, \mathbf{y}_\ell, \mathbf{p}_\ell^\perp\right\}$ is a linearly independent set; otherwise, $\mathbf{p}_\ell^\perp = \alpha\mathbf{x}_\ell + \beta\mathbf{y}_\ell$ for some $\alpha, \beta \in \mathbb{R}$, which implies that all leaders share the same position — a contradiction to Definition 2.1.1. Therefore, $\mathbf{u}_f = \mathbf{0}$ is the only solution to the equation $S_{ff}\mathbf{u}_f = \mathbf{0}$, and S_{ff} is nonsingular. ■

The following result shows that fixability can be determined from the infinitesimal rigidity of an augmented formation with all leaders connected.

Corollary 2.4.1 *A leader-follower formation* $(\mathcal{V}, \mathbf{p}, K, \mathcal{L})$ *with* $|\mathcal{L}| \geq 2$ *is fixable if the augmented formation* $(\mathcal{V}, \mathbf{p}, \hat{K})$ *is infinitesimally rigid. Here,* $\hat{K}$ *is the augmented matrix obtained from* K *by setting the connectivity coefficients between every pair of leaders strictly positive.*

Proof Observe from (2.4) that S_{ff} is independent from the connectivity coefficients between anchors. Hence, we may arbitrarily increase k_{ij} for $i, j \in \mathcal{L}$, without affecting the fixability of the anchored formation graph. Now if $(\mathcal{V}, \mathbf{p}, \hat{K})$ is infinitesimally rigid, by Theorem 2.4.1 $(\mathcal{V}, \mathbf{p}, \hat{K}, \mathcal{L})$ is fixable, and so is $(\mathcal{V}, \mathbf{p}, K, \mathcal{L})$. ■

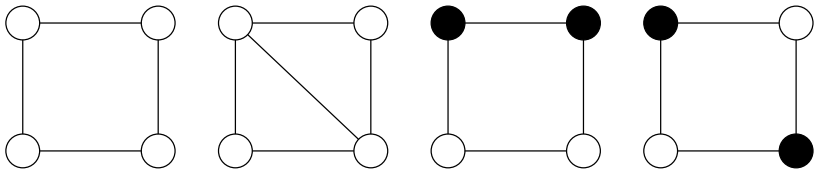

(a) Not rigid (b) Rigid (c) Not fixable (d) Fixable

Fig. 2.3.: Examples illustrating infinitesimal rigidity and fixability

To illustrate the concepts of rigidity and fixability, some example formations are shown in Fig. 2.3. The circles represent followers and the black dots represent leaders with fixed locations. An edge between two vertices indicates that they are connected and hence their distance is fixed. The (leaderless) formation in Fig. 2.3(a) is not rigid because its shape can be deformed without changing edge lengths, whereas the one in Fig. 2.3(b) is infinitesimally rigid (though not globally rigid). The leader-follower formation in Fig. 2.3(c) is not fixable since the two followers on the bottom can be parallelly slided without altering the lengths of the edges. The leader-follower formation in Fig. 2.3(d) on the other hand is fixable. The fixability of Fig. 2.3(d) can be deduced from the infinitesimal rigidity of Fig. 2.3(b) by using Corollary 2.4.1.

2.5 Looseness of Leader-follower Formations

In this section, we probe the properties regarding the *looseness* of a leader-follower formation.

Definition 2.5.1 (Looseness) *A leader-follower formation* $(\mathcal{V}, \mathbf{p}, K, \mathcal{L})$ *is called* loose*, if for an arbitrary infinitesimal motion of the leaders* $\dot{\mathbf{p}}_\ell$*, there is an infinitesimal motion of the followers* $\dot{\mathbf{p}}_f$ *satisfying* $R_f\dot{\mathbf{p}}_f + R_\ell\dot{\mathbf{p}}_\ell = \mathbf{0}$*; otherwise it is* tight*.*

In contrast to the fixability property where the leaders are assumed fixed, the looseness property determines the abilities of the followers to adapt to *arbitrary movements* of the leaders. If a leader-follower formation is tight, then there must be some directions in which if the leaders move, the followers will be unable to move accordingly while maintaining all

the distance constraints. In physical analogy, a tight formation is "stretched to extreme" by the leaders in those directions, and further movements will cause some distance constraints to break inevitably.

Proposition 2.5.1 *The following statements are equivalent:*

1) Leader-follower formation $(\mathcal{V}, \mathbf{p}, K, \mathcal{L})$ *is loose;*

2) $\mathrm{rank}(R_f) = \mathrm{rank}(R)$*;*

3) $\mathrm{colsp}(R_\ell) \subseteq \mathrm{colsp}(R_f)$*;*

4) Equation $R_f X = R_\ell$ *admits a solution.*

Proof These are obviously the linear algebraic conditions equivalent to that in Definition 2.5.1. ■

Remark 2.5.1 *Proposition 2.5.1 implies that the looseness property of a leader-follower formation is determined only by the* set *of edges (that is, the binary topology of the underlying graph), not the nonzero connectivity coefficients of the edges.*

Corollary 2.5.1 *For* $\mathcal{L} \subset \mathcal{L}' \subset \mathcal{V}$*, if* $(\mathcal{V}, \mathbf{p}, K, \mathcal{L})$ *is tight, then* $(\mathcal{V}, \mathbf{p}, K, \mathcal{L}')$ *is tight; if* $(\mathcal{V}, \mathbf{p}, K, \mathcal{L}')$ *is loose, then* $(\mathcal{V}, \mathbf{p}, K, \mathcal{L})$ *is loose.*

Proof This can be readily seen from Proposition 2.5.1 and the definition of R_f. ■

Corollary 2.5.2 *A leader-follower formation having only one leader is loose.*

Proof It is easy to verify that $R\,(\mathbf{1}_n \otimes I_2) = O$, or $R_f\,(\mathbf{1}_{n-1} \otimes I_2) + R_\ell = O$, which implies that both columns of R_ℓ are linear combinations of those of R_f. Hence, $\mathrm{rank}(R_f) = \mathrm{rank}(R)$. ■

Corollary 2.5.3 *If* $(\mathcal{V}, \mathbf{p}, K)$ *is rigid, then given any leader set* $\mathcal{L} \subset \mathcal{V}$ *with* $|\mathcal{L}| \geq 2$*, the leader-follower formation is tight.*

Proof Since $(\mathcal{V}, \mathbf{p}, K)$ is rigid, $\mathrm{rank}(R) = 2|\mathcal{V}| - 3$, whereas $\mathrm{rank}(R_f) \leq 2|\mathcal{V}| - 2|\mathcal{L}| \leq 2|\mathcal{V}| - 4$ when $|\mathcal{L}| \geq 2$. Thus the leader-follower formation must be tight. ■

Proposition 2.5.2 *If there exist two leaders directly connected with each other, then the leader-follower formation is tight.*

Proof Suppose the leader-follower formation has only two leaders, namely i and j, with $k_{ij} > 0$. Consider $\dot{\mathbf{p}}_\ell = \begin{bmatrix}\mathbf{e}_{ij}^\top & \mathbf{e}_{ji}^\top\end{bmatrix}^\top$,

$$\left[\begin{array}{c|c} R_f & R_\ell \end{array}\right] \left[\begin{array}{c} \dot{\mathbf{p}}_f \\ \hline \dot{\mathbf{p}}_\ell \end{array}\right] = \left[\begin{array}{ccc|cc} * & \cdots & * & * & * \\ \mathbf{0} & \cdots & \mathbf{0} & \sqrt{k_{ij}}\mathbf{e}_{ij}^\top & \sqrt{k_{ij}}\mathbf{e}_{ji}^\top \\ * & \cdots & * & * & * \end{array}\right] \left[\begin{array}{c} * \\ \vdots \\ * \\ \hline \mathbf{e}_{ij} \\ \mathbf{e}_{ji} \end{array}\right] = \begin{bmatrix} * \\ 2\sqrt{k_{ij}} \\ * \end{bmatrix} \neq \mathbf{0},$$

which, according to Definition 2.5.1, implies that the leader-follower formation is tight. The case with more than two leaders can be readily proven by Corollary 2.5.1. ■

Proposition 2.5.3 *Given leader-follower formation $(\mathcal{V}, \mathbf{p}, K, \mathcal{L})$ with two leaders $\mathcal{L} = \{i, j\}$, if $(\mathcal{V}, \mathbf{p}, K, \mathcal{L})$ is both fixable and tight, then $(\mathcal{V}, \mathbf{p}, K)$ is rigid.*

Proof By Proposition 2.4.1, the fixability of the leader-follower formation indicates that $\operatorname{rank}(R_f) = 2|\mathcal{F}| = 2|\mathcal{V}| - 2|\mathcal{L}| = 2|\mathcal{V}| - 4$. On the other hand, the tightness implies that $\operatorname{rank}(R_f) < \operatorname{rank}(R)$ by Proposition 2.5.1. Therefore, $\operatorname{rank}(R) = 2|\mathcal{V}| - 3$, and $(\mathcal{V}, \mathbf{p}, K)$ is rigid. ■

2.6 Subformations and Rigid Components

Definition 2.6.1 (Induced Subformation) *Given formation $(\mathcal{V}, \mathbf{p}, K)$ and $\mathcal{V}' \subset \mathcal{V}$, the* induced subformation *is defined as the formation obtained from removing all vertices in $\mathcal{V} \setminus \mathcal{V}'$ and all corresponding the rows and columns of K and $\mathbf{p}$. The subformation induced by $\mathcal{V}'$ from $(\mathcal{V}, \mathbf{p}, K)$ is denoted by $(\mathcal{V}, \mathbf{p}, K)[\mathcal{V}']$.[1] Likewise, the induced subformation of a leader-follower formation $(\mathcal{V}, \mathbf{p}, K, \mathcal{L})$ by the vertex subset $\mathcal{V}'$, denoted by $(\mathcal{V}, \mathbf{p}, K, \mathcal{L})[\mathcal{V}']$, is the induced subformation $(\mathcal{V}, \mathbf{p}, K)[\mathcal{V}']$ with leader set $\mathcal{L} \cap \mathcal{V}'$.*

[1]Note that an induced subformation may have an index set that is not consecutive or starting from 1, but this is easily fixed by relabeling the vertices without causing confusion.

Theorem 2.6.1 *Given leader-follower formation $(\mathcal{V}, \mathbf{p}, K, \mathcal{L})$, if there exists $\mathcal{V}' \subseteq \mathcal{V}$ such that $(\mathcal{V}, \mathbf{p}, K, \mathcal{L})[\mathcal{V}']$ is tight, then $(\mathcal{V}, \mathbf{p}, K, \mathcal{L})$ is tight.*

Proof We claim that if $(\mathcal{V}, \mathbf{p}, K, \mathcal{L})[\mathcal{V}']$ is tight, then $(\mathcal{V}, \mathbf{p}, K, \mathcal{L})[\mathcal{V}' \cup \{i\}]$, $\forall i \in \mathcal{V} \setminus \mathcal{V}'$ is tight. To see this, let R denote the rigidity matrix of $(\mathcal{V}, \mathbf{p}, K, \mathcal{L})[\mathcal{V}']$. By Proposition 2.5.1, $\mathrm{colsp}(R_\ell) \not\subseteq \mathrm{colsp}(R_f)$. If $i \in \mathcal{F} \setminus \mathcal{V}'$, then the rigidity matrix R' of $(\mathcal{V}, \mathbf{p}, K, \mathcal{L})[\mathcal{V}' \cup \{i\}]$ has the following structure:

$$R' = \left[\begin{array}{c|c} R'_f & R'_\ell \end{array}\right] = \left[\begin{array}{cc|c} R_f & O & R_\ell \\ * & * & * \end{array}\right].$$

If $i \in \mathcal{L} \setminus \mathcal{V}'$, then R' has the following structure:

$$R' = \left[\begin{array}{c|c} R'_f & R'_\ell \end{array}\right] = \left[\begin{array}{c|cc} R_f & R_\ell & * \\ * & * & * \end{array}\right].$$

In both cases, $\mathrm{colsp}(R'_\ell) \not\subseteq \mathrm{colsp}(R'_f)$, hence $(\mathcal{V}, \mathbf{p}, K, \mathcal{L})[\mathcal{V}' \cup \{i\}]$ is tight.

By induction, $(\mathcal{V}, \mathbf{p}, K, \mathcal{L})$ is tight. ■

Corollary 2.6.1 *If leader-follower formation $(\mathcal{V}, \mathbf{p}, K, \mathcal{L})$ is loose, then for any $\mathcal{V}' \subseteq \mathcal{V}$ such that $\mathcal{V}' \cap \mathcal{L} \neq \emptyset$, the induced subformation $(\mathcal{V}, \mathbf{p}, K, \mathcal{L})[\mathcal{V}']$ is also loose.*

Proof By contraposition of Theorem 2.6.1. ■

Theorem 2.6.2 (Theorem of Rigid Merging) *Given formation $(\mathcal{V}, \mathbf{p}, K)$, let $\mathcal{V}_1, \mathcal{V}_2$ be the subsets of $\mathcal{V}$ such that $|\mathcal{V}_1 \cap \mathcal{V}_2| \geq 2$. If both induced subformations $(\mathcal{V}, \mathbf{p}, K)[\mathcal{V}_1]$ and $(\mathcal{V}, \mathbf{p}, K)[\mathcal{V}_2]$ are rigid, then $(\mathcal{V}, \mathbf{p}, K)[\mathcal{V}_1 \cup \mathcal{V}_2]$ is rigid.*

Proof Pick any two vertices $i, j \in \mathcal{V}_1 \cap \mathcal{V}_2$ and let $\mathcal{L} = \{i, j\}$. Since $(\mathcal{V}, \mathbf{p}, K)[\mathcal{V}_1]$ and $(\mathcal{V}, \mathbf{p}, K)[\mathcal{V}_2]$ are rigid, $(\mathcal{V}, \mathbf{p}, K, \mathcal{L})[\mathcal{V}_1]$ and $(\mathcal{V}, \mathbf{p}, K, \mathcal{L})[\mathcal{V}_2]$ are both fixable and tight. Thus, $(\mathcal{V}, \mathbf{p}, K, \mathcal{L})[\mathcal{V}_1 \cup \mathcal{V}_2]$ is tight; moreover, $(\mathcal{V}, \mathbf{p}, K, \mathcal{L})[\mathcal{V}_1 \cup \mathcal{V}_2]$ is also fixable by Definition 2.4.1. Therefore by Proposition 2.5.3, $(\mathcal{V}, \mathbf{p}, K)[\mathcal{V}_1 \cup \mathcal{V}_2]$ is rigid. ■

Definition 2.6.2 (Rigid Component) *Given formation $(\mathcal{V}, \mathbf{p}, K)$, an induced subformation $(\mathcal{V}, \mathbf{p}, K)[\mathcal{V}']$ $(\mathcal{V}' \subseteq \mathcal{V})$ is called a* rigid component*, if it is rigid and there does not exist $\mathcal{V}'' \supset \mathcal{V}'$ such that $(\mathcal{V}, \mathbf{p}, K)[\mathcal{V}'']$ is rigid.*

In other words, $\mathcal{V}'$ is a maximal subset of vertices such that the induced subformation is rigid. For notation simplicity, the vertex set $\mathcal{V}'$ may also be used to denote the rigid component $(\mathcal{V}, \mathbf{p}, K)[\mathcal{V}']$ $(\mathcal{V}' \subseteq \mathcal{V})$ where confusion is unlikely.

Proposition 2.6.1 *Given formation $(\mathcal{V}, \mathbf{p}, K)$, if $(\mathcal{V}, \mathbf{p}, K)[\mathcal{V}_1]$ and $(\mathcal{V}, \mathbf{p}, K)[\mathcal{V}_2]$ are distinct rigid components, then $|\mathcal{V}_1 \cap \mathcal{V}_2| \leq 1$.*

Proof Suppose $|\mathcal{V}_1 \cap \mathcal{V}_2| \geq 2$, since both $(\mathcal{V}, \mathbf{p}, K)[\mathcal{V}_1]$ and $(\mathcal{V}, \mathbf{p}, K)[\mathcal{V}_2]$ are rigid, by Theorem 2.6.2, $(\mathcal{V}, \mathbf{p}, K)[\mathcal{V}_1 \cup \mathcal{V}_2]$ is also rigid. This contradicts with the maximality of either $\mathcal{V}_1$ or $\mathcal{V}_2$. ■

Corollary 2.6.2 *Given formation $(\mathcal{V}, \mathbf{p}, K)$ and $i, j \in \mathcal{V}$ with $k_{ij} > 0$, the rigid component containing $\{i, j\}$ uniquely exists.*

Proof First, note that $(\mathcal{V}, \mathbf{p}, K)[\{i, j\}]$ is rigid, hence there exists at least one rigid component containing $\{i, j\}$. The uniqueness is given by Proposition 2.6.1 ■

Using Corollary 2.6.2, it can be seen that for any given formation $(\mathcal{V}, \mathbf{p}, K)$, there exists a unique collection of vertex set $\mathcal{R}$, such that $\mathcal{R}$ is a cover of $\mathcal{V}$ and for each $\mathcal{V}' \in \mathcal{R}$, $(\mathcal{V}, \mathbf{p}, K)[\mathcal{V}']$ is a rigid component. We also define the *pivot set* $\mathcal{V}_p$ as

$$\mathcal{V}_p \triangleq \bigcup_{V' \in \mathcal{R},\, V'' \in \mathcal{R} \setminus \{V'\}} \bigcup (V' \cap V'')\,, \tag{2.10}$$

and each vertex in $\mathcal{V}_p$ is called a *pivot*.

Definition 2.6.3 (Skeleton Graph) *The* skeleton graph G_S *of formation $(\mathcal{V}, \mathbf{p}, K)$ is an undirected graph with vertex set $\mathcal{R} \cup \mathcal{V}_p$ and edge set $\{\{v, \mathcal{V}'\} : v \in \mathcal{V}_p, \mathcal{V}' \in \mathcal{R}, v \in \mathcal{V}'\}$.*

Proposition 2.6.2 *The skeleton graph G_S has the following properties:*

1) G_S is bipartite;

2) Every leaf (vertex with degree 1) in G_S is an element in $\mathcal{R}$.

3) The girth of G_S (size of smallest cycle) must be greater than or equal to 6;

Proof Property 1) and 2) can be readily observed from Definition 2.6.3 and the fact that its girth $g(G_S) \geq 6$ results from Proposition 2.6.1. ■

Definition 2.6.4 (Trailer) *A formation is called a* trailer *if its skeleton graph is a tree (i.e., connected and acyclic).*

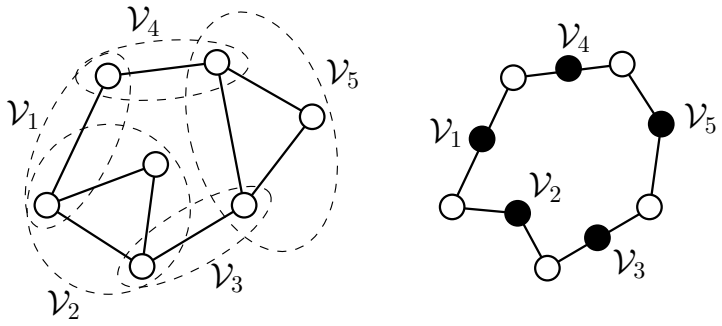

(a) Rigid components (b) Skeleton graph

Fig. 2.4.: Rigid components and the skeleton graph of a general nonrigid formation

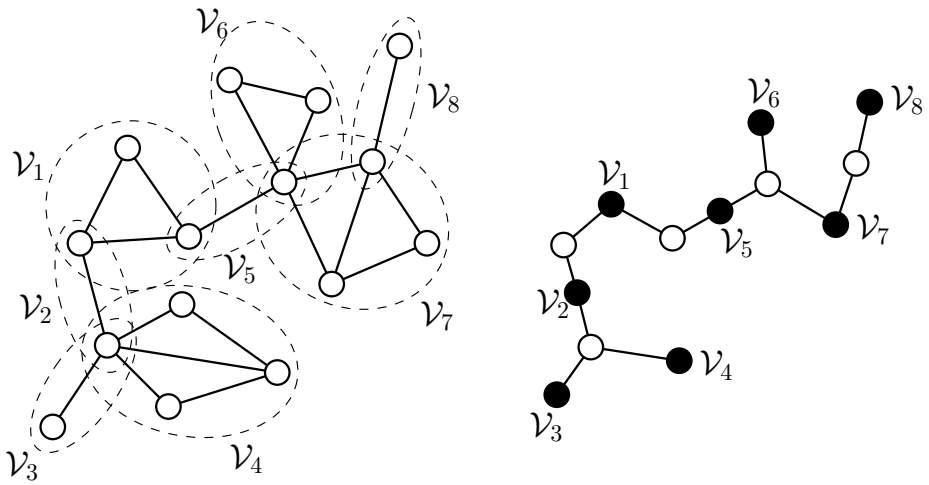

(a) Rigid components (b) Skeleton graph

Fig. 2.5.: Rigid components and the skeleton graph of a trailer

Two formations, as plotted in Fig. 2.4(a) and Fig. 2.5(a), are given as examples of rigid components. Each rigid component is encircled with a dashed ellipse in the plot and

labeled by $\mathcal{V}_i$, denoting the vertex subset corresponding to that rigid component. We see from the figures that any two adjacent rigid components share only one pivot vertex. The skeleton graphs of the formations are illustrated in Fig. 2.4(b) and Fig. 2.5(b), where the black vertices denote the rigid components in $\mathcal{R}$ and the white vertices represent the pivot vertices. The two ends of any edge in the skeleton graphs consist of one black vertex and one white vertex, hence the skeleton graphs are bipartite. Moreover, the formation in Fig. 2.5(a) is a trailer, since the skeleton graph in Fig. 2.5(b) is a tree.

2.7 Comparison with Graph-theoretic Concepts

In Table 2.1 below, the concepts proposed in this chapter are compared with their counterparts (if any) in classic graph theory. Since the concept of leader is not widely adopted in the classic graph theory, notions specifically related to leader-follower formations, such as fixability and looseness, have no well-known counterparts therein.

Table 2.1: Table of corresponding concepts

Concept in algebraic formation theory	Graph-theoretic counterpart [43]
formation	(undirected weighted) graph
induced subformation	(vertex-)induced subgraph
rigidity matrix R	incidence matrix C
stiffness matrix $S = R^\top R$	graph Laplacian matrix $L = C^\top C$
$\mathrm{rank}(S) = 2n - 3 \Rightarrow$ formation is *rigid*	$\mathrm{rank}(L) = 2n - 1 \Rightarrow$ graph is *connected*
worst-case rigidity index[‡] $r_{\mathrm{w}} \triangleq \lambda_4(S)$	algebraic connectivity $a \triangleq \lambda_2(L)$
trailer	tree
rigid component (no shared edge)	connected component (no shared vertex)

[‡] The definition of worst-case rigidity index r_{w} is given in Section 3.1.

2.8 Summary

In this chapter, multi-agent formations were formalized as mathematical objects and studied using algebraic methods. First in Section 2.2 and 2.3, rigidity matrices and stiffness matrices were proposed as quantities that describe both positional and topological information of formations. These quantities also give rise to some key properties of formations (both leaderless and leader-follower) such as rigidity, fixability, looseness, which were discussed in Section 2.4 and 2.5. Lastly in Section 2.6, it was shown that every general nonrigid formation can be decomposed into a unique collection of rigid components, and a special family of formations called trailers was defined, which will become useful in the later chapters of this thesis.

3. RIGIDITY INDEXES

This chapter is focused on the concept of rigidity indexes, numerical metrics of formation rigidity derived from the stiffness matrix. Various interesting properties of rigidity indexes are discussed through proofs and numerical examples. Finally, the usefulness of these indexes is justified through their intimate relation with multi-agent system applications.

3.1 Rigidity Indexes of Leaderless Formations

We recall that the stiffness matrix S in (2.3) is a generalization of the spring constant k in the single spring case. Just as k indicates the elasticity of the single spring, S can be used to characterize the rigidity of the formation graph. Intuitively, the formation is "more rigid" if a larger tension force $\mathbf{f}$ is resulted by the same perturbation $\dot{\mathbf{p}}$, or equivalently, if exerting the same amount of force $\mathbf{f}$ leads to a smaller displacement $\dot{\mathbf{p}}$ in vertex positions.

An arbitrary infinitesimal perturbation $\dot{\mathbf{p}}$ in (2.3) can be decomposed as $\dot{\mathbf{p}} = \mathbf{u} + \mathbf{v}$, where $\mathbf{u} \in \mathrm{iso}_n(\mathbf{p})$ and $\mathbf{v} \in \mathrm{iso}_n(\mathbf{p})^{\perp}$. Since $\mathbf{u}$ moves the whole formation as a rigid body and only $\mathbf{v}$ effectively deforms the formation shape, when analyzing infinitesimal formation rigidity we can ignore $\mathbf{u}$ and focus on the case that $\dot{\mathbf{p}} \in \mathrm{iso}_n(\mathbf{p})^{\perp}$.

Definition 3.1.1 (Worst-case Rigidity Index) *The worst-case rigidity index (WRI) of the formation $(\mathcal{V}, \mathbf{p}, K)$ is defined as*

$$r_{\mathrm{w}}(K, \mathbf{p}) \triangleq \min_{\mathbf{q} \in \mathrm{iso}_n(\mathbf{p})^{\perp}} \frac{\mathbf{q}^{\top} S(K, \mathbf{p}) \mathbf{q}}{\mathbf{q}^{\top} \mathbf{q}} = \lambda_4(S(K, \mathbf{p})), \tag{3.1}$$

where $\lambda_4(S(K, \mathbf{p}))$ denotes the fourth smallest eigenvalue of the stiffness matrix $S(K, \mathbf{p})$.

The WRI measures the robustness of the formation graph against perturbations in its most vulnerable direction. We will show later that it characterizes the convergence speed of the multi-agent formation control algorithm in Section 3.5.1.

Definition 3.1.2 (Mean Rigidity Index) *The mean rigidity index (MRI) of the formation graph $(\mathcal{V}, \mathbf{p}, K)$ is defined as the harmonic mean of the largest $2n-3$ eigenvalues $\lambda_{2n} \geq \lambda_{2n-1} \geq \cdots \geq \lambda_4$ of the stiffness matrix $S(K, \mathbf{p})$:*

$$r_{\mathrm{m}}(K, \mathbf{p}) \triangleq \frac{2n-3}{\lambda_{2n}^{-1} + \cdots + \lambda_4^{-1}} = \begin{cases} 0, & \text{if } \mathrm{rank}(S(K, \mathbf{p})) < 2n-3 \\ \frac{2n-3}{\mathrm{tr}(S(K,\mathbf{p})^{\dagger})}, & \text{if } \mathrm{rank}(S(K, \mathbf{p})) = 2n-3, \end{cases} \tag{3.2}$$

where $S(K, \mathbf{p})^{\dagger}$ is the pseudo-inverse of $S(K, \mathbf{p})$. Note that the last equality follows as the nonzero eigenvalues of $S(K, \mathbf{p})^{\dagger}$ are reciprocal of the nonzero eigenvalues of $S(K, \mathbf{p})$.

Obviously, we have $r_{\mathrm{w}}(K, \mathbf{p}) \leq r_{\mathrm{m}}(K, \mathbf{p})$. It will be shown in Section 3.5.2 that the MRI measures the robustness of the formation graph against a random perturbation $\dot{\mathbf{p}}$ isotropically distributed in $\mathrm{iso}_n(\mathbf{p})^{\perp}$, and can characterize the localization error for the network localization problem described in Section 1.2.2. The potential application value of these indexes are also revealed through the appearance of similar quantities in some recent work, such as [30, 44], despite not being identified there as quantities related to graph rigidity.

Remark 3.1.1 *We note that the arithmetic mean of the largest $2n-3$ eigenvalues of the stiffness matrix $S(K, \mathbf{p})$ is exactly $\sum_{i,j \in \mathcal{V}} k_{ij}/(2n-3)$ by Proposition 2.3.3, which is independent of the vertex locations $\mathbf{p}$ and as such not an effective rigidity measure.*

3.2 Rigidity Indexes of Leader-follower Formations

For leader-follower formations, we can still apply the mass-spring analogy in Section 2.3 to study their robustness under the perturbations of the followers. Assume that the leaders' positions are precisely known, we set $\dot{\mathbf{p}}_\ell = \mathbf{0}$, thus,

$$\begin{bmatrix} \dot{\mathbf{f}}_f \\ \dot{\mathbf{f}}_\ell \end{bmatrix} = - \begin{bmatrix} S_{ff} & S_{f\ell} \\ S_{f\ell}^{\top} & S_{\ell\ell} \end{bmatrix} \begin{bmatrix} \dot{\mathbf{p}}_f \\ \mathbf{0} \end{bmatrix}$$

from which we have the relation between $\dot{\mathbf{p}}$ and $\dot{\mathbf{f}}$,

$$\dot{\mathbf{f}}_f = -S_{ff} \dot{\mathbf{p}}_f. \tag{3.3}$$

Being a principal minor of the positive semidefinite matrix S, S_{ff} is also positive semidefinite hence has nonnegative eigenvalues. On the other hand, different from S which always has a three-dimensional null space $\mathrm{iso}_n(\mathbf{p})$ corresponding to infinitesimal rigid body motions, S_{ff} is not necessarily singular, as fixing one leader eliminates the freedom of translations and fixing two eliminates the freedom of rotations.

Definition 3.2.1 (Rigidity Indexes of Leader-follower Formations) *For leader-follower formation $(\mathcal{V}, \mathbf{p}, K, \mathcal{L})$, its worst-case rigidity index r_{w} and mean rigidity index r_{m} are defined as*

$$r_{\mathrm{w}}(K, \mathbf{p}; \mathcal{L}) \triangleq \lambda_1(S_{ff})$$

$$r_{\mathrm{m}}(K, \mathbf{p}; \mathcal{L}) \triangleq \begin{cases} 0, & \textit{if } \lambda_1(S_{ff}) = 0 \\ 2|\mathcal{F}| \left[\mathrm{tr}\left(S_{ff}^{-1}\right)\right]^{-1}, & \textit{otherwise}, \end{cases}$$

where $|\mathcal{F}|$ is the number of followers.

Both rigidity indexes are nonnegative. Moreover, the leader-follower formation is fixable if and only if r_{w} or r_{m} is strictly greater than zero. These indexes give numeric measures of the rigidity of leader-follower formations in the sense similar to that of leaderless formations.

3.3 Properties of Rigidity Indexes

We next discuss some notable properties of the two rigidity indexes defined in the previous section, the WRI r_{w} and the MRI r_{m}. For commonly held properties, the generic notation $r(K, \mathbf{p})$ is used to indicate both indexes. Note that the properties possessed by $r(K, \mathbf{p})$ also apply to $r(K, \mathbf{p}; \mathcal{L})$ with fixed $\mathcal{L}$, unless otherwise indicated.

Proposition 3.3.1 *Both rigidity indexes $r(K, \mathbf{p})$ have the following properties:*

*1) (**Nonnegativeness**) $r(K, \mathbf{p}) \geq 0$. Further, $r(K, \mathbf{p}) \neq 0$ if and only if $(\mathcal{V}, \mathbf{p}, K)$ is rigid (or fixable for leader-follower formations).*

*2) (**Homogeneity**) $r(\alpha K, \mathbf{p}) = \alpha\, r(K, \mathbf{p})$, $\forall\, \alpha \in \mathbb{R}_+$.*

*3) (**Similarity Invariance**)* $\mathbf{p} \sim \mathbf{p}' \Rightarrow r(K, \mathbf{p}) = r(K, \mathbf{p}')$.

*4) (**Monotonicity**)* $r(K, \mathbf{p})$ *is nondecreasing with respect to each entry* k_{ij} *of* $K \in \mathcal{K}$.

*5) (**Boundedness**) For a fixed* $K \in \mathcal{K}$, $r(K, \mathbf{p}) \leq \frac{1}{2n-3} \sum \sum_{i,j \in \mathcal{V}} k_{ij}$, $\forall\, \mathbf{p} \in \mathbb{R}^{2n}$.

Proof Let S be the stiffness matrix of the formation $(\mathcal{V}, \mathbf{p}, K)$.

1). That $r(K, \mathbf{p}) \geq 0$ follows from the nonnegative definiteness of S. Further, for either index, $r(K, \mathbf{p}) \neq 0$ if and only if S has rank $2n - 3$, which by Corollary 2.3.1 is equivalent to the rigidity of the formation. For leader-follower formations, see the discussion in Section 3.2.

2) and 3). These two properties follow directly from Proposition 2.3.1 as the stiffness matrix $S(K, \mathbf{p})$ is linear in K and similar (hence of the same spectrum) for similar configurations.

4). Consider $K, K' \in \mathcal{K}$ where $K' - K$ has nonnegative entries. Then, $S(K', \mathbf{p}) - S(K, \mathbf{p}) \succeq 0$ as it is the stiffness matrix of the formation $(\mathcal{V}, \mathbf{p}, K' - K)$. By [45, Corollary 4.3.3], the sorted eigenvalues of the two matrices satisfy $\lambda_i[S(K', \mathbf{p})] \geq \lambda_i[S(K, \mathbf{p})]$ for $i = 1, \ldots, 2n$. This implies that $r(K', \mathbf{p}) \geq r(K, \mathbf{p})$.

5). The inequality is trivial for non-rigid formations. Assume the formation is rigid. Then,

$$r_{\mathrm{w}}(K, \mathbf{p}) \leq r_{\mathrm{m}}(K, \mathbf{p}) \leq \frac{1}{2n-3} \sum_{k=4}^{2n-3} \lambda_k(S) = \frac{\mathrm{tr}(S)}{2n-3} = \frac{1}{2n-3} \sum_{i,j \in \mathcal{V}} \sum k_{ij}.$$

The second inequality above follows by the Arithmetic-Harmonic Mean inequality [46]. ■

The monotonicity property implies that strengthening the connectivity between any pair of vertices can only increase (or at least not decrease) the rigidity of the formation, which is consistent with one's intuition.

To derive the next property, we need the following lemma.

Lemma 3.3.1 *For any symmetric positive definite matrices* A *and* B *of the same dimension,*

$$\left[\mathrm{tr}\left((A+B)^{-1}\right)\right]^{-1} \geq \left[\mathrm{tr}\left(A^{-1}\right)\right]^{-1} + \left[\mathrm{tr}\left(B^{-1}\right)\right]^{-1}.$$

Proof Let $\Delta = B - A$. Since both A and B are positive definite, so is $A + t\Delta$ for each $t \in [0, 1]$. Define

$$f(t) \triangleq \left(\mathrm{tr}\left((A + t\Delta)^{-1}\right)\right)^{-1}, \quad t \in [0, 1].$$

For the desired conclusion, we need only to show that $f(t)$ is concave on $[0, 1]$. To this purpose, we compute

$$\frac{d}{dt}f(t) = \frac{\mathrm{tr}\left((A + t\Delta)^{-1}\Delta(A + t\Delta)^{-1}\right)}{[\mathrm{tr}\left((A + t\Delta)^{-1}\right)]^2} = \frac{\mathrm{tr}\left(G\Delta G\right)}{[\mathrm{tr}\left(G\right)]^2},$$

where $G \triangleq (A + t\Delta)^{-1} \succ 0$. Note that

$$\frac{d}{dt}\mathrm{tr}\left(G\Delta G\right) = \mathrm{tr}\left(\frac{dG}{dt}\Delta G + G\Delta\frac{dG}{dt}\right) = -2\,\mathrm{tr}\left(G\Delta G\Delta G\right),$$

we have

$$\frac{d^2}{dt^2}f(t) = \frac{d}{dt}\left(\frac{\mathrm{tr}\left(G\Delta G\right)}{[\mathrm{tr}\left(G\right)]^2}\right) = \frac{2}{[\mathrm{tr}\left(G\right)]^3}\left([\mathrm{tr}(G\Delta G)]^2 - \mathrm{tr}(G)\mathrm{tr}(G\Delta G\Delta G)\right).$$

Since $G \succ 0$, $G = H^\top H$ for some $H \succ 0$. By the Cauchy-Schwarz inequality,

$$[\mathrm{tr}(G\Delta G)]^2 = \left[\mathrm{tr}(H^\top H\Delta G)\right]^2 \leq \mathrm{tr}(H^\top H)\mathrm{tr}(G^\top\Delta^\top H^\top H\Delta G) = \mathrm{tr}(G)\mathrm{tr}(G\Delta G\Delta G).$$

As $\mathrm{tr}(G) > 0$, we conclude that $\frac{d^2}{dt^2}f(t) \leq 0, \forall t \in [0, 1]$, i.e., $f(t)$ is a concave function on $[0, 1]$. ■

Proposition 3.3.2 (Superadditivity) *$r(K_1 + K_2, \mathbf{p}) \geq r(K_1, \mathbf{p}) + r(K_2, \mathbf{p})$, $\forall\, \mathbf{p} \in \mathbb{R}^{2n}$, $K_1, K_2 \in \mathcal{K}$.*

Proof For simplicity, denote by $S(K)$ the stiffness matrix of the formation $(\mathcal{V}, \mathbf{p}, K)$. Note that $S(K_1 + K_2) = S(K_1) + S(K_2)$. For the WRI, the conclusion is immediate from (3.1) using the superadditivity of the $\min$ operation.

For the MRI, if the MRI corresponding to either of K_1 and K_2, say $r_{\mathrm{m}}(K_1)$, is zero, then the desired conclusion $r_{\mathrm{m}}(K_1+K_2) \geq r_{\mathrm{m}}(K_2)$ follows immediately from the monotonicity property of r_{m}. Assume $r_{\mathrm{m}}(K_1) > 0$ and $r_{\mathrm{m}}(K_2) > 0$, i.e., both $S(K_1)$ and $S(K_2)$ have rank $2n - 3$. For each $K \in \mathcal{K}$, define $\hat{S}(K) \triangleq V^\top S(K)V$, where $V = [\mathbf{v}_1 \ \cdots \ \mathbf{v}_{2n-3}] \in \mathbb{R}^{2n\times(2n-3)}$ whose columns form an orthonormal basis of $\mathrm{iso}_n\,(\mathbf{p})^\perp$. Then $r_{\mathrm{m}}(K) = (2n -$

3) $\left[\mathrm{tr}(S(K)^{\dagger})\right]^{-1} = (2n-3)[\mathrm{tr}(\hat{S}(K)^{-1})]^{-1}$ for all $K \in \mathcal{K}$ such that $S(K)$ has rank $2n-3$.

By Lemma 3.3.1,

$$\frac{r_{\mathrm{m}}(K_1+K_2)}{2n-3} = \left[\mathrm{tr}\left(\hat{S}(K_1+K_2)^{-1}\right)\right]^{-1} = \left[\mathrm{tr}\left(\left(\hat{S}(K_1)+\hat{S}(K_2)\right)^{-1}\right)\right]^{-1}$$
$$\geq \left[\mathrm{tr}\left(\hat{S}(K_1)^{-1}\right)\right]^{-1} + \left[\mathrm{tr}\left(\hat{S}(K_2)^{-1}\right)\right]^{-1} = \frac{r_{\mathrm{m}}(K_1)+r_{\mathrm{m}}(K_2)}{2n-3},$$

which is exactly the desired conclusion for the MRI. ■

The following property is a direct result of the superadditivity and the homogeneity of $r(K, \mathbf{p})$.

Corollary 3.3.1 (Concavity) $r(\alpha K_1 + (1-\alpha)K_2, \mathbf{p}) \geq \alpha r(K_1, \mathbf{p}) + (1-\alpha) r(K_2, \mathbf{p})$, $\forall\, \alpha \in [0,1]$, $K_1, K_2 \in \mathcal{K}$.

In other words, either of the two rigidity indexes is a concave function of the connectivity matrix $K \in \mathcal{K}$. This makes it possible for us to find the efficient solutions of the rigidity maximization problems in Section 5.

3.4 Numerical Examples

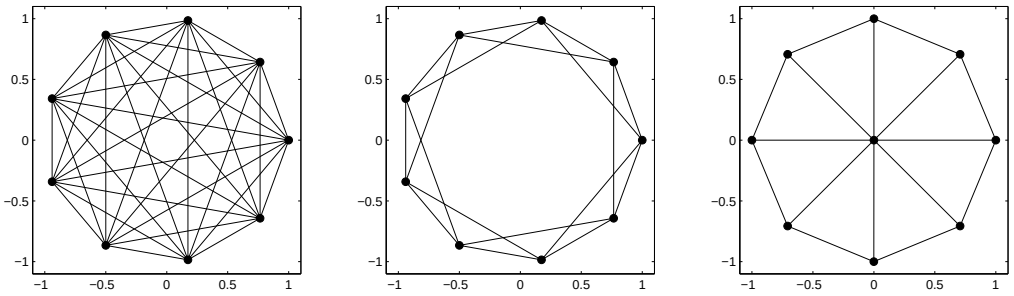

(a) Complete (b) Two-hop ring (c) Wheel

Fig. 3.1.: Three typical formation graphs ($n = 9$)

Table 3.1: WRI and MRI of the three special types of formations in Fig. 3.1

n	WRI			MRI		
	(a)	(b)	(c)	(a)	(b)	(c)
6	3	1	0.917	3.177	2.118	1.688
7	3.5	0.377	0.849	3.667	1.300	1.563
8	4	0.152	0.802	4.160	0.722	1.463
9	4.5	0.068	0.763	4.655	0.400	1.382
10	5	0.033	0.727	5.152	0.230	1.315

Consider three special formations of n vertices whose instances with $n = 9$ are plotted in Fig. 3.1. Assume unit connectivity $k_{ij} = 1$ for each link depicted. The WRI and the MRI of these formations are computed numerically for the cases $n = 6, 7, \ldots, 10$ and summarized in Table 3.1. As can be expected, the completely connected (equilateral) formation is the most rigid as measured by either index due to the maximum connections it possesses; it indeed becomes even more rigid as the number of vertices increases. On the other hand, the two-hop ring graph, despite having more connections than the wheel graph, quickly becomes much less rigid than the wheel graph as well as the completely connected formation as n increases. Intuitively, the connections of all the other vertices with the central vertex in the wheel formation strengthen the overall structure against the many vulnerabilities suffered by the two-hop formation.

Remark 3.4.1 *The rigidity indexes of a formation with a uniform nonzero value for all connectivity coefficients (i.e., with a completely connected graph with uniform weights), as illustrated in Fig. 3.1(a), can be found analytically. Without loss of generality, assume its* n *vertices are located at* $\mathbf{p}_i = \frac{1}{\sqrt{n}}[\cos(2i\pi/n), \sin(2i\pi/n)]$, $i = 1, \ldots, n$, *on a circle of radius* $\sqrt{n}$. *Let* $W \in \mathbb{R}^{2n\times 3}$ *be such that its columns are the three directions of infinitesimal rigid body motions in* $\mathrm{iso}_n(\mathbf{p})$, $W = \frac{1}{\sqrt{n}}[\mathbf{x}, \mathbf{y}, \mathbf{r}]$, *where* $\mathbf{x}$ *and* $\mathbf{y}$ *denote the simultaneous translations along* x*- and* y*-directions and* $\mathbf{r}$ *with* $\mathbf{r}_i = \left[-\sin\left(\frac{2i\pi}{n}\right), \cos\left(\frac{2i\pi}{n}\right)\right]^\top$, $i = 1, \ldots, n$,

denotes the simultaneous rotation around the origin. Note that $W^\top W = I_3$*. Now, one can verify that the stiffness matrix* S_n *can be written in the following form,*

$$S_n = \frac{n}{2}\left(I_{2n} + \mathbf{p}\mathbf{p}^\top - WW^\top\right).$$

Since $W^\top \mathbf{p} = 0$*, we conclude that the eigenvalues of* S_n *are* 0 *(with multiplicity* 3*),* n *(with multiplicity* 1*) and* $n/2$ *(with multiplicity* $2n-4$*). Hence, the WRI and the MRI are, respectively,*

$$r_{\mathrm{w}} = \frac{n}{2}, \quad r_{\mathrm{m}} = \frac{2n^2 - 3n}{4n - 7}.$$

3.5 Application Examples of Rigidity Indexes

3.5.1 Performance Evaluation for Formation Control Systems

Consider the multi-agent formation control problem described in Section 1.2.1, where the configuration $\mathbf{q}$ of n agents is controlled by the feedback controller (1.2) to achieve a set of formation constraints: $\|\mathbf{q}_i - \mathbf{q}_j\| = d_{ij}^*$ for $(i,j) \in \mathcal{E}$. Recall that $\mathbf{p}$ is assumed to be a configuration satisfying all the formation constraints. Then the formation constraint function defined in (1.1))satisfies $F(\mathbf{p}) = 0$ and $\mathbf{p}$ is an equilibrium point of the dynamics (1.2).

For agent configurations $\mathbf{q}$ very close to $\mathbf{p}$, the dynamics of the deviation $\delta\mathbf{p} \triangleq \mathbf{q} - \mathbf{p}$ can be approximated by linearizing equation (1.2) around $\mathbf{p}$ as:

$$\frac{d}{dt}\mathbf{q} = -S\,\mathbf{q}, \tag{3.4}$$

where S is exactly the stiffness matrix for the formation $(\mathcal{V}, \mathbf{p}, K)$. Here, the connectivity matrix K is defined such that k_{ij} is the penalty weight in the formation constraint function (1.1) for violating the formation constraint $\|\mathbf{p}_i - \mathbf{p}_j\| = d_{ij}^*$ for any agent pair $(i,j) \in \mathcal{E}$ and zero otherwise. Indeed, the formation constraint function $F(\mathbf{q})$ is exactly the total elastic energy function $J(\mathbf{q})$ defined by 2.6 in the mass-spring analogy.

Since both $\mathrm{iso}_n(\mathbf{p})$ and $\mathrm{iso}_n(\mathbf{p})^\perp$ are invariant subspaces of S, the solution to (3.4) can be decomposed into $\mathbf{q}(t) = \mathbf{u}(t) + \mathbf{v}(t)$, where $\mathbf{u}(t) \in \mathrm{iso}_n(\mathbf{p})$ and $\mathbf{v}(t) \in \mathrm{iso}_n(\mathbf{p})^\perp$ for all

t. We can disregard $\mathbf{u}(t)$ because rigid body motions will not result in shape deformation hence violations of formation constraints. Thus, convergence to formation is equivalent to $\mathbf{v}(t) \to 0$, which occurs at the exponential rate $\lambda_4(S)$ in the worst case.

In summary, the formation $\mathbf{p}$ satisfying all the formation constraints can be successfully recovered (up to a rigid body transformation) by the controller (1.2) after small perturbations if and only if the formation graph $(\mathcal{V}, \mathbf{p}, K)$ is rigid; and the exponential rate of the recovery is precisely the WRI of $(\mathcal{V}, \mathbf{p}, K)$.

3.5.2 Bound of Estimation Errors in Network Localization

Recall that in the network localization problem described in Section 1.2.2, noisy measurements $z_{ij} = \|\mathbf{p}_i - \mathbf{p}_j\| + \varepsilon_{ij}$ of the distances between certain pairs of sensor nodes $(i,j) \in \mathcal{E}$ are available, with the variance of the error ε_{ij} being σ_{ij}. A set $\hat{\mathcal{P}}$ of the estimates of the node locations $\mathbf{p}$ can then be obtained according to (1.3), where k_{ij} penalizes the discrepancy with the measurement z_{ij} resulted by the estimate. Generally speaking, the more accurate the measurement z_{ij}, the higher the penalty k_{ij}. We assume in the following that $k_{ij} = \sigma_{ij}^{-2}$ for $(i,j) \in \mathcal{E}$. A formation graph $(\mathcal{V}, \mathbf{p}, K)$ can then be constructed whose connectivity matrix K is defined by $k_{ij} = \sigma_{ij}^{-2}$ for $(i,j) \in \mathcal{E}$ and $k_{ij} = 0$ if otherwise.

When the formation $(\mathcal{V}, \mathbf{p}, K)$ is rigid and the measurement errors ε_{ij} are small, at least one estimate $\hat{\mathbf{p}}$ in $\hat{\mathcal{P}}$ should be close to $\mathbf{p}$, i.e., $\hat{\mathbf{p}} = \mathbf{p} + \dot{\mathbf{p}}$ for some small estimation error $\dot{\mathbf{p}}$. Note that $\hat{\mathbf{p}}$ by definition minimizes the function $\sum_{(i,j)\in\mathcal{E}} k_{ij}(\|\hat{\mathbf{p}}_i - \hat{\mathbf{p}}_j)\| - z_{ij})^2$ which can be thought of as the total elastic energy in a mass-spring system. By the principle of minimum energy, such $\hat{\mathbf{p}}$ is an equilibrium configuration of the mass-spring system, in which the total force acting on each node should be zero:

$$\sum_{j\in\mathcal{V}\setminus\{i\}} k_{ij}\mathbf{e}_{ij}(\|\hat{\mathbf{p}}_j - \hat{\mathbf{p}}_i\| - z_{ij}) = 0, \quad \forall\, i \in \mathcal{V}. \tag{3.5}$$

Using the following approximation (see Fig. 2.1),

$$\begin{aligned}\|\hat{\mathbf{p}}_j - \hat{\mathbf{p}}_i\| - z_{ij} &= \|\hat{\mathbf{p}}_i - \hat{\mathbf{p}}_j\| - \|\mathbf{p}_i - \mathbf{p}_j\| + \|\mathbf{p}_i - \mathbf{p}_j\| - z_{ij} \\ &= \mathbf{e}_{ij}^\top (\dot{\mathbf{p}}_j - \dot{\mathbf{p}}_i) - \varepsilon_{ij} + o(\|\dot{\mathbf{p}}\|), \end{aligned} \tag{3.6}$$

we can rewrite equation (3.5) as below,

$$\sum_{j\in\mathcal{V}\setminus\{i\}} k_{ij}\mathbf{e}_{ij}\mathbf{e}_{ij}^{\top}\left(\dot{\mathbf{p}}_j-\dot{\mathbf{p}}_i\right)\simeq\sum_{j\in\mathcal{V}\setminus\{i\}} k_{ij}\mathbf{e}_{ij}\varepsilon_{ij},\ \ \forall\, i\in\mathcal{V}. \tag{3.7}$$

By stacking all ε_{ij} for $i<j$ into a column vector $\mathbf{e}\in\mathbb{R}^m$, we write (3.7) in matrix form as

$$S\,\dot{\mathbf{p}}\simeq HD\mathbf{e}.$$

Here, S is the stiffness matrix of the formation $(\mathcal{V},\mathbf{p},K)$, $D\in\mathbb{R}^{m\times m}$ is a diagonal matrix with the diagonal entries $\sqrt{k_{ij}}=\sigma_{ij}^{-1}$ and $H\in\mathbb{R}^{2n\times m}$ has columns $\mathbf{h}_{ij}$, indexed by the same order of the pairs (i,j) as in $\mathbf{e}$. Each column $\mathbf{h}_{ij}\in\mathbb{R}^{2n}$ is the vertical stacking of n vectors in $\mathbb{R}^2$: $\sqrt{k_{ij}}\,\mathbf{e}_{ij}$ at the ith position, $\sqrt{k_{ji}}\,\mathbf{e}_{ji}$ at the jth position and zero elsewhere. It can be verified that $HH^{\top}=S$.

From the above derivation, the best estimate $\hat{\mathbf{p}}$ deviates from the true location $\mathbf{p}$ by $\dot{\mathbf{p}}\simeq S^{\dagger}HD\mathbf{e}$. By assumption, $\mathbf{e}$ is a random vector with the covariance $E\left[\mathbf{e}\mathbf{e}^{\top}\right]=\Sigma=\mathrm{diag}(\sigma_{ij}^2)$. The mean square error is then

$$E\left[(e_{\hat{\mathcal{P}}})^2\right]=E\left[\|\dot{\mathbf{p}}\|^2\right]\simeq E\left[\mathbf{e}^{\top}DH^{\top}S^{\dagger}S^{\dagger}HD\,\mathbf{e}\right]=\mathrm{tr}\left(H^{\top}S^{\dagger}S^{\dagger}HD\Sigma D\right).$$

Note that $D\Sigma D$ is the identity matrix. Consequently,

$$E\left[(e_{\hat{\mathcal{P}}})^2\right]\simeq\mathrm{tr}\left(S^{\dagger}\left(HH^{\top}\right)S^{\dagger}\right)=\mathrm{tr}(S^{\dagger})=\frac{2n-3}{r_{\mathrm{m}}(S)}. \tag{3.8}$$

That is, for small measurement noises, the mean square error (MSE) of the developed estimator is determined by the reciprocal of the MRI of the formation graph $(\mathcal{V},\mathbf{p},K)$. A more rigid graph implies a smaller MSE hence a more accurate best estimation, up to a rigid body transformation. The value in (3.8) has also been shown to be the Cramér-Rao lower bound of the localization estimator [47].

3.6 Summary

In this chapter, two quantitative metrics of formation rigidity, namely the *worst-case rigidity index* and the *mean rigidity index*, are derived from the eigenvalues of the stiffness

matrix associated with the formation. It was shown that both indexes possess interesting properties: They are both nonnegative, monotonically increasing with respect to connectivity coefficients, and invariant among similar formations. Both rigidity indexes were also proven to be concave functions of the connectivity coefficients, which implies that formation optimization by maximizing these rigidity indexes is a convex program that can be solved effectively and efficiently, as will be demonstrated later in Chapter 5.

In addition to the theoretic results regarding rigidity indexes, their usefulness in practice was also demonstrated by two instances of multi-agent system application. It was particularly shown that that the performance of a class of formation control strategy is precisely indicated by the worst-case rigidity index, whereas the error bounds of many distance-based localization algorithms can be characterized by the mean rigidity index. Therefore, rigidity indexes are useful in assessing the general "goodness" of a given formation.

4. MANIPULABILITY INDEXES

In this chapter, the concept of *manipulability indexes* is proposed with its properties and methods of computation discussed. Like rigidity indexes, manipulability indexes also quantifies the capability of the leaders to influence or manipulate the configuration of the followers in a leader-follower formation. The definition of manipulability index was first proposed by Kawashima *et. al* in [30] and further developed in [31]. Most of the results in this chapter supplement the previous works by providing alternative formulations of the manipulability indexes, newly discovered properties and improved computational methods.

4.1 Manipulability Matrix and Manipulability Indexes

Let us consider a formation control scenario, which is similar to the example in Section 1.2.1, except that there are leaders whose movements are controlled exogenously. Let $(\mathcal{V}, \mathbf{p}, K, \mathcal{L})$ denote the leader-follower network, and $\mathbf{q}_i$ the displacement of vertex i from its original position $\mathbf{p}_i$. Suppose that the leaders positions are changed from $\mathbf{p}_\ell$ to $\mathbf{p}_\ell + \mathbf{q}_\ell$ and that $\mathbf{q}_\ell$ is very small, then the dynamics of the followers under the control law (1.2) becomes

$$\begin{cases} \dot{\mathbf{q}}_f = -S_{ff}\mathbf{q}_f - S_{f\ell}\mathbf{q}_\ell, \\ \dot{\mathbf{q}}_\ell = \mathbf{0}. \end{cases} \tag{4.1}$$

Assume that the dynamics start from zero initial state, i.e. $\mathbf{q}_f(t_0) = \mathbf{0}$. Then, using the final value theorem [48], we have

$$\begin{aligned} \mathbf{q}_f(\infty) \triangleq \lim_{t\to+\infty} \mathbf{q}_f(t) &= \lim_{s\to 0} s\left(sI + S_{ff}\right)^{-1}\left(-S_{f\ell}\right)\frac{\mathbf{q}_\ell}{s} \\ &= -\lim_{s\to 0}\left(sI + S_{ff}\right)^{-1} S_{f\ell}\mathbf{q}_\ell \\ &= -S_{ff}^{\dagger} S_{f\ell}\mathbf{q}_\ell, \end{aligned}$$

where the last equality follows from the fact that S_{ff} is symmetric and that $\mathrm{null}(S_{ff}) \perp \mathrm{colsp}(S_{f\ell})$ according to (2.9). The amount of "energy" transferred from the leaders to the followers can be formulated using the Rayleigh quotient:

$$m = \frac{\mathbf{q}_f(\infty)^\top \mathbf{q}_f(\infty)}{\mathbf{q}_\ell^\top \mathbf{q}_\ell} = \frac{\mathbf{q}_\ell^\top \left(S_{f\ell}^\top S_{ff}^\dagger S_{ff}^\dagger S_{f\ell} \right) \mathbf{q}_\ell}{\mathbf{q}_\ell^\top \mathbf{q}_\ell} \triangleq \frac{\mathbf{q}_\ell^\top M \mathbf{q}_\ell}{\mathbf{q}_\ell^\top \mathbf{q}_\ell}, \tag{4.2}$$

where $M \triangleq S_{f\ell}^\top S_{ff}^\dagger S_{ff}^\dagger S_{f\ell}$ is called the *manipulability matrix* of the leader-follower formation.

Based on the manipulability matrix, we define the *manipulability indexes* as follows.

Definition 4.1.1 (Manipulability Indexes) *The* minimum*,* maximum *and* mean manipulability indexes*, denoted by $m_{\min}, m_{\max}, \bar{m}$ respectively, are defined as*

$$m_{\min} \triangleq \lambda_{\min}(M), \qquad m_{\max} \triangleq \lambda_{\max}(M), \qquad \bar{m} \triangleq \frac{1}{2|\mathcal{L}|}\mathrm{tr}(M).$$

4.1.1 An Alternative Formulation

The manipulability matrix can be derived alternatively from the perspective of real-time optimization. Suppose the leader-follower formation $(\mathcal{V}, \mathbf{p}, K, \mathcal{L})$ reaches an equilibrium state at time t_0, that is, the global edge-tension energy as defined in (1.1) is locally minimized:

$$\mathbf{p}_f(t_0) = \arg\min_{\mathbf{p}_f} F(\mathbf{p}_f, \mathbf{p}_\ell(t_0)).^1$$

As a result,

$$\frac{\partial F(\mathbf{p}_f(t_0), \mathbf{p}_\ell(t_0))}{\partial \mathbf{p}_f} = 0. \tag{4.3}$$

Note that only the followers have the freedom to decide their locations autonomously. Now if we assume that in a small amount of time δt, the leaders move from $\mathbf{p}_\ell(t_0)$ to $\mathbf{p}_\ell(t_0) + \delta \mathbf{p}_\ell$,

[1] Here the equality is a little abuse of notation since there could be many local minima for the edge-tension energy function. We can consider any one of them.

and the followers reached the new equilibrium state instantaneously[2], then using Taylor expansion at point $(\mathbf{p}_f(t_0), \mathbf{p}_\ell(t_0))$ and (2.6),

$$\begin{aligned} &F\left(\mathbf{p}_f(t_0+\delta t), \mathbf{p}_\ell(t_0+\delta t)\right) = \\ &\quad F\left(\mathbf{p}_f(t_0), \mathbf{p}_\ell(t_0)\right) + \frac{\partial F\left(\mathbf{p}_f(t_0), \mathbf{p}_\ell(t_0)\right)}{\partial \mathbf{p}_f}\delta\mathbf{p}_f + \frac{\partial F\left(\mathbf{p}_f(t_0), \mathbf{p}_\ell(t_0)\right)}{\partial \mathbf{p}_\ell}\delta\mathbf{p}_\ell \\ &\quad + \frac{1}{2}\left(\delta\mathbf{p}_f^\top S_{ff}\delta\mathbf{p}_f + 2\cdot\delta\mathbf{p}_f^\top S_{f\ell}\delta\mathbf{p}_\ell + \delta\mathbf{p}_\ell^\top S_{\ell\ell}\delta\mathbf{p}_\ell\right) + \text{h.o.t.} \end{aligned}$$

where $S_{ff}, S_{f\ell}$ and $S_{\ell\ell}$ are parts of the stiffness matrix S correspond to the leader-follower formation at time t_0.

Since we assume that at time $t_0 + \delta t$ the formation reaches another equilibrium state, the edge-tension energy is again minimized. Hence,

$$\begin{aligned} \frac{\partial F\left(\mathbf{p}_f(t_0), \mathbf{p}_\ell(t_0)\right)}{\partial(\delta\mathbf{p}_f)} &= \frac{\partial F\left(\mathbf{p}_f(t_0), \mathbf{p}_\ell(t_0)\right)}{\partial \mathbf{p}_f} + \delta\mathbf{p}_f^\top S_{ff} + \delta\mathbf{p}_\ell^\top S_{f\ell}^\top + \text{h.o.t.} \\ &= \delta\mathbf{p}_f^\top S_{ff} + \delta\mathbf{p}_\ell^\top S_{f\ell}^\top + \text{h.o.t.} = 0 \end{aligned} \tag{4.4}$$

We derive the instantaneous velocities by dividing both sides in (4.4) by δt and taking the limit $\delta t \downarrow 0$, which yields

$$S_{ff}(t)\dot{\mathbf{p}}_f(t) + S_{f\ell}(t)\dot{\mathbf{p}}_\ell(t) = 0. \tag{4.5}$$

We hereby substitute t_0 with t to emphasize that this relation holds for every time instant t, and that the parameters S_{ff} and $S_{f\ell}$ are time-variant. If S_{ff} is nonsingular, then without ambiguity

$$\dot{\mathbf{p}}_f(t) = -S_{ff}^{-1}(t)S_{f\ell}(t)\dot{\mathbf{p}}_\ell(t). \tag{4.6}$$

If S_{ff} is singular, then the possible instantaneous velocities $\dot{\mathbf{p}}_f$ at time t form a nontrivial affine subspace. The solution having the least norm is given by the Moore-Penrose pseudoinverse as follows

$$\dot{\mathbf{p}}_f(t) = -S_{ff}^{\dagger}(t)S_{f\ell}(t)\dot{\mathbf{p}}_\ell(t), \tag{4.7}$$

which gives a solution whose projected components in the null space of S_{ff} are all zero. From the perspective of physics, the vertices can be regarded as having no inertia, as they

[2]This assumption is similar to letting $s \to \infty$ for the rigid-link approximation proposed in [30].

will not drift at a nonzero speed within the null space of S_{ff} (equivalently, $\mathrm{null}(R_f)$). This formulation is consistent with the rigid-link approximation proposed in [30]. Since for nonsingular S_{ff}, we have $S_{ff}^{-1} = S_{ff}^{\dagger}$, the two cases in (4.6) and (4.7) can be consolidated into (4.7), which gives rise to the same expression of the manipulability matrix as in (4.2).

4.2 Properties of Manipulability Matrix

Proposition 4.2.1 *The manipulability indexes $M(K, \mathbf{p})$ possess the following properties:*

1) *(**Nonnegative Definiteness**) $M \succeq 0$. Furthermore, $M = O$ if and only if there exists no edge between $\mathcal{L}$ and $\mathcal{F}$.*

2) *(**Scale Invariance**) $M(K, \mathbf{p}) = M(\beta K, \gamma \mathbf{p}),\ \forall\, \beta, \gamma \in \mathbb{R}_+$.*

3) *(**Translation Invariance**) $M(K, \mathbf{p}) = M(K, \mathbf{p} \oplus \mathbf{w}),\ \forall\, \mathbf{w} \in \mathbb{R}^2$, where*

$$\mathbf{p} \oplus \mathbf{w} \triangleq \left[(\mathbf{p}_1 + \mathbf{w})^\top \ \cdots \ (\mathbf{p}_n + \mathbf{w})^\top\right]^\top.$$

4) *(**Rotation/Reflection Invariance**) For any orthogonal matrix $Q \in \mathbb{O}_2 \triangleq \{Q \in \mathbb{R}^{2\times 2} : QQ^\top = I\}$, denote $Q \odot \mathbf{p} \triangleq \left[(Q\mathbf{p}_1)^\top \ \cdots \ (Q\mathbf{p}_n)^\top\right]^\top$. Then,*

$$M(K, Q \odot \mathbf{p}) = (I_n \otimes Q) M(K, \mathbf{p}) (I_n \otimes Q)^\top,$$

where $\otimes$ denotes the Kronecker product of matrices.

Proof Properties 2)–4) are direct results of Proposition 2.3.1. We now prove the latter part of the nonnegative definiteness property.

If there exists no edge between $\mathcal{L}$ and $\mathcal{F}$, that is, $k_{ij} = 0,\ \forall\, i \in \mathcal{L}, j \in \mathcal{F}$, then $S_{f\ell} = O \ \Rightarrow\ M = O$.

Conversely, $M = O$ implies that $S_{ff}^{\dagger} S_{f\ell} = O$. Thus, $\mathrm{colsp}(S_{f\ell}) \subseteq \mathrm{null}(S_{ff}^{\dagger}) = \mathrm{null}(S_{ff})$, or $S_{ff} S_{f\ell} = O$. According to (2.4), if there is a nonzero 2-by-2 block in the j-th block-row of $S_{f\ell}$, then the (j, j)-th block of S_{ff} is also nonzero, thus the product $S_{ff} S_{f\ell}$. Therefore, $S_{ff} S_{f\ell} = O$ holds only if all the blocks in $S_{f\ell}$ is zero, indicating that there exists no edge between the leaders $\mathcal{L}$ and the followers $\mathcal{F}$. ■

Lemma 4.2.1 *$S_{ff}^\dagger S_{f\ell} = R_f^\dagger R_\ell$ for any leader-follower formation $(\mathcal{V}, \mathbf{p}, K, \mathcal{L})$.*

Proof Recalling from (2.8) and using Moore-Penrose pseudoinverse identities [49],

$$S_{ff}^\dagger S_{f\ell} = \left(R_f^\top R_f\right)^\dagger R_f^\top R_\ell = R_f^\dagger \left(R_f^\top\right)^\dagger R_f^\top R_\ell = R_f^\dagger R_\ell, \tag{4.8}$$

which is the desired conclusion. ■

Remark 4.2.1 *As a result of Lemma 4.2.1, $M = R_\ell^\top R_f^{\dagger\top} R_f^\dagger R_\ell$ is an equivalent expression of the manipulability matrix.*

The main nontrivial property of the manipulability matrix is the following theorem, which states that for loose formations, the manipulability matrix M only depends the topology given by $\mathcal{E}(K)$, not the relative nonzero values of k_{ij}. The sufficiency part of the following result was previously proposed in [30, Theorem 5.1].

Theorem 4.2.1 *Given the vertex set $\mathcal{V}$, leader set $\mathcal{L}$ and configuration $\mathbf{p}$, for all the leader-follower formations sharing the same set of edges, i.e., $\mathcal{E}(K) \triangleq \{(i,j) : k_{ij} > 0\}$, the quantity $R_f^\dagger R_\ell$, is invariant if and only if the formations are loose (i.e., $\operatorname{rank}(R_f) = \operatorname{rank}(R)$.*

Proof First we note that by Remark 2.5.1, all such leader-follower formations share the same looseness property. Therefore, the proposition is well-defined.

By the definitions of rigidity matrices, $R_f = \Lambda_K^{\frac{1}{2}} \bar{R}_f$ and $R_\ell = \Lambda_K^{\frac{1}{2}} \bar{R}_\ell$. Without causing confusion, we hereby assume that the zero diagonal entries in Λ_K and the corresponding rows in $\bar{R}_f$ and $\bar{R}_\ell$ are already removed, so that only those rows corresponding to the elements in $\mathcal{E}(K)$ are retained. Hence Λ_K is positive definite.

First we prove sufficiency and assume $\operatorname{rank}(R_f) = \operatorname{rank}(R)$. Observe the equation $R_f X = R_\ell$ has at least one solution under this assumption, and so does $\bar{R}_f X = \bar{R}_\ell$ by left-multiplying $\Lambda_K^{-\frac{1}{2}}$ (a positive definite matrix) on both sides. Note that, by the property of Moore-Penrose pseudoinverse, $R_f^\dagger R_\ell$ and $\bar{R}_f^\dagger \bar{R}_\ell$ can be regarded as the unique optimal solutions to the following problems, respectively:

$$\begin{array}{ll} \underset{X}{\text{minimize}} & \|X\|_F \\ \text{subject to} & R_f X = R_\ell, \end{array} \quad \text{and} \quad \begin{array}{ll} \underset{X}{\text{minimize}} & \|X\|_F \\ \text{subject to} & \bar{R}_f X = \bar{R}_\ell, \end{array}$$

which are identical problems and hence the unique solutions must coincide.

For necessity, assume $\mathrm{rank}(R_f) < \mathrm{rank}(R)$, then $R_f X = R_\ell$ admits no solution, and $R_f^\dagger R_\ell$ is the least-square solution, i.e., the solution of the following problem,

$$\underset{X}{\text{minimize}} \quad \|\Lambda_K^{\frac{1}{2}} \left(\bar{R}_f X - \bar{R}_\ell\right) \|_F$$

The first-order necessary condition of the above optimization implies

$$\bar{R}_f^\top \Lambda_K \left(\bar{R}_f X^* - \bar{R}_\ell\right) = O. \tag{4.9}$$

Suppose that given $\bar{R}_f$ and $\bar{R}_\ell$, (4.9) holds for arbitrary positive definite diagonal matrix Λ_K. Rewriting (4.9) by decomposing both $\bar{R}_f$ and $\bar{R}_\ell$ into rows, denoted by $\bar{\mathbf{r}}_{ij,f}^\top$ and $\bar{\mathbf{r}}_{ij,\ell}^\top$ respectively , we have

$$\begin{aligned}
& \sum_{(i,j)\in\mathcal{E}(K)} k_{ij} \bar{\mathbf{r}}_{ij,f} \left(\bar{\mathbf{r}}_{ij,f}^\top X^* - \bar{\mathbf{r}}_{ij,\ell}^\top\right) = O, \text{ with arbitrary } k_{ij} > 0. \\
\Leftrightarrow \quad & \bar{\mathbf{r}}_{ij,f} \left(\bar{\mathbf{r}}_{ij,f}^\top X^* - \bar{\mathbf{r}}_{ij,\ell}^\top\right) = O, \ \forall (i,j) \in \mathcal{E}(K). \\
\Leftrightarrow \quad & \bar{\mathbf{r}}_{ij,f}^\top X^* - \bar{\mathbf{r}}_{ij,\ell}^\top = O, \ \forall (i,j) \in \mathcal{E}(K). \\
\Leftrightarrow \quad & \bar{R}_f X^* = \bar{R}_\ell
\end{aligned}$$

which is an obvious contradiction. Thus, $R_f^\dagger R_\ell$ cannot be invariant. ■

Remark 4.2.2 *By Lemma 4.2.1, the invariance of the quantity $S_{ff}^\dagger S_{f\ell}$ and the manipulability matrix M depends on exactly the same condition described in Theorem 4.2.1.*

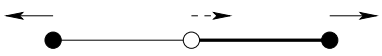

Fig. 4.1.: Scenario where the distance constraint is about to be violated

Fig. 4.1 gives an example of a tight leader-follower formation, where $R_f^\dagger R_\ell$ depends on not only the binary topology but also the connectivity coefficients. The two black dots represent the leaders, moving away from each other at the same speed, while the white dot in the middle represents the follower. Let the connectivity coefficient for the bolder edge in

the figure be denoted by k_1 and for the other edge k_2, and suppose $k_1 > k_2$. It can be seen intuitively that the follower will move toward right, because otherwise the edge-tension energy would increase more. This shows that the movement of the followers in a tight leader-follower formation depend on the relative values of the connectivity coefficients.

4.3 Properties of Manipulability Indexes

In this section, we discuss some notable properties of the manipulability indexes defined in the previous section. For commonly held properties, the generic notation $m(K, \mathbf{p})$ is used to indicate all three indexes, namely $m_{\min}, m_{\max}$ and $\bar{m}$. Throughout the section we assume there is an underlying leader-follower formation $(\mathcal{V}, \mathbf{p}, K, \mathcal{L})$.

Proposition 4.3.1 *The manipulability indexes $m(K, \mathbf{p})$ possess the following properties:*

*1) (**Nonnegativeness**) $m(K, \mathbf{p}) \geq 0$. Further, $m_{\max}(K, \mathbf{p}) = 0$ or $\bar{m}(K, \mathbf{p}) = 0$ if and only if there exists no edge between $\mathcal{L}$ and $\mathcal{F}$.*

*2) (**Scale Invariance**) $m(K, \mathbf{p}) = m(\alpha K, \mathbf{p}),\ \forall\, \alpha \in \mathbb{R}_+$.*

*3) (**Similarity Invariance**) $\mathbf{p} \sim \mathbf{p}' \ \Rightarrow\ m(K, \mathbf{p}) = m(K, \mathbf{p}')$*

Proof These properties directly result from Proposition 4.2.1. ■

Proposition 4.3.2 *The following statements are equivalent:*

1) $m_{\min} > 0$;

2) $S_{f\ell}$ has full column rank;

3) R_ℓ has full column rank and $\mathrm{colsp}(R_\ell) \cap \mathrm{colsp}(R_f)^\perp = \{\mathbf{0}\}$;

4) No leader lies on the same line with all its follower-neighbors.

Proof 1) $\Leftrightarrow$ 2): Since $\mathrm{rowsp}(R_f^\dagger) = \mathrm{rowsp}(R_f^\top)$ by property of Moore-Penrose pseudoinverse [49], there exists $V \in GL(2|\mathcal{F}|, \mathbb{R})$ such that $R_f^\dagger = V R_f^\top$. Therefore,

$$\begin{aligned} m_{\min} > 0 \ &\Leftrightarrow\ \mathrm{rank}(R_f^\dagger R_\ell) = 2|\mathcal{L}| \ \Leftrightarrow\ \mathrm{rank}(V R_f^\top R_\ell) = \mathrm{rank}(V S_{f\ell}) = 2|\mathcal{L}| \\ &\Leftrightarrow\ \mathrm{rank}(S_{f\ell}) = 2|\mathcal{L}|. \end{aligned}$$

2) $\Leftrightarrow$ 4): Recalling the structure of $S_{f\ell}$ as defined in (2.4) and (2.9), it can be easily seen that the column rank becomes deficient if and only if all the projection matrices P_{ij} with $k_{ij} > 0$ in a block-column of $S_{f\ell}$ are identical, which indicates that the edges connecting that leader and all its neighbors in the follower set are collinear (or in more trivial cases, there is only one or no edge connecting a follower and that leader).

2) $\Leftrightarrow$ 3): $S_{f\ell}$ having full column rank is equivalent to the following statement by definition of linear independence:

$$R_f^\top R_\ell \mathbf{u} = \mathbf{0} \;\leftrightarrow\; \mathbf{u} = \mathbf{0}.$$

The above statement is true if and only if both of the following holds true:

a) R_ℓ has full column rank;

b) $\mathrm{colsp}(R_\ell) \cap \mathrm{null}(R_f^\top) = \{\mathbf{0}\}$.

Since $\mathrm{null}(R_f^\top) = \mathrm{colsp}(R_f)^\perp$, this concludes the proof. ■

Proposition 4.3.3 *The minimum manipulability $m_{\min}$ is upper bounded by $\frac{|\mathcal{F}|}{|\mathcal{L}|}$.*

Proof For any $\mathbf{u} \in \mathbb{R}^2 \setminus \{\mathbf{0}\}$, we have $R\left(\mathbf{1}_n \otimes \mathbf{u}\right) = \mathbf{0}$, or equivalently,

$$R_f\left(\mathbf{1}_{|\mathcal{F}|} \otimes \mathbf{u}\right) = -R_\ell\left(\mathbf{1}_{|\mathcal{L}|} \otimes \mathbf{u}\right).$$

From the above equation, we see that $R_f\mathbf{x} = -R_\ell\left(\mathbf{1}_{|\mathcal{L}|} \otimes \mathbf{u}\right)$ has at least one solution, hence by property of Moore-Penrose pseudoinverse [49], $\mathbf{x}^* = -R_f^\dagger R_\ell\left(\mathbf{1}_{|\mathcal{L}|} \otimes \mathbf{u}\right)$ is the solution having the minimum Euclidean norm. Therefore, $\|\mathbf{x}^*\| \leq \|\mathbf{1}_{|\mathcal{F}|} \otimes \mathbf{u}\|$. Now,

$$\begin{aligned} m_{\min} &= \min_{\mathbf{q} \in \mathbb{R}^{2|\mathcal{L}|} \setminus \{\mathbf{0}\}} \frac{\mathbf{q}^\top R_\ell^\top R_f^{\dagger\top} R_f^\dagger R_\ell \mathbf{q}}{\mathbf{q}^\top \mathbf{q}} \\ &\leq \frac{\left(\mathbf{1}_{|\mathcal{L}|} \otimes \mathbf{u}\right)^\top R_\ell^\top R_f^{\dagger\top} R_f^\dagger R_\ell \left(\mathbf{1}_{|\mathcal{L}|} \otimes \mathbf{u}\right)}{\left(\mathbf{1}_{|\mathcal{L}|} \otimes \mathbf{u}\right)^\top \left(\mathbf{1}_{|\mathcal{L}|} \otimes \mathbf{u}\right)} \\ &\leq \frac{\left(\mathbf{1}_{|\mathcal{F}|} \otimes \mathbf{u}\right)^\top \left(\mathbf{1}_{|\mathcal{F}|} \otimes \mathbf{u}\right)}{\left(\mathbf{1}_{|\mathcal{L}|} \otimes \mathbf{u}\right)^\top \left(\mathbf{1}_{|\mathcal{L}|} \otimes \mathbf{u}\right)} = \frac{|\mathcal{F}|}{|\mathcal{L}|}, \end{aligned}$$

which concludes the proof. ■

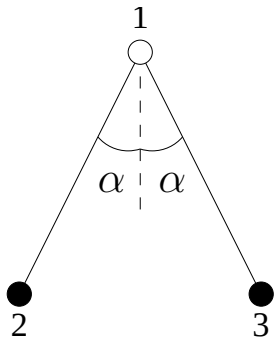

Fig. 4.2.: Example of a leader-follower formation whose maximum and mean manipulability indexes are potentially unbounded

Remark 4.3.1 *In general, there does not an upper bound in terms of $K, |\mathcal{F}|$ and $|\mathcal{L}|$ for either $m_{\max}$ or $\bar{m}$. To see this, consider a three-vertex formation with two leaders as illustrated in Fig. 4.2. We can explicitly write the rigidity matrix of the leader-follower formation as below,*

$$\left[\begin{array}{c|c} R_f & R_\ell \end{array}\right] = \left[\begin{array}{cc|cccc} -\sin\alpha & -\cos\alpha & \sin\alpha & \cos\alpha & 0 & 0 \\ \sin\alpha & -\cos\alpha & 0 & 0 & -\sin\alpha & \cos\alpha \end{array}\right].$$

Therefore,

$$\begin{aligned} R_f^\dagger R_\ell &= R_f^{-1} R_\ell \\ &= \begin{bmatrix} -\frac{1}{2\sin\alpha} & \frac{1}{2\sin\alpha} \\ -\frac{1}{2\cos\alpha} & -\frac{1}{2\cos\alpha} \end{bmatrix} \begin{bmatrix} \sin\alpha & \cos\alpha & 0 & 0 \\ 0 & 0 & -\sin\alpha & \cos\alpha \end{bmatrix} \\ &= -\frac{1}{2} \begin{bmatrix} 1 & \cot\alpha & 1 & -\cot\alpha \\ \tan\alpha & 1 & -\tan\alpha & 1 \end{bmatrix}, \\ m_{\max} &= \lambda_{\max}\left(R_\ell^\top R_f^{\dagger\top} R_f^\dagger R_\ell\right) = \lambda_{\max}\left(R_f^\dagger R_\ell R_\ell^\top R_f^{\dagger\top}\right) \\ &= \lambda_{\max}\left(\frac{1}{2}\begin{bmatrix} \frac{1}{\sin^2\alpha} & 0 \\ 0 & \frac{1}{\cos^2\alpha} \end{bmatrix}\right) = \max\left\{\frac{1}{2\sin^2\alpha}, \frac{1}{2\cos^2\alpha}\right\}. \end{aligned}$$

The maximum manipulability index $m_{\max}$ is unbounded as $\alpha \to 0$ or $\frac{\pi}{2}$, and so it is with the mean manipulability index $\bar{m}$.

4.4 Manipulability Indexes of Single-leader Rigid Formations

Definition 4.4.1 *The* centroid *of a formation* $(\mathcal{V}, \mathbf{p}, K)$ *or a leader-follower formation* $(\mathcal{V}, \mathbf{p}, K, \mathcal{L})$*, denoted by* $\mathbf{p}_\odot$*, is defined as*

$$\mathbf{p}_\odot \triangleq \frac{1}{n}\sum_{j\in\mathcal{V}} \mathbf{p}_j.$$

The torque ratio*, denoted by* τ*, is defined as*

$$\tau \triangleq \frac{\sum_{i\in\mathcal{L}} \|\mathbf{p}_i - \mathbf{p}_\odot\|^2}{\sum_{j\in\mathcal{V}} \|\mathbf{p}_j - \mathbf{p}_\odot\|^2},$$

particularly, the torque ratio τ *is zero for leaderless formations.*

Proposition 4.4.1 *Given leader-follower formation* $(\mathcal{V}, \mathbf{p}, K, \mathcal{L})$*, if formation* $(\mathcal{V}, \mathbf{p}, K)$ *is rigid and* $|\mathcal{L}| = 1$*, then*

1) $m_{\max} = |\mathcal{F}| = n - 1$*;*

2) $m_{\min} = \frac{n}{n\tau+1} - 1$*, where* τ *is the torque ratio.*

Proof For the case where $|\mathcal{L}| = 1$ and the formation is rigid, the rigidity matrix R can be partitioned as $R = [R_f \ R_\ell]$, where $R_f \in \mathbb{R}^{m\times 2n-2}$ and $R_\ell \in \mathbb{R}^{m\times 2}$. Apply the singular value decomposition on R and remove all the degenerate rows and columns, we can get

$$R = \underbrace{U}_{m\times 2n-3} \quad \underbrace{\Sigma}_{2n-3\times 2n-3} \quad \underbrace{V^\top}_{2n-3\times 2n} = U\Sigma \begin{bmatrix} V_f^\top & V_\ell^\top \end{bmatrix} = \tilde{U} \begin{bmatrix} V_f^\top & V_\ell^\top \end{bmatrix},$$

where $\tilde{U} = U\Sigma$ and Σ is a positive definite diagonal matrix. By unitarity,

$$V^\top V = V_f^\top V_f + V_\ell^\top V_\ell = I_{2n-3}.$$

Notice that for the $|\mathcal{L}| = 1$ case, $\mathrm{rank}(R_f) = \mathrm{rank}(R) = 2n - 3$ by Corollary 2.5.2. Therefore $R_f = \tilde{U}V_f^\top$ is a full-rank decomposition, which implies that

$$R_f^\dagger = V_f(V_f^\top V_f)^{-1}(\tilde{U}^\top \tilde{U})^{-1}\tilde{U}^\top.$$

Hence,

$$\begin{aligned}
-R_f^\dagger R_\ell &= -V_f(V_f^\top V_f)^{-1}(\tilde{U}^\top\tilde{U})^{-1}\tilde{U}^\top\tilde{U}V_\ell^\top \\
&= -V_f(V_f^\top V_f)^{-1}V_\ell^\top \\
&= -V_f\left(I_{2n-3} - V_\ell^\top V_\ell\right)^{-1}V_\ell^\top \\
&= -V_f\left(I_{2n-3} + V_\ell^\top\left(I_2 - V_\ell V_\ell^\top\right)^{-1}V_\ell\right)V_\ell^\top \\
&= -V_fV_\ell^\top - V_fV_\ell^\top\left(I_2 - V_\ell V_\ell^\top\right)^{-1}\left(V_\ell V_\ell^\top - I_2\right) - V_fV_\ell^\top\left(I_2 - V_\ell V_\ell^\top\right)^{-1} \\
&= -V_fV_\ell^\top\left(I_2 - V_\ell V_\ell^\top\right)^{-1} \qquad (4.10)
\end{aligned}$$

Recall that $\mathrm{colsp}(V)\oplus\mathrm{iso}_n(\mathbf{p}) = \mathbb{R}^{2n}$ (the vector space). Let $\mathbf{x},\mathbf{y},\mathbf{r}$ denote the vectors corresponding to x-translation, y-translation and simultaneous rotation, respectively, with proper scaling such that the following unitarity equation holds,

$$\begin{bmatrix} V_f^\top & V_\ell^\top \\ \mathbf{x}_f^\top & \mathbf{x}_\ell^\top \\ \mathbf{y}_f^\top & \mathbf{y}_\ell^\top \\ \mathbf{r}_f^\top & \mathbf{r}_\ell^\top \end{bmatrix}\begin{bmatrix} V_f & \mathbf{x}_f & \mathbf{y}_f & \mathbf{r}_f \\ V_\ell & \mathbf{x}_\ell & \mathbf{y}_\ell & \mathbf{r}_\ell \end{bmatrix} = I_{2n} \quad\Leftrightarrow\quad \begin{bmatrix} V_f & \mathbf{x}_f & \mathbf{y}_f & \mathbf{r}_f \\ V_\ell & \mathbf{x}_\ell & \mathbf{y}_\ell & \mathbf{r}_\ell \end{bmatrix}\begin{bmatrix} V_f^\top & V_\ell^\top \\ \mathbf{x}_f^\top & \mathbf{x}_\ell^\top \\ \mathbf{y}_f^\top & \mathbf{y}_\ell^\top \\ \mathbf{r}_f^\top & \mathbf{r}_\ell^\top \end{bmatrix} = I_{2n}. \qquad (4.11)$$

The above equations yields

$$\begin{aligned}
V_fV_\ell^\top &= -\mathbf{x}_f\mathbf{x}_\ell^\top - \mathbf{y}_f\mathbf{y}_\ell^\top - \mathbf{r}_f\mathbf{r}_\ell^\top, \\
V_\ell V_\ell^\top &= I_2 - \mathbf{x}_\ell\mathbf{x}_\ell^\top - \mathbf{y}_\ell\mathbf{y}_\ell^\top - \mathbf{r}_\ell\mathbf{r}_\ell^\top.
\end{aligned}$$

Plugging these into (4.10), we have

$$-R_f^\dagger R_\ell = \left(\mathbf{x}_f\mathbf{x}_\ell^\top + \mathbf{y}_f\mathbf{y}_\ell^\top + \mathbf{r}_f\mathbf{r}_\ell^\top\right)\underbrace{\left(\mathbf{x}_\ell\mathbf{x}_\ell^\top + \mathbf{y}_\ell\mathbf{y}_\ell^\top + \mathbf{r}_\ell\mathbf{r}_\ell^\top\right)^{-1}}_{\triangleq W \text{ symmetric}}.$$

We compute the manipulability matrix M using the relations established in (4.11),

$$\begin{aligned}
M = R_\ell^\top R_f^{\dagger\top} R_f^\dagger R_\ell &= W\left(\mathbf{x}_\ell\mathbf{x}_f^\top + \mathbf{y}_\ell\mathbf{y}_f^\top + \mathbf{r}_\ell\mathbf{r}_f^\top\right)\left(\mathbf{x}_f\mathbf{x}_\ell^\top + \mathbf{y}_f\mathbf{y}_\ell^\top + \mathbf{r}_f\mathbf{r}_\ell^\top\right)W \\
&= W\left(\mathbf{x}_\ell\mathbf{x}_f^\top\mathbf{x}_f\mathbf{x}_\ell^\top + \mathbf{x}_\ell\mathbf{x}_f^\top\mathbf{y}_f\mathbf{y}_\ell^\top + \mathbf{x}_\ell\mathbf{x}_f^\top\mathbf{r}_f\mathbf{r}_\ell^\top + \mathbf{y}_\ell\mathbf{y}_f^\top\mathbf{x}_f\mathbf{x}_\ell^\top + \mathbf{y}_\ell\mathbf{y}_f^\top\mathbf{y}_f\mathbf{y}_\ell^\top + \right. \\
&\qquad \left. \mathbf{y}_\ell\mathbf{y}_f^\top\mathbf{r}_f\mathbf{r}_\ell^\top + \mathbf{r}_\ell\mathbf{r}_f^\top\mathbf{x}_f\mathbf{x}_\ell^\top + \mathbf{r}_\ell\mathbf{r}_f^\top\mathbf{y}_f\mathbf{y}_\ell^\top + \mathbf{r}_\ell\mathbf{r}_f^\top\mathbf{r}_f\mathbf{r}_\ell^\top\right)W \\
&= W\left(\mathbf{x}_\ell\left(1-\mathbf{x}_\ell^\top\mathbf{x}_\ell\right)\mathbf{x}_\ell^\top + \mathbf{x}_\ell\cdot 0\cdot\mathbf{y}_\ell^\top + \mathbf{x}_\ell\left(-\mathbf{x}_\ell^\top\mathbf{r}_\ell\right)\mathbf{r}_\ell^\top + \mathbf{y}_\ell\cdot 0\cdot\mathbf{x}_\ell^\top + \right. \\
&\qquad \mathbf{y}_\ell\left(1-\mathbf{y}_\ell^\top\mathbf{y}_\ell\right)\mathbf{y}_\ell^\top + \mathbf{y}_\ell\left(-\mathbf{y}_\ell^\top\mathbf{r}_\ell\right)\mathbf{r}_\ell^\top + \mathbf{r}_\ell\left(-\mathbf{r}_\ell^\top\mathbf{x}_\ell\right)\mathbf{x}_\ell^\top + \mathbf{r}_\ell\left(-\mathbf{r}_\ell^\top\mathbf{y}_\ell\right)\mathbf{y}_\ell^\top + \\
&\qquad \left.\mathbf{r}_\ell\left(1-\mathbf{r}_\ell^\top\mathbf{r}_\ell\right)\mathbf{r}_\ell^\top\right)W. \qquad (4.12)
\end{aligned}$$

Finally, observing the following identities,

$$\mathbf{x}_\ell^\top\mathbf{x}_\ell = \mathbf{y}_\ell^\top\mathbf{y}_\ell = \frac{1}{n}, \quad \mathbf{x}_\ell\mathbf{x}_\ell^\top + \mathbf{y}_\ell\mathbf{y}_\ell^\top = \frac{1}{n}I_2,$$

and also the following according to Woodbury Matrix Identity [45],

$$W = \left(\frac{1}{n}I_2 + \mathbf{r}_\ell\mathbf{r}_\ell^\top\right)^{-1} = n\cdot I_2 - \frac{n^2\mathbf{r}_\ell\mathbf{r}_\ell^\top}{1+n\mathbf{r}_\ell^\top\mathbf{r}_\ell}$$

Equation (4.12) can be simplified as below,

$$\begin{aligned}
M &= W\left(\frac{n-1}{n^2}I_2 + \left(1-\frac{2}{n}\right)\mathbf{r}_\ell\mathbf{r}_\ell^\top - \mathbf{r}_\ell\mathbf{r}_\ell^\top\mathbf{r}_\ell\mathbf{r}_\ell^\top\right)W \\
&= (n-1)I_2 - \frac{n^2r^2}{1+nr^2}P_{\mathbf{r}_\ell}, \qquad (4.13)
\end{aligned}$$

where

$$r^2 \triangleq \mathbf{r}_\ell^\top\mathbf{r}_\ell, \quad P_{\mathbf{r}_\ell} \triangleq \frac{\mathbf{r}_\ell\mathbf{r}_\ell^\top}{\mathbf{r}_\ell^\top\mathbf{r}_\ell}.$$

Now recall that $\mathbf{r} \perp \mathbf{x}$ and $\mathbf{r} \perp \mathbf{y}$. It can be seen with some calculation that

$$\mathbf{r} = \beta\left(\mathbf{p} - \mathbf{1}_n \otimes \mathbf{p}_\odot\right),$$

where $\beta = \left(\sum_{j\in\mathcal{V}}\|\mathbf{p}_j - \mathbf{p}_\odot\|^2\right)^{-1}$ is the normalization coefficient. It is not difficult to verify that $\tau = r^2$ according to Definition 4.4.1. Therefore, the minimum and maximum manipulability indexes are

$$m_{\min} = (n-1) - \frac{n^2\tau}{1+n\tau} = \frac{n}{n\tau+1} - 1, \quad m_{\max} = n-1. \qquad (4.14)$$

This concludes the proof. ■

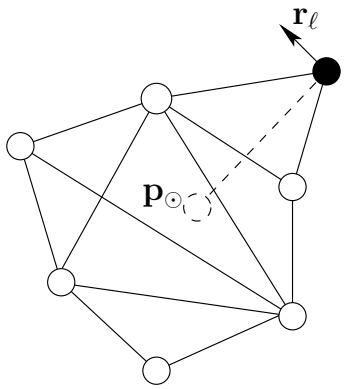

Fig. 4.3.: A single-leader rigid formation

Proposition 4.4.2 *For single-leader formations,* $0 \leq \tau \leq \dfrac{n-1}{n}$.

Proof By Proposition 4.3.1, the nonnegativeness property indicates that $m_{\min} = \frac{n}{n\tau+1} - 1 \geq 0$, which implies $\tau \leq \frac{n-1}{n}$. The other inequality is evident by Definition 4.4.1. Note that the inequalities hold even for nonrigid formations since the definition of τ is independent of K. ■

Theorem 4.4.1 *For the single leader case (*$|\mathcal{L}| = 1$*), the minimum manipulability of a rigid formation is maximized when the leader agent is located at the centroid of the formation.*

Proof Note that $m_{\min} \leq n - 1 = m_{\max}$, where the equality is attained when $\tau = 0$, which implies $\mathbf{p}_\ell = \mathbf{p}_\odot$. ■

Fig. 4.3 gives a single-leader rigid formation. The solid dot represents the leader and the dashed circle in the middle denotes the centroid of the formation. The minimum manipulability index, according to (4.13), corresponds to the leader's movement in $\mathbf{r}_\ell$ as plotted in Fig. 4.3. The maximum manipulability index corresponds to the movement of the leader along the direction from the leader to the centroid. Such movement will not result in any rotation of the formation; instead, all the followers will be pushed or pulled parallelly by the same displacement of the leader.

4.5 Manipulability Indexes of Single-leader Trailers

For a general nonrigid formation $(\mathcal{V}, \mathbf{p}, K)$, the manipulability index is usually found by first computing the manipulability matrix M and then analyze its spectrum. This process involves the computation of the Moore-Penrose pseudoinverse matrix $S_{ff}^{\dagger}$ (or $R_f^{\dagger}$). As the formation becomes larger in the number of followers, the computation of $S_{ff}^{\dagger}$ may encounter numerical stability issues, because the Moore-Penrose pseudoinverse operation is discontinuous at the set of rank-deficient matrices.

In this section, the computation of manipulability matrix and indexes for trailers as defined in Section 2.6 is discussed. A hierarchical recursive algorithm based on dynamic programming is proposed to compute these quantities in a fast and stable manner.

Trailers are nonrigid formations whose skeleton graph is a tree (Definition 2.6.4). In other words, the rigid components of a trailer do not form any loops. Therefore, it is possible to specify one of its rigid components as a "root" (denoted by $\mathcal{V}_0$) and build a hierarchical structure of the other rigid components by inspecting the corresponding rooted version of the skeleton graph. Rigid component $\mathcal{V}_1$ is called an *ancestor* of $\mathcal{V}_2$, denoted by $\mathcal{V}_1 \prec \mathcal{V}_2$, if $\mathcal{V}_1$ is an ancestor of $\mathcal{V}_2$ in the skeleton graph with root $\mathcal{V}_0$. Likewise, $\mathcal{V}_1$ is a *descendant* of $\mathcal{V}_2$, denoted by $\mathcal{V}_1 \succ \mathcal{V}_2$ if $\mathcal{V}_2 \prec \mathcal{V}_1$. If $V_2 \succ \mathcal{V}_1$ and $\mathcal{V}_1 \cap \mathcal{V}_2 \neq \emptyset$, then $\mathcal{V}_2$ is a *successor* of $\mathcal{V}_1$, and V_1 the *predecessor* of V_2. Note that in a trailer, a rigid component may have many successors, but can only have one predecessor (except for the root component which has no predecessor). The set of all successors of V_1 is denoted by $\mathrm{succ}(\mathcal{V}_2)$.

Given the trailer in Fig. 4.4, assume that rigid component $\mathcal{V}_1$ is the root, i.e., $\mathcal{V}_0 \triangleq \mathcal{V}_1$. We have $\mathcal{V}_1 \prec \mathcal{V}_i, i = \{2, \ldots, 8\}$, $\mathcal{V}_8 \prec \mathcal{V}_5$, $\mathcal{V}_6 \in \mathrm{succ}(\mathcal{V}_7)$, etc. However, $\mathcal{V}_8 \notin \mathrm{succ}(\mathcal{V}_5)$ (they are not adjacent) and $\mathcal{V}_3 \not\prec \mathcal{V}_4$. If we set $\mathcal{V}_3$ as the root, then $\mathcal{V}_3 \prec \mathcal{V}_4$.

Definition 4.5.1 (Subtrailer) *Given trailer $(\mathcal{V}, \mathbf{p}, K)$ with root $\mathcal{V}_0$, a* rigid subtrailer *from $\mathcal{V}' \in \mathcal{R}$ is the induced subformation of the union set of $\mathcal{V}'$ and all its successors.*

We use the notation $\mathcal{V}'_{\succeq}$ to denote the vertex set of the subtrailer from $\mathcal{V}'$. if the trailer has a single leader ℓ, then by default we assume that the rigid component containing ℓ is the root component. Each of its subtrailers is also assumed to have a single leader, which

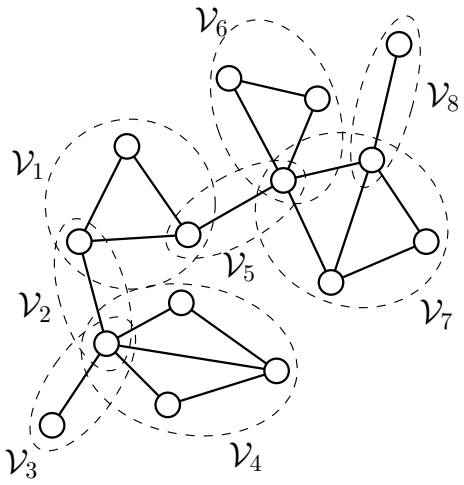

Fig. 4.4.: An example trailer

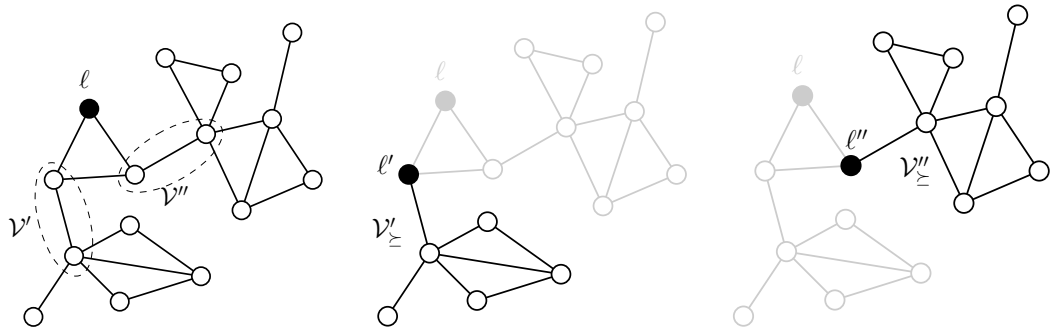

(a) Trailer (b) Subtrailer from $\mathcal{V}'$ (c) Subtrailer from $\mathcal{V}''$

Fig. 4.5.: Trailer and its subtrailers

is the pivot connecting it to its ancestors. The notation $\mathring{\mathcal{V}}$ denotes the subset of $\mathcal{V}$ excluding all leaders.

Fig. 4.5 illustrates the subtrailers of a single-leader trailer. Fig. 4.5(b) depicts the subtrailer from $\mathcal{V}'$, denoted by $\mathcal{V}'_{\succeq}$, and the connecting pivot ℓ' is also assigned to be the leader of $\mathcal{V}'_{\succeq}$. Fig. 4.5(c) depicts a different subtrailer from $\mathcal{V}''$, with the connecting pivot ℓ'' as its leader.

With the above notation setup, we now derive the formula for computing the manipulability matrix of a trailer with single leader ℓ. By property of Moore-Penrose pseudoinverse,

the quadratic form involving manipulability matrix M can be written in the form of an optimization problem as follows,

$$\mathbf{q}_\ell^\top M \mathbf{q}_\ell = \left\| -R_f^\dagger R_\ell \mathbf{q}_\ell \right\|^2 = \min \left\{ \|\mathbf{q}_f\|^2 : R_f \mathbf{q}_f + R_\ell \mathbf{q}_\ell = \mathbf{0} \right\}. \tag{4.15}$$

We can split the term $\|\mathbf{q}_f\|^2$ (which is in fact a sum) into the rigid component $\mathcal{V}_0$ and the subtrailers from its successors. Let $\mathbf{p}_{\mathcal{V}'}$ denote the components of $\mathbf{p}$ corresponding to the vertices in $\mathcal{V}'$. For each subtrailer $\mathcal{V}'_{\succeq}$ with $\mathcal{V}' \in \mathrm{succ}(\mathcal{V}_0)$, let ℓ' denote the connecting pivot. The optimization problem can be rewritten as

$$\underset{\mathbf{q}_i, i \in \mathcal{F}}{\text{minimize}} \quad \sum_{i \in \mathring{\mathcal{V}}_0} \|\mathbf{q}_i\|^2 + \sum_{\mathcal{V}' \in \mathrm{succ}(\mathcal{V}_0),\, j \in \mathring{\mathcal{V}}'_{\succeq}} \sum \|\mathbf{q}_j\|^2 \tag{4.16}$$

$$\text{subject to} \quad R_{\mathring{\mathcal{V}}_0} \mathbf{q}_{\mathring{\mathcal{V}}_0} + R_\ell \mathbf{q}_\ell = \mathbf{0} \tag{4.17}$$

$$R_{\mathring{\mathcal{V}}'_{\succeq}} \mathbf{q}_{\mathring{\mathcal{V}}'_{\succeq}} + R_{\ell'} \mathbf{q}_{\ell'} = \mathbf{0}, \forall\, \mathcal{V}' \in \mathrm{succ}(\mathcal{V}_0). \tag{4.18}$$

The first summation in (4.16) corresponds to the total movements in the root component $\mathcal{V}_0$. The double summation in the second part correspond to all the remaining subtrailers (excluding the connecting pivots to avoid double counting with the first summation). Likewise, the equality constraint (4.17) describes the movements of the vertices in $\mathcal{V}_0$ under the leading of ℓ. In (4.18), for each successor $\mathcal{V}'$, the equality constraint describes the movements of the vertices in the corresponding rigid subtrailer under the leading of the pivot connecting $\mathcal{V}'$ and $\mathcal{V}_0$. One can show that the combination (4.17) and (4.18) is equivalent to $R_f \mathbf{q}_f + R_\ell \mathbf{q}_\ell = \mathbf{0}$, as there is no edge shared by the root component and the rigid subtrailers.

According to the dynamic programming rule, we may substitute the parts corresponding to the subtrailers in the optimization problem (4.16) by the value function $G_{\mathcal{V}'}(\cdot)$ defined as follows,

$$G_{\mathcal{V}'}(\mathbf{q}_{\ell'}) \triangleq \min \left\{ \sum_{j \in \mathring{\mathcal{V}}'_{\succeq}} \|\mathbf{q}_j\|^2 : R_{\mathring{\mathcal{V}}'_{\succeq}} \mathbf{q}_{\mathring{\mathcal{V}}'_{\succeq}} + R_{\ell'} \mathbf{q}_{\ell'} = \mathbf{0} \right\}. \tag{4.19}$$

The optimization problem (4.16) now becomes

$$\underset{\mathbf{q}_i, i\in\mathcal{V}_0\setminus\{\ell\}}{\text{minimize}} \quad \sum_{i\in\mathring{\mathcal{V}}_0} \|\mathbf{q}_i\|^2 + \sum_{\mathcal{V}'\in\text{succ}(\mathcal{V}_0)} G_{\mathcal{V}'}(\mathbf{q}_{\ell'}) \tag{4.20}$$

$$\text{subject to} \quad R_{\mathring{\mathcal{V}}_0}\mathbf{q}_{\mathring{\mathcal{V}}_0} + R_\ell \mathbf{q}_\ell = \mathbf{0}. \tag{4.21}$$

Notice that (4.19) can be written as $\mathbf{q}_\ell^\top M \mathbf{q}_\ell = G_{\mathcal{V}_0}(\mathbf{q}_\ell)$, therefore,

$$G_{\mathcal{V}_0}(\mathbf{q}_\ell) = \min\left\{ \sum_{i\in\mathring{\mathcal{V}}_0} \|\mathbf{q}_i\|^2 + \sum_{\mathcal{V}'\in\text{succ}(\mathcal{V}_0)} G_{\mathcal{V}'}(\mathbf{q}_{\ell'}) : R_{\mathring{\mathcal{V}}_0}\mathbf{q}_{\mathring{\mathcal{V}}_0} + R_\ell \mathbf{q}_\ell = \mathbf{0} \right\}.$$

By substituting root component $\mathcal{V}_0$ with a general rigid component $\mathcal{V}'' \in \mathcal{R}$, and leader ℓ with connecting pivot ℓ'' of $\mathcal{V}''$, a recursive expression can be derived as follows,

$$G_{\mathcal{V}''}(\mathbf{q}_{\ell''}) = \min\left\{ \sum_{i\in\mathring{\mathcal{V}}''} \|\mathbf{q}_i\|^2 + \sum_{\mathcal{V}'\in\text{succ}(\mathcal{V}'')} G_{\mathcal{V}'}(\mathbf{q}_{\ell'}) : R_{\mathring{\mathcal{V}}''}\mathbf{q}_{\mathring{\mathcal{V}}''} + R_{\ell''}\mathbf{q}_{\ell''} = \mathbf{0} \right\}, \tag{4.22}$$

Since the rigid component $\mathcal{V}''$ itself is rigid, the rank deficiency of $R_{\mathring{\mathcal{V}}''}$ is equal to 1, thus the feasible set defined by the equality constraint in (4.22) can be expressed as

$$\left\{ -R^\dagger_{\mathring{\mathcal{V}}''} R_{\ell''}\mathbf{q}_{\ell''} + \alpha\mathbf{w} : \alpha \in \mathbb{R} \right\},$$

where $\mathbf{w} \in \text{null}\left(R_{\mathring{\mathcal{V}}''}\right)$ is the unit vector representing the simultaneous rotation of $\mathring{\mathcal{V}}''$ about the pivot ℓ'', or explicitly,

$$\mathbf{w} = \frac{1}{\sum\limits_{i\in\mathring{\mathcal{V}}''} \|\mathbf{p}_i - \mathbf{p}_{\ell''}\|^2} \left(\mathbf{p}_{\mathring{\mathcal{V}}''} - \mathbf{1}_{|\mathcal{V}''|-1} \otimes \mathbf{p}_{\ell''}\right)^\perp.$$

For notation simplicity, let W denote the matrix $-R^\dagger_{\mathring{\mathcal{V}}''} R_{\ell''}$. Then (4.22) can be manipulated into an unconstrained optimization problem,

$$\begin{aligned} G_{\mathcal{V}''}(\mathbf{q}_{\ell''}) &= \min_\alpha \left\{ \sum_{i\in\mathring{\mathcal{V}}''} \|W_i\mathbf{q}_{\ell''} + \alpha\mathbf{w}_i\|^2 + \sum_{\mathcal{V}'\in\text{succ}(\mathcal{V}''),} G_{\mathcal{V}'}\left(W_{\ell'}\mathbf{q}_{\ell''} + \alpha\mathbf{w}_{\ell'}\right) \right\} \\ &= \min_\alpha \left\{ \alpha^2 + \sum_{i\in\mathring{\mathcal{V}}''} \|W_i\mathbf{q}_{\ell''}\|^2 + \sum_{\mathcal{V}'\in\text{succ}(\mathcal{V}'')} G_{\mathcal{V}'}\left(W_{\ell'}\mathbf{q}_{\ell''} + \alpha\mathbf{w}_{\ell'}\right) \right\}, \end{aligned} \tag{4.23}$$

where $W_{\ell'}$ and $\mathbf{w}_{\ell'}$ refer to the block rows of W and $\mathbf{w}$ corresponding to vertex ℓ', respectively.

For each rigid component $\mathcal{V}''$ whose corresponding vertices in the skeleton graph are leaves, it can be readily seen that $G_{\mathcal{V}''}(\mathbf{q}_{\ell''}) = \mathbf{q}_{\ell''}^\top M_{\mathcal{V}''} \mathbf{q}_{\ell''}$ where $M_{\mathcal{V}''}$ is the manipulability matrix for the rigid component $\mathcal{V}''$ with pivot ℓ'' as the leader. For a general rigid component $\mathcal{V}''$, assume that for each successor $\mathcal{V}' \in \mathrm{succ}(\mathcal{V}'')$, $G_{\mathcal{V}'}(\mathbf{q}_{\ell'})$ is quadratic, i.e. $G_{\mathcal{V}'}(\mathbf{q}_{\ell'}) = \mathbf{q}_{\ell'}^\top M_{\mathcal{V}'} \mathbf{q}_{\ell'}$ for some real symmetric matrix $M_{\mathcal{V}'} \in \mathbb{R}^{2\times 2}$. Now, observing the first order necessary condition for the optimality of (4.23) yields

$$
\begin{aligned}
& 2\alpha^* + 2 \sum_{\mathcal{V}' \in \mathrm{succ}(\mathcal{V}'')} \left(W_{\ell'} \mathbf{q}_{\ell''} + \alpha^* \mathbf{w}_{\ell'}\right)^\top M_{\mathcal{V}'} \mathbf{w}_{\ell'} = 0 \\
\Rightarrow \quad & \alpha^* = A \mathbf{q}_{\ell''}, \;\; A \triangleq -\frac{\displaystyle\sum_{\mathcal{V}' \in \mathrm{succ}(\mathcal{V}'')} \mathbf{w}_{\ell'}^\top M_{\mathcal{V}'} W_{\ell'}}{1 + \displaystyle\sum_{\mathcal{V}' \in \mathrm{succ}(\mathcal{V}'')} \mathbf{w}_{\ell'}^\top M_{\mathcal{V}'} \mathbf{w}_{\ell'}} \in \mathbb{R}^{1\times 2}.
\end{aligned}
$$

Substituting into (4.23), we have

$$
G_{\mathcal{V}''}(\mathbf{q}_{\ell''}) = \mathbf{q}_{\ell''}^\top \underbrace{\left[A^\top A + W^\top W + \sum_{\mathcal{V}' \in \mathrm{succ}(\mathcal{V}'')} \left(W_{\ell'} + \mathbf{w}_{\ell'} A\right)^\top M_{\mathcal{V}'} \left(W_{\ell'} + \mathbf{w}_{\ell'} A\right) \right]}_{M_{\mathcal{V}''}} \mathbf{q}_{\ell''}. \tag{4.24}
$$

By induction on the tree structure, $G_{\mathcal{V}'}(\cdot)$ is a quadratic form for every rigid component $\mathcal{V}'$ in the trailer, and the update formula for $G_{\mathcal{V}'}(\cdot)$ is given by (4.24), which by applying recursively yields $M_{\mathcal{V}_0}$, the manipulability matrix of the rigid trailer.

The advantage of this dynamic programming approach is that the entire process involves only the propagation of 2-by-2 matrices, and hence is much more numerically stable. The Moore-Penrose pseudoinverse operation is done only on rigid component, whose rank deficiency is equal to one and has a much smaller scale compared to the entire trailer.

4.6 Summary

The relation between the leaders' infinitesimal movements and the resultant reactions of followers can be established via the *manipulability matrix*. The *manipulability indexes*, derived from the singular values of this matrix, are the quantitative measures of leaders' amplification effect on followers, which can be viewed as an indicator of the effectiveness

of leader-follower formations. In this chapter, the formulation of the manipulability matrix and indexes was given in two approaches, followed by the discussion of their properties. The properties and computation methods of the manipulability indexes for two particular cases were studied: single-leader rigid formations and single-leader trailers. Explicit expressions of the manipulability indexes for both cases were derived.

5. FORMATION OPTIMIZATION USING RIGIDITY INDEXES

This chapter[1] is focused on the problems of finding favorable formations in terms of greater rigidity measured by the rigidity indexes proposed in Chapter 3. In practical applications, such formations are often robust to perturbation or measurement inaccuracy (see Section 3.5 for application examples in formation control and network localization). The general problem of finding the most rigid formation is to solve the following formation optimization problem

$$\text{maximize} \quad r(K, \mathbf{p}) \tag{5.1}$$

subject to certain constraints on the connectivity matrix K and the configure $\mathbf{p}$, where r is either the worst-case rigidity index or the mean rigidity index. With different combinations of objectives and constraints, various optimization problems are formulated in this chapter. For nonconvex optimization problems, several approximate algorithms with high computational efficiency are also proposed with numerical examples illustrating their effectiveness in solving the problems.

5.1 Optimal Link Resource Allocation

In this section, problem (5.1) is studied by assuming a fixed vertex position $\mathbf{p}$ and optimizing with respect to the connectivity K only, which is referred to as the *optimal link resource allocation problem*, since entries of K model the strength of links between vertices which typically require consuming resources (transmission power, etc.) to maintain. The more general case of optimizing with respect to both K and $\mathbf{p}$ will be studied in the next section.

[1] Most of the results presented in this chapter are previously published in [50] and [51].

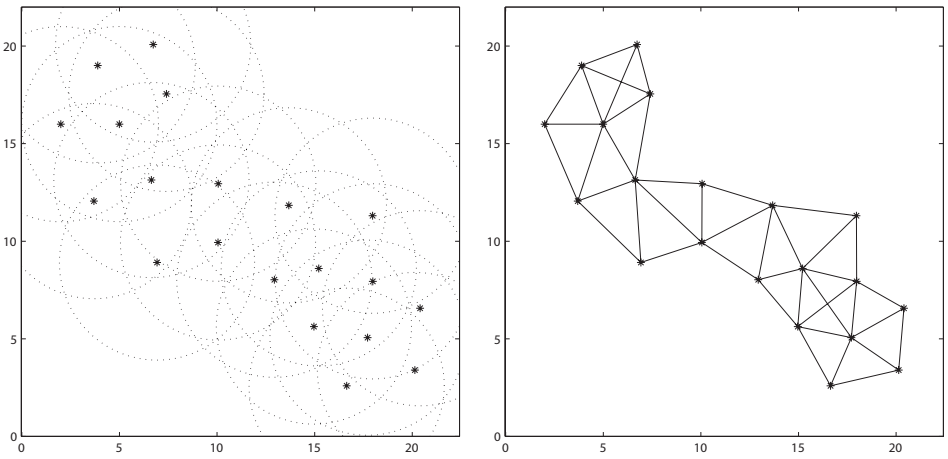

(a) (b)

Fig. 5.1.: A formation generated using a communication range $R = 5$.

Specifically, the following optimal link resource allocation problem is considered:

$$\underset{K \in \mathcal{K}}{\text{maximize}} \quad r(K, \mathbf{p}) \tag{5.2}$$

$$\text{subject to} \quad \sum_{i<j} k_{ij} \leq c, \quad \text{and} \quad k_{ij} = 0 \ \text{ for } \ (i,j) \notin \mathcal{E}. \tag{5.3}$$

Here, $\mathbf{p}$ is assumed to be fixed and the rigidity index r to be optimized is either the WRI r_w or the MRI r_m. We denote by $\mathcal{E} \subset \mathcal{V} \times \mathcal{V}$ the set of active links. For instance, $\mathcal{L}$ could be chosen so that $(i,j) \in \mathcal{E}$ if and only if vertices i and j are within a communication range R of each other (see Fig. 5.1 for an example). In the constraint (5.3), $c > 0$ is the total amount of resources to be allocated over all active links. For example, wireless localization schemes using Time of Arrival (TOA) estimation [52] can be modeled by formations with k_{ij} being the inverse of the Cramér-Rao Bound (CRB) of distance sensing errors and proportional to the power of the sensing signals [47]. Thus, c can be interpreted as the total power of pulse signals used for distance measurements, with k_{ij} being the portion of the power used for measuring the distance between vertices i and j. Solving (5.2) will then show how the signal power should be allocated over all active links for the most efficient network localization.

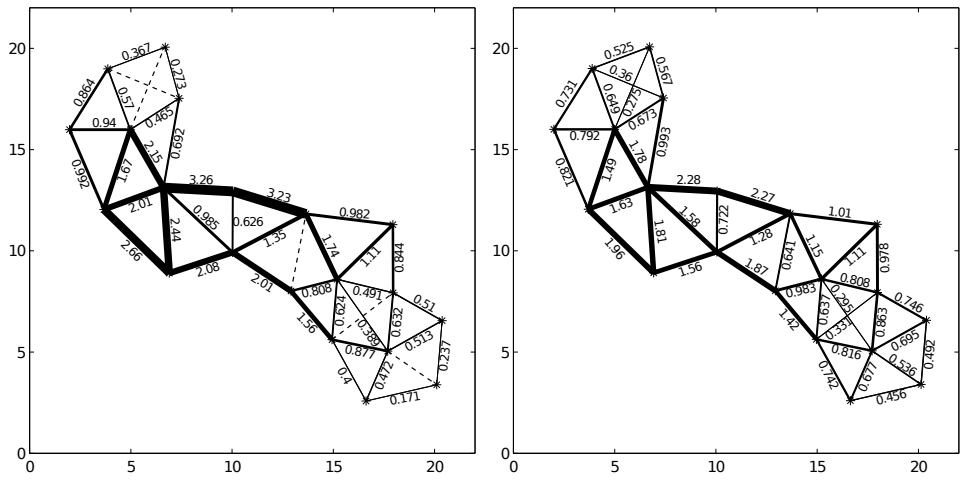

(a) WRI (b) MRI

Fig. 5.2.: Computed optimal link resource allocations for the formation in Fig. 5.1.

Since both $r_{\mathrm{w}}(K, \mathbf{p})$ and $r_{\mathrm{m}}(K, \mathbf{p})$ are concave continuous functions of K and the constraint (5.3) defines a compact convex feasible subset of $\mathcal{K}$, problem (5.2) is a convex optimization problem whose solution exists and can be effectively solved by existing numerical methods, e.g, the CVX toolbox for MATLAB [53]. As an example, consider the formation in Fig. 5.1 with the total resource c set as $|\mathcal{E}|$, i.e., each link is allocated unit amount of resources on average. The computed optimal allocations with respect to r_{w} and r_{m} are plotted in Fig. 5.2a and 5.2b, respectively. A thicker line segment indicates that a larger portion of resources should be allocated to that link; whereas a dashed line indicates that the link has been eliminated (k_{ij} drops to zero) in the optimal solution.

Several observations can be made by comparing Fig. 5.2a and Fig. 5.2b. Both results show that the "bottleneck" links in between the two end clusters need significantly more resources than peripheral links. Furthermore, the optimal allocation in Fig. 5.2a is more polarized than that in Fig. 5.2b, with several links in the original formation eliminated (as shown by the dashed lines) after the optimization. Experiments show that allocations obtained by optimizing r_{m} tend to be more smoothly distributed. On the other hand, through

optimizing r_{w}, dispensable links that contribute little to the overall formation rigidity can be identified. This is especially useful when the number of active links needs to be reduced.

5.1.1 Sensitivity Analysis

We next investigate how sensitive the rigidity indexes are to changes in link connectivity. First consider the WRI r_{w}, which by definition is the fourth smallest eigenvalue λ_4 of the stiffness matrix $S(K)$. If λ_4 is a distinct eigenvalue of $S(K)$, the partial derivative of r_{w} with respect to k_{ij} has been derived in [54] as

$$\frac{\partial r_{\mathrm{w}}}{\partial k_{ij}} = \mathbf{v}_4^\top \left(\frac{\partial S}{\partial k_{ij}} \right) \mathbf{v}_4,$$

where $\mathbf{v}_4(K)$ is the unit eigenvector corresponding to the eigenvalue λ_4. Noting that $\frac{\partial S}{\partial k_{ij}} = \mathbf{q}_{ij}\mathbf{q}_{ij}^\top$ where $\mathbf{q}_{ij}$ is defined in (2.7), the *WRI sensitivity* with respect to link (i,j) can be expressed as

$$\frac{\partial r_{\mathrm{w}}}{\partial k_{ij}} = \left| \mathbf{v}_4^\top \mathbf{q}_{ij} \right|^2. \tag{5.4}$$

The fact that $\frac{\partial r_{\mathrm{w}}}{\partial k_{ij}} \geq 0$ for all k_{ij} confirms the monotonicity property of the WRI r_{w}.

For the MRI r_{m}, suppose the formation $(\mathcal{V}, \mathbf{p}, K)$ is rigid. Then the MRI $r_{\mathrm{m}} = (2n-3)\left(\mathrm{tr}(S(K)^\dagger)\right)^{-1}$. Since both S and $S^\dagger$ are symmetric, we have

$$\frac{\partial r_{\mathrm{m}}(K)}{\partial k_{ij}} = \frac{\partial}{\partial k_{ij}} \left(\frac{2n-3}{\mathrm{tr}(S^\dagger)} \right) = -\frac{2n-3}{\left(\mathrm{tr}(S^\dagger)\right)^2} \cdot \mathrm{tr}\left(\frac{\partial S^\dagger}{\partial k_{ij}} \right) = \frac{2n-3}{\left(\mathrm{tr}(S^\dagger)\right)^2} \cdot \mathrm{tr}\left(S^\dagger \frac{\partial S}{\partial k_{ij}} S^\dagger \right).$$

By noting again that $\frac{\partial S}{\partial k_{ij}} = \mathbf{q}_{ij}\mathbf{q}_{ij}^\top$, the *MRI sensitivity* with respect to link (i,j) at K can be written as

$$\frac{\partial r_{\mathrm{m}}}{\partial k_{ij}} = \frac{2n-3}{\left(\mathrm{tr}(S^\dagger)\right)^2} \cdot \left\| S^\dagger \mathbf{q}_{ij} \right\|^2. \tag{5.5}$$

As in the WRI case, $\frac{\partial r_{\mathrm{m}}}{\partial k_{ij}} \geq 0$ for all k_{ij}, verifying the monotonicity property of the MRI r_{m}.

For the formation in Fig. 5.1, we compute the sensitivities of the rigidity indexes with respect to all the active links at two different K. Fig. 5.3 illustrates the sensitivity distributions of both the WRI r_{w} and the MRI r_{m} at their respective optimal allocation schemes (as plotted in Fig. 5.2a and Fig. 5.2b). In both cases, the sensitivity values are identical for

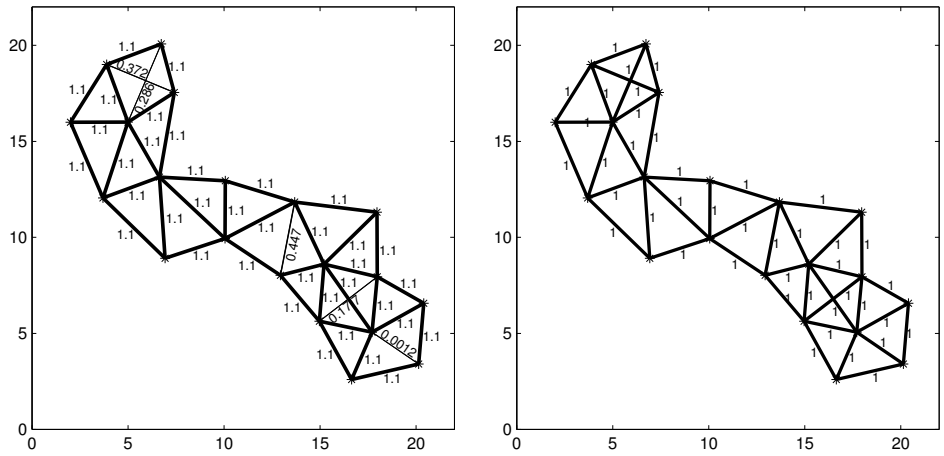

(a) WRI (b) MRI

Fig. 5.3.: Sensitivity of rigidity indexes at the optimal allocation K^*.

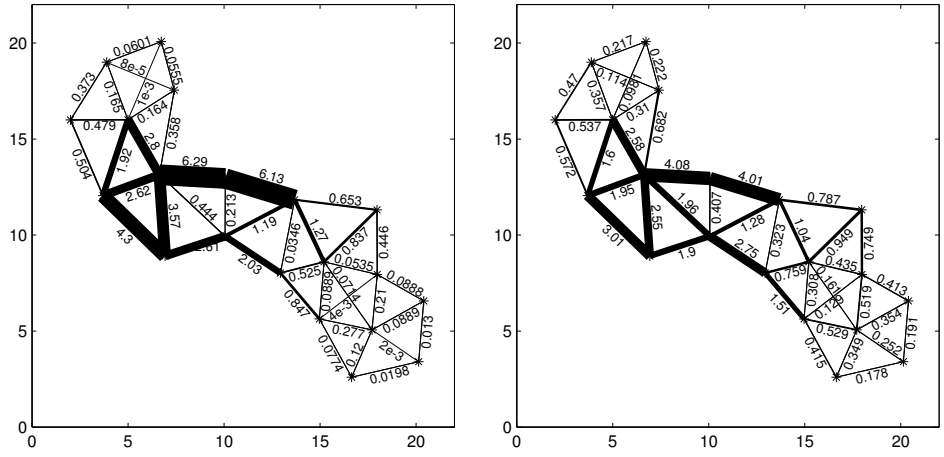

(a) WRI (b) MRI

Fig. 5.4.: Sensitivity of rigidity indexes at the equal allocation.

all active links except for a few links in Fig. 5.3a that are allocated zero resources in the WRI-optimal scheme, i.e., those depicted by dashed lines in Fig. 5.2a. This is consistent with the optimality of both schemes, as the rigidity indexes cannot be further increased by shifting resources from one link to another.

Next, we compute the sensitivity distributions of both rigidity indexes at the equal allocation scheme, i.e., each link is allocated the same unit amount of resources. The computed sensitivity distribution is shown in Fig. 5.4. The thicker line segments indicate the more "sensitive" links. Shifting resources from other links to these more sensitive ones will result in an increase of the rigidity indexes. As a result, it can be expected that these links will demand more resources in the optimal allocation schemes, as is verified by the plots in Fig. 5.2.

5.2 Configuration Optimization

In the configuration optimization problem, one assumes a fixed connectivity K and tries to find the vertex configuration $\mathbf{p}$ resulting in the largest rigidity index. Take the example of MRI. The optimization to be solved is:

$$\underset{\mathbf{p}\in\mathbb{R}^{2n}}{\text{maximize}} \;\; r_{\mathrm{m}}(K,\mathbf{p}). \tag{5.6}$$

Note that K is fixed and there is no constraint on $\mathbf{p}$. Since the MRI is invariant to similarity transformations, only the shape of $\mathbf{p}$ is to be optimized, while its absolute location, orientation, and size have no effect.

Assume that throughout the optimization process the formation remains rigid, i.e., $r_{\mathrm{m}}(K,\mathbf{p}) > 0$. Under this assumption, by recalling (3.2), problem (5.6) is equivalent to

$$\underset{\mathbf{p}\in\mathbb{R}^{2n}}{\text{minimize}} \;\; \mathrm{tr}(S(K,\mathbf{p})^{\dagger}), \tag{5.7}$$

which is a nonlinear and nonconvex optimization problem. One solution approach is the gradient descent method.

Lemma 5.2.1 *Denote* $X \triangleq S(K,\mathbf{p})^{\dagger}S(K,\mathbf{p})^{\dagger} = [X_{ij}]_{i,j\in\mathcal{V}}$ *for some* $X_{ij} \in \mathbb{R}^{2\times 2}$ *satisfying* $X_{ij} = X_{ji}^{\top}$. *Then*

$$\frac{\partial \mathrm{tr}\left(S^{\dagger}\right)}{\partial \mathbf{p}_l} = 2\sum_{i\in\mathcal{V}\setminus\{l\}} \frac{k_{il}(\mathbf{p}_i-\mathbf{p}_l)^{\top}(X_{ll}-X_{il}-X_{li})(I-P_{il})}{\|\mathbf{p}_l-\mathbf{p}_i\|^2}, \quad \textit{for } l\in\mathcal{V}. \tag{5.8}$$

Proof For notational simplicity, we drop the arguments in S. By [55], for each $l \in \mathcal{V}$,

$$\frac{\partial \mathrm{tr}(S^\dagger)}{\partial \mathbf{p}_l} = -\mathrm{tr}\left(S^\dagger \frac{\partial S}{\partial \mathbf{p}_l} S^\dagger\right) = -\mathrm{tr}\left(X \frac{\partial S}{\partial \mathbf{p}_l}\right) = -\sum_{i,j\in\mathcal{V}} \mathrm{tr}\left(X_{ij} \frac{\partial S_{ij}}{\partial \mathbf{p}_l}\right). \tag{5.9}$$

According to (2.4), $\partial S_{ij}/\partial \mathbf{p}_l = 0$ unless either $i = l$ or $j = l$. For each $i \in \mathcal{V}$ with $i \neq l$, we have

$$\frac{\partial \mathrm{tr}\left(X_{il} S_{il}\right)}{\partial \mathbf{p}_l} = -k_{il} \frac{\partial \left(\mathbf{e}_{il}^\top X_{ij} \mathbf{e}_{il}\right)}{\partial \mathbf{p}_l} = -k_{il} \mathbf{e}_{il}^\top (X_{ij} + X_{ij}^\top) \frac{\partial \mathbf{e}_{il}}{\partial \mathbf{p}_l} = k_{il} \mathbf{e}_{il}^\top (X_{ij} + X_{ij}^\top) \frac{I - P_{il}}{\|\mathbf{p}_i - \mathbf{p}_l\|}.$$

Similarly, we can compute $\partial \mathrm{tr}\left(X_{lj} S_{lj}\right)/\partial \mathbf{p}_l$ for $j \in \mathcal{V}$ with $j \neq l$, and $\partial \mathrm{tr}\left(X_{ll} S_{ll}\right)/\partial \mathbf{p}_l$. Plugging these into (5.9) yields the desired conclusion. ■

By stacking the partial derivatives in (5.8) for all $l \in \mathcal{V}$, we obtain the gradient of the objective function of the optimization problem (5.7) with respect to $\mathbf{p}$. Gradient descent methods such as the Newton and quasi-Newton methods [56] can then be applied to find a (generally suboptimal) solution to problem (5.6).

Remark 5.2.1 *At a given configuration* $\mathbf{p}$*, denote by* $\mathbf{v}_4$ *the eigenvector of the stiffness matrix* $S(K, \mathbf{p})$ *corresponding to its fourth smallest eigenvalue* λ_4*. Then, it is known [54] that the gradient of the WRI at* $\mathbf{p}$ *is given by*

$$\frac{\partial r_{\mathrm{w}}(K, \mathbf{p})}{\partial \mathbf{p}_l} = \mathbf{v}_4^\top \left(\frac{\partial S(K, \mathbf{p})}{\partial \mathbf{p}_l}\right) \mathbf{v}_4, \quad l \in \mathcal{V}.$$

Thus, the above gradient-based methods can be similarly applied to optimize r_{w} *with respect to* $\mathbf{p}$*. One needs to be aware that when* λ_4 *is a multiple eigenvalue, the concept of subgradient is involved. (See [57] for more details.)*

5.3 Topology Optimization

In the topology optimization subproblem, the vertex configuration $\mathbf{p}$ is assumed to be fixed, and the rigidity index is optimized with respect to the connectivity K that quantifies the topology of the formation:

$$\underset{K \in \mathcal{K}_0}{\text{maximize}} \;\; r(K, \mathbf{p}),$$

for some feasible set $\mathcal{K}_0 \subset \mathcal{K}$ of K. A version of this problem has already been studied in Section 5.1 with $\mathcal{K}_0$ defined through the constraints (5.3). In the following, we consider the following more challenging version, where the feasible set $\mathcal{K}_0$ is a discrete set defined by

$$\mathcal{K}_0 = \left\{ K : \|K\|_0 = \ell, \text{ and } k_{ij} \in \{0, \hat{k}_{ij}\}, \ \forall\, i, j \in \mathcal{V} \right\}. \tag{5.10}$$

Here, $\|K\|_0$ denotes the number of nonzero entries, ℓ is a positive integer and $\hat{K} = \left[\hat{k}_{ij}\right]$ with $\hat{k}_{ij} > 0$ is a preset connectivity matrix. In other words, each edge is either on or off, and there are no more than ℓ "on" edges. For simplicity, choose the rigidity index to be optimized as the WRI r_{w}.

The optimization problem with the 0-1 constraint on K is NP-hard in graph size. To find a sub-optimal solution, we propose a method that swaps edges iteratively. In each iteration, an absent edge is first added to increase the WRI the most, followed by the removal of an edge that results in the least decrease of the WRI. Thus the WRI will never decrease in each step. The process terminates when the same edge is being added and removed in a single step.

Assume that the initial formation with the configuration $\mathbf{p}$ and the topology K is rigid. When a single edge, say, between vertices i and j, is added/removed, the original stiffness matrix S is updated by a rank-one modification $\tilde{S} = S + \rho \cdot \Delta S$, where $\Delta S = \hat{k}_{ij}\mathbf{q}_{ij}\mathbf{q}_{ij}^\top$ with $\mathbf{q}_{ij}$ defined in (2.7), and ρ is $+1$ or -1 if the edge is added or removed. According to the following theorem, if the edge is added, then $\lambda_4(\tilde{S})$ is between $\lambda_4(S)$ and $\lambda_5(S)$; while if the edge is removed, then $\lambda_4(\tilde{S})$ is between 0 and $\lambda_4(S)$.

Lemma 5.3.1 (Cauchy's Interlace Theorem [58]) *Let $C = D + \sigma \mathbf{b}\mathbf{b}^\top$, where matrix $D = \mathrm{diag}(d_1, d_2, \ldots, d_{2n}) \in \mathbb{R}^{2n\times 2n}$ is diagonal; $\mathbf{b} \in \mathbb{R}^{2n}$ and $\sigma \in \mathbb{R}$. Suppose $\bar{d}_1 \le \bar{d}_2 \le \cdots \le \bar{d}_{2n}$ are the eigenvalues of C. Then,*

$$d_1 \le \bar{d}_1 \le d_2 \le \bar{d}_2 \le \cdots \le d_{2n} \le \bar{d}_{2n}, \quad \text{if } \sigma > 0$$
$$\bar{d}_1 \le d_1 \le \bar{d}_2 \le d_2 \le \cdots \le \bar{d}_{2n} \le d_{2n}, \quad \text{if } \sigma < 0.$$

To characterize the eigenvalues of $\tilde{S}$, we write $S = QDQ^\top$, where $Q \in \mathbb{R}^{2n\times 2n}$ is orthogonal and $D = \mathrm{diag}(\lambda_1, \lambda_2, \ldots, \lambda_{2n})$ with λ_i's being the eigenvalues of S. Suppose

$\tilde{\lambda}$ is an eigenvalue of $\tilde{S} = S + \rho\delta S$ with $\tilde{\mathbf{v}}$ a corresponding eigenvector. Then $\tilde{\lambda}$ must be a root of the following *secular equation* [58]:

$$\begin{aligned} \tilde{S}\tilde{\mathbf{v}} = (S + \rho\hat{k}_{ij}\mathbf{q}_{ij}\mathbf{q}_{ij}^\top)\tilde{\mathbf{v}} = \tilde{\lambda}\tilde{\mathbf{v}} \quad &\Rightarrow \quad 1 + \rho\hat{k}_{ij}\bar{\mathbf{q}}_{ij}^\top(D - \tilde{\lambda}I)^{-1}\bar{\mathbf{q}}_{ij} = 0 \\ &\Rightarrow \quad \omega_{ij}(\mu) \triangleq 1 + \rho\hat{k}_{ij}\sum_{m=1}^{2n}\frac{\xi_m^2}{\lambda_m - \mu} = 0, \end{aligned} \tag{5.11}$$

where $\bar{\mathbf{q}}_{ij} = Q^\top\mathbf{q}_{ij} = [\xi_1, \xi_2, \ldots, \xi_{2n}]^\top$ is constant for varying ρ.

The secular equation (5.11) is a monotonically increasing equation on the interval $(\lambda_4(S), \lambda_5(S))$. Denote by $\mathcal{E}^{\text{on}}$ and $\mathcal{E}^{\text{off}}$ the set of edges that are currently on and off, respectively. When an edge $(i,j) \in \mathcal{E}^{\text{off}}$ is turned on, the new WRI can be obtained by solving the secular equation using a bisection algorithm.

In fact, instead of solving (5.11) for each individual edges that can be added, the following algorithm, inspired by [59] and summarized in Table 5.1, can simultaneously solve all the secular equations through a single bisection algorithm. At each step $t = 0, 1, \ldots$, let l and u be a lower bound and an upper bound of the largest WRI r_{w}^* achievable by adding edges in the feasible set $\mathcal{A}_t$, and let $m = (l+u)/2$. We can classify links (i,j) in $\mathcal{A}_t$ into two groups $\mathcal{A}^- = \{(i,j) \in \mathcal{A}_t | \lambda_4(\tilde{S}) \in [l, m)\}$ and $\mathcal{A}^+ = \{(i,j) \in \mathcal{A}_t | \lambda_4(\tilde{S}) \in [m, u]\}$ according to whether the corresponding secular equation satisfies $\omega_{ij}(m) > 0$ or not. After this classification, if $\mathcal{A}^+$ is empty, then the midpoint m becomes the new upper bound and the new feasible set $\mathcal{A}_{t+1}$ is updated to $\mathcal{A}^-$. Otherwise m becomes the new lower bound and $\mathcal{A}_{t+1}$ is updated to $\mathcal{A}^+$. This process is repeated until the required precision is achieved.

The above idea can also be applied to the similar problem of deleting one edge that results in the least decrease in the WRI. In this case, the new WRI lies inside the interval $(0, \lambda_4(S))$; and since $\rho = -1$, each secular equation $\omega_{ij}(\mu)$ is non-increasing on this interval. The algorithm in Table 5.1 can be modified to obtain the *Edge Removal Bisection Algorithm*. By alternating between the edge addition and removal algorithms, we obtain a combined iteration algorithm, called the *Edge Swapping Algorithm*, that at each step relocates an edge within the formation graph. This algorithm is stopped whenever the same edge is added and removed in a single step.

Table 5.1: Edge Addition Bisection Algorithm

Input	$\rho = 1$, $l = \lambda_4(S)$, $u = \lambda_5(S)$, $m = (l+u)/2$, $\mathcal{A}_0 = \mathcal{E}^{\text{off}}$ and $t = 0$
Step 1	If $\lvert\mathcal{A}_t\rvert = 1$, then go to Output; otherwise, $\mathcal{A}^+ = \emptyset$, $\mathcal{A}^- = \emptyset$, and go to **Step 2**.
Step 2	For each $(i,j) \in \mathcal{A}_t$, if $\omega_{ij}(m) > 0$, then $\mathcal{A}^- \leftarrow \mathcal{A}^- \cup \{(i,j)\}$; Otherwise, $\mathcal{A}^+ \leftarrow \mathcal{A}^+ \cup \{(i,j)\}$
Step 3	If $\lvert\mathcal{A}^+\rvert = 0$, $u \leftarrow m$ and $\mathcal{A}_{t+1} = \mathcal{A}^-$ otherwise, $l \leftarrow m$ and $\mathcal{A}_{t+1} = \mathcal{A}^+$
Step 4	$t \leftarrow t+1$ and go to **Step 1**
Output	$\mathcal{A}_t$ (singleton)

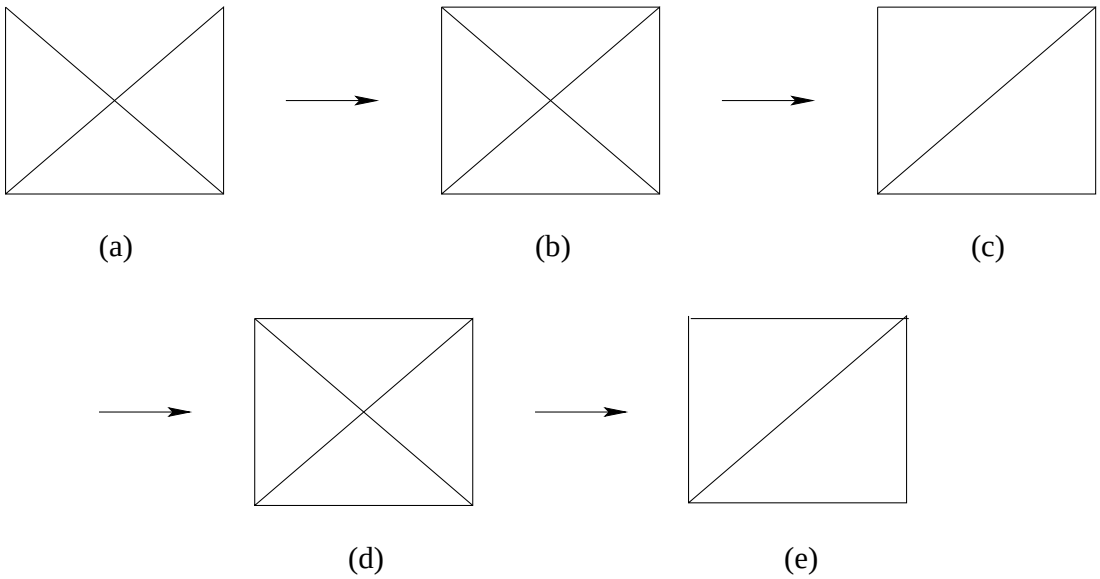

Fig. 5.5.: Edge Switching Algorithm (a) **Input** $\rightarrow$ (b) **Step 1** $\rightarrow$ (c) **Step 2, Step 3** $\rightarrow$ (d) **Step 1** $\rightarrow$ (e) **Step 2, Step 3** then **Output**

Fig. 5.5 shows a step-by-step illustration of applying the Edge Swapping Algorithm to a simple example where all $\hat{k}_{ij}$ are assumed to be 1. As a result, the WRI increases from the initial 0.268 to 0.586 at the end.

Table 5.2: Alternating Optimization Algorithm

Input	Original formation $\left(\mathcal{V}, K^{(0)}, \mathbf{p}^{(0)}\right), \mathcal{X}, t := 0, \epsilon$
Step 1	Fix $K^{(t)}$, optimize $\mathbf{p}' := \arg\max_{\mathbf{p}} \; r_{\mathrm{m}}\left(K^{(t)}, \mathbf{p}\right)$ from $\mathbf{p}^{(t)}$
Step 2	Fix $\mathbf{p}^{(t+1)}$, optimize $K^{(t+1)} := \arg\max_{K \in \mathcal{X}} \; r_{\mathrm{w}}\left(K, \mathbf{p}^{(t+1)}\right)$ from $K^{(t)}$
Step 3	If $r_{\mathrm{m}}\left(K^{(t+1)}, \mathbf{p}^{(t+1)}\right) < r_{\mathrm{m}}\left(K^{(t)}, \mathbf{p}^{(t)}\right) + \epsilon$, go to **Output**
Step 4	$t := t + 1$, go to **Step 1**
Output	$K^{(t)}, \mathbf{p}^{(t)}$

5.4 Hybrid Configuration/Topology Optimization

The two optimization algorithms discussed in the previous two subsections can be combined to solve the general formation optimization problems. The idea is to alternatively apply the configuration optimization and the topology optimization until both fail to improve the formation rigidity any further. The combined algorithm is described in Table 5.2. An advantage of the combined algorithm is that it can avoid some local extrema with poor overall value associated with either the configuration optimization or the topology optimization individually.

Fig. 5.6 depicts the simulation results of the combined formation optimization algorithm for a five-vertex formation under the constraint $\ell = 6$. The initial formation has random vertex positions and a given topology as shown in Fig. 5.6(a). We first apply the configuration optimization with the fixed initial topology to obtain a solution in Fig. 5.6(a), where the initial and the final vertex positions are shown by hollow and solid dots, respectively, and the dashed lines represent the trajectories of the intermediate results during the gradient descent optimization. We then apply the topology optimization with fixed vertex configuration as in Fig. 5.6(a) to obtain the solution in Fig. 5.6(c). Another configuration optimization leads to the final solution in Fig. 5.6(d). In Fig. 5.7 we plot the WRI and the MRI of the resulted formations as a function of the number of iterations during this

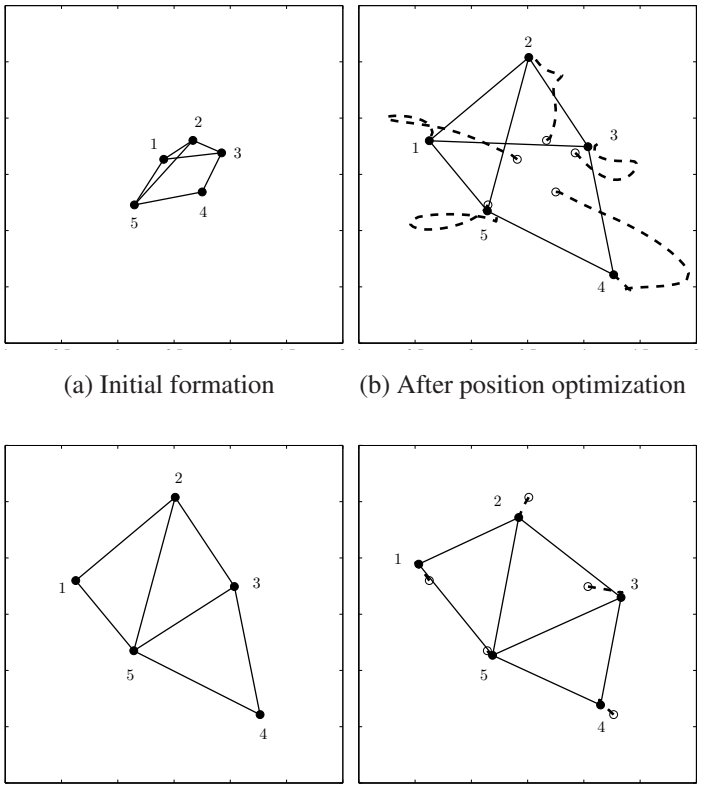

(a) Initial formation (b) After position optimization

(c) After topology optimization (d) Final formation

Fig. 5.6.: Example on Alternating Optimization Algorithm

optimization process. Both rigidity indexes increase over iterations, with the WRI grows from 0.0145 to 0.837 while the MRI grows from 0.0959 to 1.458. The sudden jumps of the two rigidity indexes at the time step 50 are due to the swapping of an edge caused by the topology optimization. It is observed that the MRI exhibits a similar general trend but with a smoother variation compared with the WRI.

5.5 Optimal Leader Selection

A fixable formation is highly desirable in many applications due to its structural robustness and localizability. As setting up leaders in practice has often high hardware and

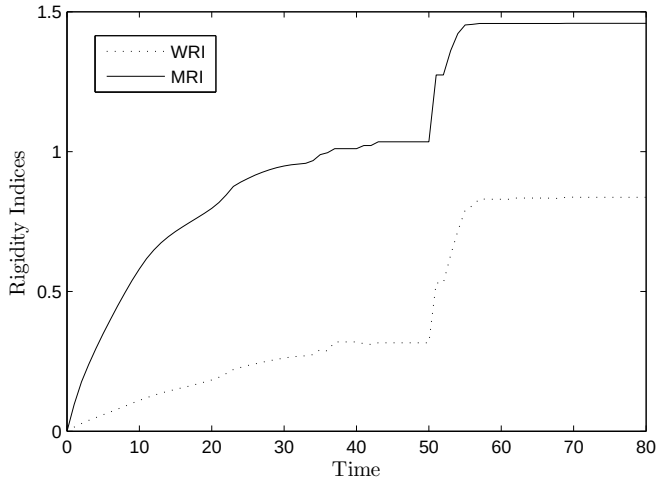

Fig. 5.7.: Rigidity indexes versus time step

energy cost, it is meaningful to find a minimum set of leaders that makes the formation fixable. Such a set is called a *minimum fixable set*.

Lemma 5.5.1 (Cauchy's Interlacing Theorem [45]) *Let $A \in \mathbb{R}^{l\times l}$ be a symmetric matrix with eigenvalues $\lambda_1, \ldots, \lambda_l$, and let $B \in \mathbb{R}^{l-1\times l-1}$ be a principal minor of A with eigenvalues $\mu_1, \ldots, \mu_{l-1}$, both sorted in ascending order. Then $\lambda_1 \leq \mu_1 \leq \lambda_2 \leq \mu_2 \leq \cdots \leq \mu_{l-1} \leq \lambda_l$.*

Proposition 5.5.1 *Let S be the stiffness matrix of a formation with n vertices. Then a minimum fixable set contains at least $n - \lfloor \mathrm{rank}(S)/2 \rfloor$ leaders.*

Proof Let $\lambda_1, \ldots, \lambda_{2n}$ be the eigenvalues of S in ascending order and suppose a set of m leaders has been chosen. Since $\tilde{S}$ of the resulting leader-follower formation is a principal minor of S of order $2n-2m$, by repeatedly applying Lemma 5.5.1, the smallest eigenvalue μ_1 of $\tilde{S}$ satisfies $\lambda_1 \leq \mu_1 \leq \lambda_{2m+1}$. If $\mu_1 > 0$, we must have $\lambda_{2m+1} > 0$, or $\mathrm{rank}(S) \geq 2n - 2m$. Since m, n are integers, this implies that $2m \geq 2n - \mathrm{rank}(S)$, or $m \geq n - \lfloor \mathrm{rank}(S)/2 \rfloor$. ■

Proposition 5.5.1 gives a generally conservative estimate on the size of the minimum fixable set, whose choice is by no means unique. In addition to finding a minimum fixable

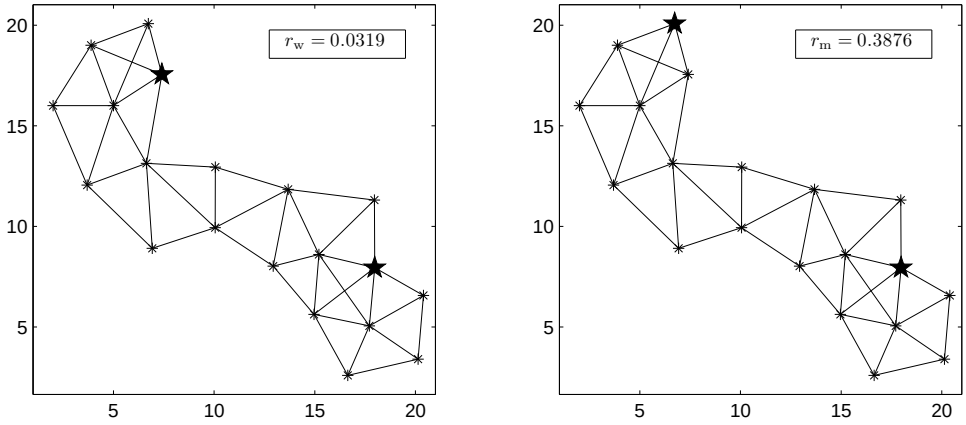

(a) WRI (b) MRI

Fig. 5.8.: Best choices of anchors with respect to the WRI and the MRI

set, a secondary objective is to find one that results in the "most fixable" leader-follower formation as measured by the rigidity index r that is either r_{w} or r_{m}. This can be formulated as the following multi-objective optimization problem:

$$\underset{\mathcal{L}}{\text{minimize}} \;\; [|\mathcal{L}|,\; 1/r(K, \mathbf{p}; \mathcal{L})] \quad \text{subject to} \quad r(K, \mathbf{p}; \mathcal{L}) > 0. \tag{5.12}$$

When both m and n are small, this problem can be solved using an exhaustive search. It is worth noting that a similar problem was previously stated in [44], in which the authors proposed an efficient relaxation method for relatively large-scale problems.

Fig. 5.8 illustrates the best choices of $m = 2$ anchors computed for an example. In both cases, the two anchors in the best schemes are chosen far from each other such that the two ends of the long narrow formation are pinned down. Intuitively, this kind of anchoring provides a better global fixation of the formation structure compared to having both anchors at one end, leaving the other end vulnerable to perturbations. We also note that the best anchoring are different for the two rigidity indexes.

5.6 Summary

In this chapter, the optimization problems of maximizing rigidity indexes were studied. Specifically, three types of optimization problems were formulated and solved. Firstly, the *optimal link resource allocation problem* assumes that both the agent positions and the connection topology are fixed and finds the optimal allocation of link resources (i.e., connectivity coefficients) over all link, with constraint on the total link resource. This problem, due to the concavity of the rigidity indexes, is a convex program and hence can be solved efficiently. Secondly, the *configuration optimization problem* assumes a fixed topology of the formation, and aims to find the optimal positions of the vertices in terms of maximizing the values of rigidity indexes, which is a highly nonlinear optimization problem. Since the gradient direction of the objective function can be given analytically, gradient-based optimization methods can used to find a locally optimal solution. Thirdly, the *topology optimization problem* assumes a fixed configuration and a designated connectivity coefficient for each pair of agents provided the link is turned on. The objective is to find an optimal set of links to turn on, while the number of on-links is constrained. This problem is a binary program and generally NP-hard. To overcome the computational difficulties, an edge-switching algorithm was developed to improve a current topology until it cannot evolve locally. The topology optimization problem can be combined with the configuration optimization problem through alternative execution to avoid local optima with poor performance. Lastly, the *optimal leader selection problem* in the context of rigidity indexes maximization was formulated and a numerical example was given.

6. FORMATION OPTIMIZATION USING MANIPULABILITY

In this chapter[1], the formation optimization problems are revisited from the distinct perspective via the manipulability indexes. Particularly, the single-leader formations receive focused study as the looseness property, hence conflict-freeness, is guaranteed for these formations. Such optimization problems often prove to be useful in designing multi-agent systems where the dynamics of the system is determined by a small subset of leaders, e.g., leader-follower multi-vehicle systems.

6.1 Optimal Leader Position

Provided we are given the freedom to adjust the position of the leader, how can we find the optimal leader's position in terms of maximizing the manipulability indexes? In this section, we will study a particular scenario where there is only one leader and the objective is to maximize the minimum manipulability index $m_{\min}$. Maximizing $m_{\min}$ is often more desirable than $m_{\max}$ in real applications as it prevents a leader-follower formation from significantly poor performance in the worst case. To solve this problem, we introduce the gradient-based method to solve this problem. For convenience, let us define the operator $\mathfrak{D}$ as $\mathfrak{D}A \triangleq \partial A/\partial\theta$, where A is a scalar or a matrix which depends on some common variable θ.

Lemma 6.1.1 *For the single leader case* ($|\mathcal{L}| = 1$)*, the following identity holds:*

$$S_{ff}^{\dagger}\mathfrak{D}\left(S_{ff}^{\dagger}S_{f\ell}\right) = S_{ff}^{\dagger}S_{ff}^{\dagger}\left((\mathfrak{D}S_{f\ell}) - (\mathfrak{D}S_{ff})S_{ff}^{\dagger}S_{f\ell}\right)$$

[1]The results presented in this chapter were partially published in [31].

Proof Recall that for the single leader case, the column space of $S_{f\ell}$ is contained in the column space of S_{ff}. Since S_{ff} is real symmetric, $S_{ff}S_{ff}^{\dagger} = S_{ff}^{\dagger}S_{ff}$. Furthermore, $S_{ff}^{\dagger}S_{ff}$ is the projection matrix into the column space of S_{ff}. The above facts imply the following,

$$S_{ff}^{\dagger}S_{ff}^{\dagger}S_{ff} = S_{ff}^{\dagger}, \quad S_{ff}S_{ff}^{\dagger}S_{f\ell} = S_{f\ell}.$$

According to [60] and the above identities, we have

$$\begin{aligned} S_{ff}^{\dagger}\left(\mathfrak{D}S_{ff}^{\dagger}\right)S_{f\ell} = S_{ff}^{\dagger}\Big(&-S_{ff}^{\dagger}(\mathfrak{D}S_{ff})S_{ff}^{\dagger} + S_{ff}^{\dagger}S_{ff}^{\dagger}(\mathfrak{D}S_{ff}) \\ &- S_{ff}^{\dagger}S_{ff}^{\dagger}(\mathfrak{D}S_{ff})S_{ff}S_{ff}^{\dagger} + (\mathfrak{D}S_{ff})S_{ff}^{\dagger}S_{ff}^{\dagger} \\ &- S_{ff}^{\dagger}S_{ff}(\mathfrak{D}S_{ff})S_{ff}^{\dagger}S_{ff}^{\dagger}\Big)S_{f\ell} \\ = -S_{ff}^{\dagger}S_{ff}^{\dagger}(\mathfrak{D}S_{ff})S_{ff}^{\dagger}S_{f\ell}&. \end{aligned}$$

Finally,

$$\begin{aligned} S_{ff}^{\dagger}\mathfrak{D}\left(S_{ff}^{\dagger}S_{f\ell}\right) &= S_{ff}^{\dagger}\left(\mathfrak{D}S_{ff}^{\dagger}\right)S_{f\ell} + S_{ff}^{\dagger}S_{ff}^{\dagger}\mathfrak{D}S_{f\ell} \\ &= S_{ff}^{\dagger}S_{ff}^{\dagger}\left((\mathfrak{D}S_{f\ell}) - (\mathfrak{D}S_{ff})S_{ff}^{\dagger}S_{f\ell}\right), \end{aligned}$$

which concludes the proof. ■

Lemma 6.1.2 ([54]) *Suppose X is a real symmetric matrix. The i-th smallest eigenvalue of X is denoted by $\lambda_i(X)$ and the corresponding normalized eigenvector by v_i. Then,*

$$\mathfrak{D}\lambda_i(X) = v_i^{\top}\left(\mathfrak{D}X\right)v_i.$$

Proposition 6.1.1 *For the single leader case ($|\mathcal{L}| = 1$), if the minimum manipulability index $m_{\min} = \lambda_{\min}(M) > 0$, then its gradient with respect to the leader's position $\mathbf{p}_\ell$ is*

$$\nabla\lambda_{\min}(M) = 2\sum_{j\in\mathcal{N}(\ell)}(X_{jj} + X_{jj}^{\top} + Y_j + Y_j^{\top})(\mathbf{p}_j - \mathbf{p}_\ell),$$

where

- *v is the normalized eigenvector associated with the eigenvalue $\lambda_{\min}(J^{\top}J)$;*

- *X_{jj} is the d-by-d block of the matrix $X \in \mathbb{R}^{2|\mathcal{F}|\times 2|\mathcal{F}|}$,*

$$X = R_f^\dagger R_\ell v v^\top R_\ell^\top R_f^{\dagger\top} S_{ff}^\dagger;$$

- *Y_j is the d-by-d block of the matrix $Y \in \mathbb{R}^{2\times 2|\mathcal{F}|}$,*

$$Y = v v^\top R_\ell^\top R_f^{\dagger\top} S_{ff}^\dagger;$$

Proof By (4.2) and Lemma 6.1.2,

$$\mathfrak{D}\lambda_{\min}(M) = v^\top (\mathfrak{D}M)\, v = \operatorname{tr}\left(vv^\top \mathfrak{D}M\right) = 2\operatorname{tr}\left(vv^\top S_{f\ell}^\top S_{ff}^\dagger \mathfrak{D}\left(S_{ff}^\dagger S_{f\ell}\right)\right)$$

Using Lemma 6.1.1 and the fact that $S_{ff}^\dagger S_{f\ell} = R_f^\dagger R_\ell$ for the single leader case, we have

$$\mathfrak{D}\lambda_{\min}(M) = 2\operatorname{tr}\left(Y\mathfrak{D}S_{f\ell}\right) - 2\operatorname{tr}\left(X\mathfrak{D}S_{ff}\right).$$

If we view X and Y as constants, it is not hard to see that

$$\begin{aligned}
\operatorname{tr}\left(Y\mathfrak{D}S_{f\ell}\right) &= \sum_{j\in\mathcal{N}(\ell)} \operatorname{tr}\left(Y_j \mathfrak{D}\left(-(\mathbf{p}_j - \mathbf{p}_\ell)(\mathbf{p}_j - \mathbf{p}_\ell)^\top\right)\right) \\
&= -\sum_{j\in\mathcal{N}(\ell)} \mathfrak{D}\left((\mathbf{p}_j - \mathbf{p}_\ell)^\top Y_j (\mathbf{p}_j - \mathbf{p}_\ell)\right) \\
&= \sum_{j\in\mathcal{N}(\ell)} (\mathbf{p}_j - \mathbf{p}_\ell)^\top \left(Y_j + Y_j^\top\right) \mathfrak{D}(\mathbf{p}_\ell - \mathbf{p}_j)
\end{aligned}$$

Similarly,

$$\operatorname{tr}\left(X\mathfrak{D}S_{ff}\right) = -\sum_{j\in\mathcal{N}(\ell)} (\mathbf{p}_j - \mathbf{p}_\ell)^\top \left(X_{jj} + X_{jj}^\top\right) \mathfrak{D}(\mathbf{p}_\ell - \mathbf{p}_j)$$

Now we replace $\mathfrak{D}$ with $\frac{\partial}{\partial \mathbf{p}_\ell}$. Note that $\frac{\partial}{\partial \mathbf{p}_\ell}(\mathbf{p}_\ell - \mathbf{p}_j) = I_2$. Therefore,

$$\frac{\partial \lambda_{\min}(M)}{\partial \mathbf{p}_\ell} = 2\sum_{j\in\mathcal{N}(\ell)} (\mathbf{p}_j - \mathbf{p}_\ell)^\top \left(X_{jj} + X_{jj}^\top + Y_j + Y_j^\top\right),$$

which implies the desired conclusion. ■

The gradient information enables us to use the gradient descent method to search for a locally optimal leader's position which maximizes the minimum (worst-case) manipulability.

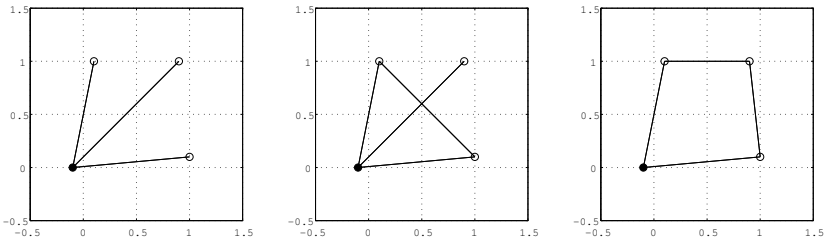

(a) G1 (b) G2 (c) G3

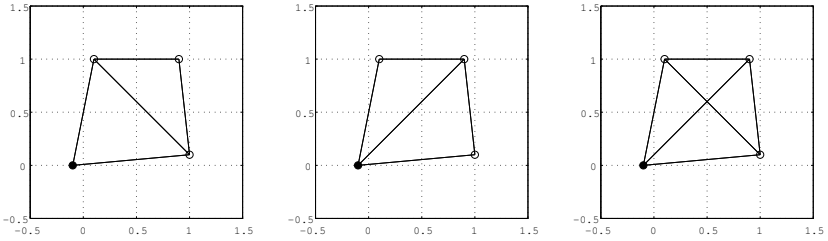

(d) G4 (e) G5 (f) G6

Fig. 6.1.: Original leader-follower formations

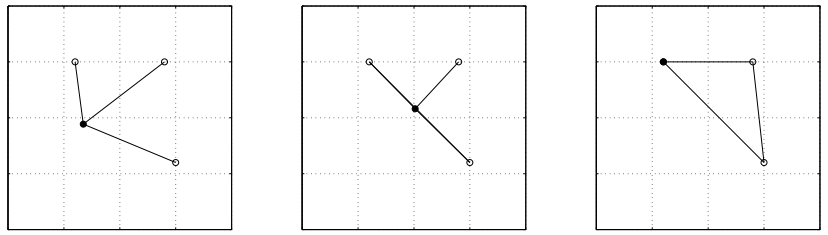

(a) G1 (b) G2 (c) G3‡

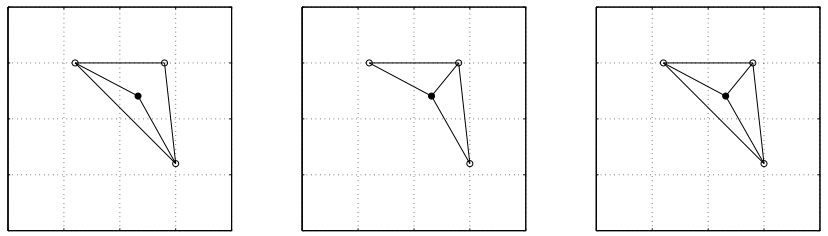

(d) G4 (e) G5 (f) G6

Fig. 6.2.: Optimal leader position for maximizing the minimum manipulability.

‡ This is the asymptotic configuration, but not a valid solution.

Fig. 6.2 depicts the optimal leader's position in each instance where the topology is given as in 6.1 and the positions of the followers are assumed fixed. It is worth noting that a legitimate solution for optimal leader's position does not always exist. For example, in G3, the optimal leader's position tends to one of the followers, but the asymptotic result does not give a valid solution (the two agents collide). Another interesting observation is that for every rigid formation (such as G4, G5 and G6), the optimal leader's position is always the centroid of the rest of the agents, in which case the manipulability is isotropic and equal to $|\mathcal{F}|$. This phenomenon was previously certified by Theorem 4.4.1.

6.2 Optimal Leader Selection

In this section, we will mostly consider the optimal leader selection problem for single-leader formations in terms of maximizing the minimum manipulability index, which can be formulated as follows,

$$\underset{\mathcal{L}\subset\mathcal{V},|\mathcal{L}|=1}{\text{maximize}} \quad m_{\min}(K,\mathbf{p};\mathcal{L}). \tag{6.1}$$

We assume that the connectivity matrix K and the configuration $\mathbf{p}$ are fixed. Therefore, the search region for the optimization problem is a finite set, and the original problem can be solved using brute force search. In terms of computational complexity, the brute force approach is tractable in that a formation with meaningful manipulability index values often has only a limited number of vertices.

Particularly, if the formation is rigid, then according to Proposition 4.4.1, the minimum manipulability index $m_{\min} = \frac{n}{n\tau+1} - 1$ is a monotonically decreasing function with respect to the torque ratio τ as defined in Definition 4.4.1. As a result, the optimal leader ℓ^* which leads to maximal $m_{\min}$ is given by

$$\ell^* = \arg\min_{\ell} \frac{\|\mathbf{p}_\ell - \mathbf{p}_\odot\|^2}{\sum_{j\in\mathcal{V}} \|\mathbf{p}_j - \mathbf{p}_\odot\|^2} = \arg\min_{\ell} \|\mathbf{p}_\ell - \mathbf{p}_\odot\|.$$

In other words, the optimal leader is the one closest to the centroid $\mathbf{p}_\odot$ of the formation. Since for rigid formations, the relative distance between the centroid and each of the vertices remain constant, thus the optimal leader remains to be ℓ^* regardless of the position and orientation of the formation.

In Fig. 6.3, two formations with same configuration and different topologies are plotted. Particularly, formation (a) is rigid and formation (b) is nonrigid. The manipulability indexes of both formations are computed with each of vertices being assumed as the single leader, and their values are listed in Table 6.1.

We first observe from Table 6.1 that for formation (a), the maximum manipulability index $m_{\max}$ is equal to 5.0000 regardless of the choice of the leader, which in compliance with Proposition 4.4.1. The largest value of minimum manipulability index $m_{\min}$ for formation (a) is obtained when vertex 4 is the leader. This also conforms with the previous discussion as vertex 4 is located near the center of the formation. The same conclusions do not hold for the nonrigid formation (b), where the largest value of $m_{\min}$ is attained when vertex 5 is the leader.

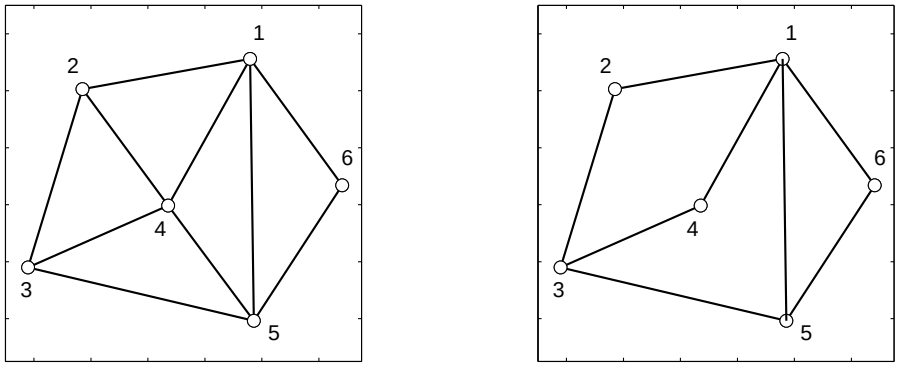

(a) Rigid formation (b) Nonrigid formation

Fig. 6.3.: Example formations for optimal leader selection

6.3 Summary

Formation optimization in the context of leader-follower manipulability was studied in this chapter, with particular emphasis on the single-leader cases. Due to the lack of the concavity properties of the manipulability indexes, the maximization problems of the manipulability indexes are much harder to solve than those of the rigidity indexes. There-

Table 6.1: Computed manipulability indexes for formations in Fig. 6.3

Leader	(a)			(b)		
	$m_{\min}$	$\bar{m}$	$m_{\max}$	$m_{\min}$	$\bar{m}$	$m_{\max}$
1	1.9560	3.4780	5.0000	1.6567	2.8424	4.0281
2	1.9402	3.4701	5.0000	1.1077	1.5596	2.0115
3	1.3158	3.1579	5.0000	1.0980	2.3093	3.5206
4	4.8015	4.9008	5.0000	0.4697	2.7348	4.9999
5	1.8496	3.4248	5.0000	1.8495	3.2203	4.5911
6	1.7286	3.3643	5.0000	1.7285	3.3394	4.6502

fore, only the gradient-based solution algorithms and exhaustive search algorithms were proposed for these problems. Nevertheless, it was proven previously in Section 4.4 and revisited by numerical examples in the chapter that for single-leader rigid formations, the optimal position of the leader is precisely the centroid of the remaining formation formed by the followers.

7. NETWORK LOCALIZATION USING ANGLE-OF-ARRIVAL INFORMATION

Network localization, which is to find the (potentially time-varying) locations of the agents based on available measurements, is one of the crucial tasks in a majority of multi-agent system (including sensor network) applications. A direct method to localize the agents is to use positioning devices such as GPS [61]. However, due to issues such as cost, energy usage, and form factor, such devices are typically available only at a subset of the agents. To localize other agents, additional inter-agent measurements are needed. Designing algorithms that only utilize local measurements to localize the whole network has become a popular research topic in the study of multi-agent systems [62].

Based on the type of measurement data available, localization algorithms can be classified into two categories: distance-based schemes and direction-based schemes. In the distance-based schemes, the neighboring agents measure their relatively distances and then attempt to recover the global positional configuration of the system. Numerous distance-based localization algorithms have been proposed in the literature using, e.g., received signal strength (RSS) [63], time of arrival (TOA) or time difference of arrival (TDOA) [64], or a combination of RF and ultrasound sensing [65]. A common issue with these algorithms however is that eliminating ambiguity, especially reflective ambiguity, is often very difficult and may result in large errors [66]. Indeed, the distance-based localization problem has been shown to be NP-hard [67,68], with unique solution existing only when the underlying graph is globally rigid [14]. Although with some additional assumptions the distance-based localization problem may be significantly simplified [69], it remains a challenging problem in general.

On the other hand, the direction-based localization methodology uses the measurements of angles of arrival (AOA) instead of relative distances. Direction-based localization schemes have not received adequate attention mainly because of two drawbacks. First, lo-

calization problem based on relative angle measurements is also an NP-hard problem [70]. However, if compasses are installed on all the agents to allow for a common global coordinate for the measured angles, the direction-based localization problem could be as easy as solving a set of linear equations [71, 72]. Second, measuring AOA of RF signals requires more advanced hardware such as antenna arrays that are usually expensive and large in size due to wavelength constraint. Nevertheless, in many environmental monitoring applications, the agents/sensors are already equipped with acoustic sensing devices [73], thus acquiring AOA information via acoustic sensors would be a natural inexpensive extension [62]. As the technologies advance in signal measurement and hardware manufacturing, these drawbacks could be alleviated to the point that AOA localization schemes become a viable alternative or at least a valuable supplement to distance-based schemes.

In this chapter[1], the AOA localization problem is studied using the quantitative analysis framework established in the previous chapters. Specifically, it is shown that solving the AOA localization problem is equivalent to finding the solution to a system of linear equations involving the stiffness matrix of the formation. To avoid the matrix inversion, we propose distributed algorithms for both continuous-time and discrete-time dynamics, which are guaranteed to globally asymptotically converge to the desired localization result. These algorithms turn out to be similar to the consensus protocol described in [33] and also the distributed formation controller proposed in [76]. The convergence, delay tolerance as well as potential performance improvements of these algorithms are also studied.

7.1 AOA Localization Problem

The direction-based localization problem that is the focus of this section has been previously formulated and studied in [71, 72] and more recently in [77], all through the rigidity matrix. Different from these studies, we present here an approach that utilizes the stiffness matrix. Although for the purpose of determining localizability the two approaches ultimately lead to equivalent rank conditions, the presented one can also be used to study

[1]Most of the results presented in this chapter are previously published in [74] and [75].

further problems such as quantifying the degree of localizability. Moreover, with a structure resembling the graph Laplacian, the stiffness matrix makes it easy to design distributed localization algorithms, such as the ones to be presented in Section 7.2 and 7.3.

Consider a sensor/agent network consisting of n nodes (vertices) modeled by the leader-follower formation $(\mathcal{V}, \mathbf{p}, K, \mathcal{L})$, where $\mathbf{p}$ represents sensor locations and K their connectivity coefficients. Recall that vertices in $\mathcal{L}$ are leaders and vertices in $\mathcal{F} = \mathcal{V} \setminus \mathcal{L}$ are followers.

Assumption 7.1.1 (Global Coordinate [72,77]) *There exists a global direction in the $\mathbb{R}^2$ plane shared by all the sensors against which the angles are measured.*

The above assumption can be satisfied by either installing compasses on all the sensors, or on a subset of sensors and letting them propagate the coordinate to the remaining ones.

The problem to be studied is formulated below.

Problem 7.1.1 (AOA Localization Problem) *Suppose that the absolute positions of the leaders $\mathbf{p}_\ell$ are known. Given the connectivity coefficients k_{ij} and the angle measurements $\theta_{ij} \in [0, 2\pi)$ for all i, j such that $k_{ij} > 0$, find the absolute positions of the followers $\mathbf{p}_f$ that satisfy $\angle(\mathbf{p}_j - \mathbf{p}_i) = \theta_{ij}$ for all $i \in \mathcal{V}$, $j \in \mathcal{F}$ and $k_{ij} > 0$.*

Remark 7.1.1 *In precedent literature on network localization, nodes with knowledge of their absolute positions are more often referred to as* anchors *or* beacons. *The use of the term* leaders *here is mainly for terminology consistency with previous chapters.*

An AOA localization problem may have no feasible solution if the given angle measurements are inconsistent, e.g., $|\theta_{ij} - \theta_{ji}| \neq \pi$. Perfect measurements generated from a given formation graph, on the other hand, is guaranteed to have at least one solution, which is itself.

Definition 7.1.1 *A leader-follower formation $(\mathcal{V}, \mathbf{p}, K, \mathcal{L})$ is called* AOA localizable *if the AOA localization problem given the anchor positions $\mathbf{p}_\ell$ and angle measurements $\theta_{ij} = \angle(\mathbf{p}_j - \mathbf{p}_i)$ admits only one solution, namely, $\mathbf{p}_f$.*

Lemma 7.1.1 *If $(\mathcal{V}, \mathbf{p}, K, \mathcal{L})$ is fixable, then*

$$\mathbf{p}_f^\perp = -S_{ff}^{-1} S_{f\ell} \mathbf{p}_\ell^\perp. \tag{7.1}$$

Proof Note that $\mathbf{p}^\perp \in \mathrm{null}(S)$ as the direction of $\mathbf{p}^\perp$ corresponds to the simultaneous infinitesimal rotation of all the vertices around the origin. Thus,

$$\begin{bmatrix} S_{ff} & S_{f\ell} \\ S_{af} & S_{aa} \end{bmatrix} \begin{bmatrix} \mathbf{p}_f^\perp \\ \mathbf{p}_\ell^\perp \end{bmatrix} = \mathbf{0} \;\Rightarrow\; S_{ff}\mathbf{p}_f^\perp + S_{f\ell}\mathbf{p}_\ell^\perp = \mathbf{0}. \tag{7.2}$$

By assumption, S_{ff} is nonsingular. The conclusion (7.1) then follows directly from (7.2). ■

Equation 7.2 is an explicit expression of the positions of followers in terms of the anchor positions and angle measurements, hence is more favorable compared to the implicit solution of an optimization problem as in [71].

Notice that S_{ff} and $S_{f\ell}$ depend on θ_{ij} and k_{ij} only, which together with $\mathbf{p}_\ell$ are assumed to be known in Problem 7.1.1. Hence, Lemma 7.1.1 gives an explicit formula for recovering the unknown positions of followers when the anchored formation graph is fixable. The following theorem states that fixability is also a necessary condition of AOA localizability.

Theorem 7.1.1 *A leader-follower formation $(\mathcal{V}, \mathbf{p}, K, \mathcal{L})$ is AOA localizable if and only if it is fixable.*

Proof Sufficiency has been shown in Lemma 7.1.1. To prove necessity, suppose S_{ff} is singular, i.e., $S_{ff}\mathbf{u}_f = \mathbf{0}$ for some $\mathbf{u}_f \neq 0$. Define $\mathbf{u} = \begin{bmatrix} \mathbf{u}_f^\top & \mathbf{0}^\top \end{bmatrix}^\top \in \mathbb{R}^{2n}$ and write it as a stacked vector of $\mathbf{u}_i \in \mathbb{R}^2$, $i \in \mathcal{V}$. Then $\mathbf{u}^\top S \mathbf{u} = 0$, which by the definition of S in (2.4) implies that

$$\sum_{i,j \in \mathcal{V}} k_{ij} (\mathbf{u}_i - \mathbf{u}_j)^\top P_{ij} (\mathbf{u}_i - \mathbf{u}_j) = 0.$$

As each term in the summation is nonnegative, it can only be zero. Hence, for i, j with $k_{ij} > 0$, $\mathbf{u}_i - \mathbf{u}_j \in \mathrm{null}(P_{ij})$, or equivalently, $\mathbf{u}_i^\perp - \mathbf{u}_j^\perp = \ell_{ij} \cdot \mathbf{e}_{ij}$ for some $\ell_{ij} \in \mathbb{R}$.

Define $\tilde{\mathbf{p}} = \mathbf{p} + \delta \cdot \mathbf{u}^{\perp}$ for some small $\delta > 0$. We claim that $\tilde{\mathbf{p}} \neq \mathbf{p}$ is also a solution to the AOA localization problem, which shows that the leader-follower formation is not AOA localizable. In fact, for any $i, j \in \mathcal{V}$ with $k_{ij} > 0$,

$$\begin{aligned}\tilde{\mathbf{p}}_j - \tilde{\mathbf{p}}_i &= (\mathbf{p}_j - \mathbf{p}_i) + \delta\,(\mathbf{u}_j - \mathbf{u}_i)^{\perp} \\ &= (\|\mathbf{p}_j - \mathbf{p}_i\| - \ell_{ij}\delta)\,\mathbf{e}_{ij}.\end{aligned}$$

Thus, $\angle(\tilde{\mathbf{p}}_j - \tilde{\mathbf{p}}_i) = \angle(\mathbf{p}_j - \mathbf{p}_i) = \angle\mathbf{e}_{ij}$ for δ small enough. ■

Fig. 7.1(a) shows a fixable anchor formation graph. One way to verify its fixability is by applying Corollary 2.4.1: after connecting the leaders, the resulting formation graph in Fig. 7.1(b) is infinitesimally rigid. By Theorem 7.1.1, it is also AOA localizable as in Fig. 7.1(c). We note that the formation in Fig. 7.1(b) is not globally rigid due to reflection ambiguity (dashed lines). Thus, this anchored formation graph can be uniquely localized by angle measurements but not by distance measurements.

On the other hand, the formation in Fig. 7.2(a) is not fixable as the augmented formation in Fig. 7.2(b) is globally but not infinitesimally rigid (infinitesimal rotations of the inner triangle do not change the distances between connected vertices). Hence its AOA localization problem admits multiple solutions as shown by the dashed circles in Fig. 7.2(c). This yields an example of anchored formations that can be localized by distance measurements but not by angle measurements.

An interesting observation from the above two examples is that, although fixability is a necessary and sufficient condition for the *direction-based* localizability, it is neither necessary nor sufficient for the *distance-based* localizability, despite the fact that fixability is originally defined via an infinitesimal analysis of distance-based localizability.

7.2 Continuous-Time AOA Localization

A distributed continuous-time AOA localization algorithm is described as follows. Suppose at each vertex $i \in \mathcal{V}$, a variable $\mathbf{x}_i \in \mathbb{R}^2$ is maintained that represents the current estimate of vertex i's position. If vertex i is an anchor which knows its position exactly,

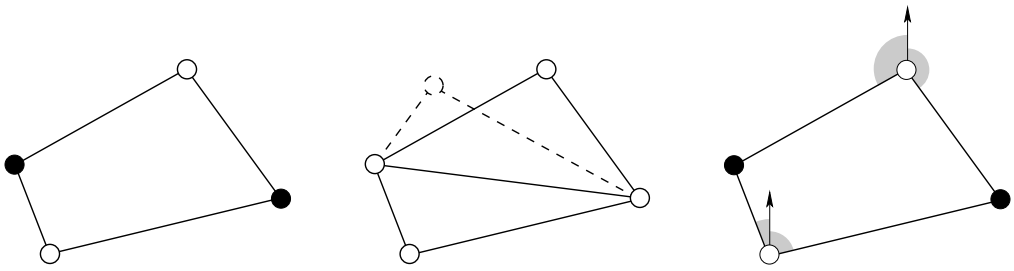

(a) Fixable (b) Infinitesimally but not globally rigid (c) AOA localizable

Fig. 7.1.: AOA localizable formation that is not distance-based localizable

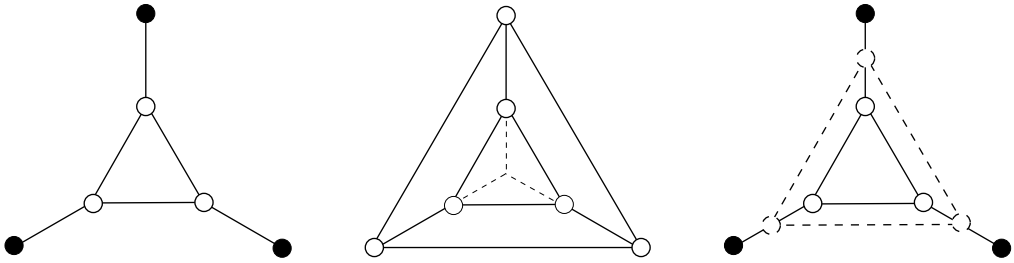

(a) Not fixable (b) Globally but not infinitesimally rigid (c) Not AOA localizable

Fig. 7.2.: Distance-based localizable formation that is not AOA localizable

the value of $\mathbf{x}_i$ is fixed to be $\mathbf{p}_i^{\perp}$. If vertex i is a follower, then with the available angle measurement data θ_{ij} for those vertices j connected with it, $\mathbf{x}_i$ is updated according to the following distributed protocol,

$$\dot{\mathbf{x}}_i(t) = -\sum_{j\in\mathcal{V}} k_{ij} P_{ij}(\mathbf{x}_j(t) - \mathbf{x}_i(t)), \quad \forall\, i \in \mathcal{F}. \tag{7.3}$$

Here, P_{ij} is the projection matrix along the direction of the angle θ_{ij}. In matrix form, equation (7.3) becomes

$$\dot{\mathbf{x}}_f = -S_{ff}\mathbf{x}_f - S_{f\ell}\mathbf{p}_\ell^{\perp}, \tag{7.4}$$

where $\mathbf{x}_f = [\mathbf{x}_i]_{i\in\mathcal{F}}$. This dynamics is similar to the continuous-time average consensus dynamics [33], with the difference being that (7.4) has vector-valued state variables and matrix-valued weights instead of scalars.

Using (7.2), the following result can be proved.

Proposition 7.2.1 *The precise AOA localization result, $\mathbf{x}_f = \mathbf{p}_f^{\perp}$, is an equilibrium point of the dynamics (7.4).*

7.2.1 Stability and Convergence Rate

We first show how the convergence of the algorithm (7.3) depends on the fixability of the underlying formation graph.

Proposition 7.2.2 *If the leader-follower formation is fixable, then under algorithm* (7.3)*, $\mathbf{x}_f \to \mathbf{p}_f^{\perp}$ exponentially fast at the rate $\lambda_1(S_{ff})$, namely, the worst-case rigidity index $r_{\mathrm{w}}(K, \mathbf{p}; \mathcal{L})$.*

Proof Let $\boldsymbol{\varepsilon}(t) = \mathbf{x}_f(t) - \mathbf{p}_f^{\perp}$ be the localization error. Using (7.2) and (7.4), the error dynamics is $\dot{\boldsymbol{\varepsilon}}(t) = -S_{ff}\boldsymbol{\varepsilon}(t)$. For fixable formations, S_{ff} is nonsingular hence positive definite. Thus, $\boldsymbol{\varepsilon}(t) \to 0$ at the exponential rate $\lambda_1(S_{ff})$ in the worst case. ■

We simulate the distributed continuous-time protocol (7.4) with a square-shaped formation consisting of 50 agents for three different set of leaders. The connectivity coefficient

between each pair of neighboring agents is set to be 2 uniformly. The simulation results are shown in Fig. 7.3, where the red filled dots denote the leaders and the white dots denote the agents to be localized. In the first case (Fig. 7.3(a)–(d)), the localization process converges to the true ground configuration fairly quickly. Intuitively speaking, if the whole formation is viewed as a mechanical structure, the selected leaders are effective in pinning down the whole formation as they are located at the corners. As we remove some of the leaders, as is shown in Fig. 7.3(e)–(h) and (i)–(l), the AOA based protocol may become less efficient in localizing the agents that are not geographically surrounded by leaders. A heuristic explanation is that the directional information is effective in distinguishing different shapes, but less effective at determining the scale of the shape. Hence, if the leaders are unable to stretch a certain part of the formation, e.g., the right wing of the case in Fig. 7.3(i)–(k), it may take very long for those agents to converge to the correct scale.

7.2.2 Delay Tolerance

We consider a more general scenario where there is a constant communication delay τ across all links. The localization dynamics with delay becomes

$$\dot{\mathbf{x}}_i(t) = -\sum_{j\in\mathcal{V}} k_{ij}P_{ij}(\mathbf{x}_j(t-\tau) - \mathbf{x}_i(t-\tau)), \quad \forall\, i \in \mathcal{F}. \tag{7.5}$$

The stability of such delayed systems is characterized by a threshold value of τ in the following proposition. The proof follows very similar lines as those of the consensus algorithm in [33].

Proposition 7.2.3 *Given an anchored formation $(\mathcal{V}, \mathbf{p}, K, \mathcal{L})$ that is fixable, the dynamics (7.5) is stable if the communication delay $\tau < \tau^*$, where $\tau^* = \pi/2\lambda_{\max}(S_{ff})$.*

7.2.3 Bounds of Performance Indexes

Knowing the values of $\lambda_1(S_{ff})$ and $\lambda_{\max}(S_{ff})$ is important as they characterize the convergence speed and the delay tolerance of the distributed algorithm (7.3). In this section,

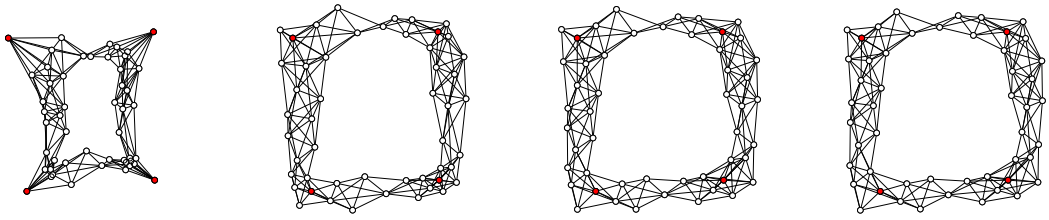

(a) $t = 1$s (b) $t = 5$s (c) $t = 15$s (d) ground truth

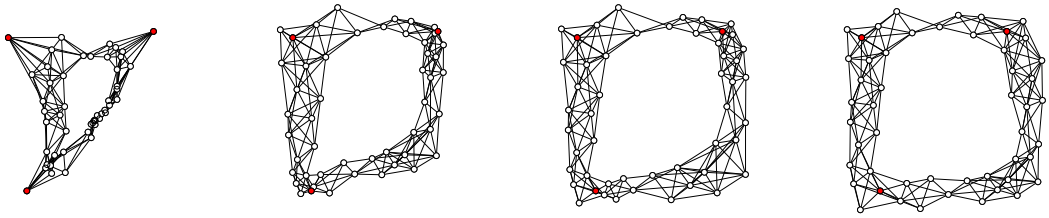

(e) $t = 1$s (f) $t = 5$s (g) $t = 15$s (h) ground truth

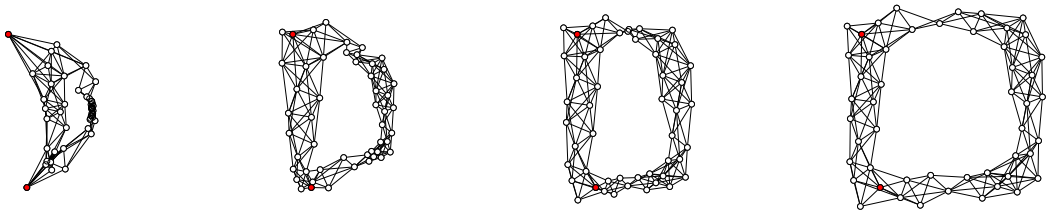

(i) $t = 1$s (j) $t = 5$s (k) $t = 15$s (l) ground truth

Fig. 7.3.: Simulation results using different sets of leaders

we derive some estimation bounds on these two quantities that can be easily computed distributively by consensus-type algorithms.

Proposition 7.2.4 *For any given leader-follower formation $(\mathcal{V}, \mathbf{p}, K, \mathcal{L})$, we have $\underline{\lambda} \leq \lambda_{\max}(S_{ff}) \leq \overline{\lambda}$, where*

$$\underline{\lambda} = \frac{\sum_{i\in\mathcal{F}} \sum_{j\in\mathcal{V}\setminus\{i\}} k_{ij}}{2|\mathcal{F}|},$$
$$\overline{\lambda} = \max_{i\in\mathcal{F}} \left\{ \lambda_{\max} \left(\sum_{j\in\mathcal{V}\setminus\{i\}} k_{ij} P_{ij} \right) + \sum_{j\in\mathcal{F}\setminus\{i\}} k_{ij} \right\}.$$

As a result, the delay margin τ^* is bounded by

$$\pi/2\overline{\lambda} \leq \tau^* \leq \pi/2\underline{\lambda}.$$

Proof For the lower bound, using (2.4) and the fact that each projection matrix P_{ij} has trace 1, we obtain

$$\sum_{k=1}^{2|\mathcal{F}|} \lambda_k(S_{ff}) = \mathrm{tr}(S_{ff}) = \sum_{i\in\mathcal{F}} \mathrm{tr} \left(\sum_{j\in\mathcal{V}\setminus\{i\}} k_{ij} P_{ij} \right) = \sum_{i\in\mathcal{F}} \sum_{j\in\mathcal{V}\setminus\{i\}} k_{ij}.$$

The lower bound follows as the maximum eigenvalue is no smaller than the average of all eigenvalues.

For the upper bound, note that each diagonal 2-by-2 block S_{ii} of S_{ff} is positive semidefinite. Let $\alpha_i \leq \beta_i$ be its only two eigenvalues, then $\|S_{ii}\|_2 = \beta_i$. Each off-diagonal 2-by-2 block satisfies $\|S_{ij}\|_2 = k_{ij}\|P_{ij}\|_2 = k_{ij}$. According to the Generalized Gershgorin Circle Theorem [78, Theorem 2], for each eigenvalue λ of S_{ff}, the following inequality must hold for at least one $i \in \mathcal{F}$,

$$\sum_{j\in\mathcal{F}\setminus\{i\}} \|S_{ij}\|_2 \geq \left(\left\| (S_{ii} - \lambda I_2)^{-1} \right\|_2 \right)^{-1} = \min\left\{ |\alpha_i - \lambda|, |\beta_i - \lambda| \right\},$$

which implies that

$$\exists\, i \in \mathcal{F} \text{ such that } \lambda \leq \beta_i + \sum_{j\in\mathcal{F}\setminus\{i\}} k_{ij}.$$

Taking the maximum value of the right hand side over all $i \in \mathcal{F}$ yields the desired result. ■

Both bounds in Proposition 7.2.4 are of a form that is amenable to distributive computation: $\underline{\lambda}$ by local computations followed by an average consensus; and $\overline{\lambda}$ by local computations followed by a max consensus. Therefore, the delay tolerance margin for the AOA localization algorithm running on any formation graph can be estimated in a distributed way.

Remark 7.2.1 *The upper bound $\overline{\lambda}$ for $\lambda_{\max}(S_{ff})$ can be further relaxed as follows,*

$$\overline{\lambda} \leq \max_{i \in \mathcal{F}} \left\{ 2 \cdot \sum_{j \in \mathcal{F} \setminus \{i\}} k_{ij} + \sum_{j \in \mathcal{L}} k_{ij} \right\}.$$

The new upper bound may be more desirable in some applications as it no longer depends on the vertex positions.

As pointed out in Section 2.3, the well studied graph Laplacian matrix has half the dimension as that of S. The following result establishes new estimation bounds on $\lambda_1(S_{ff})$ and $\lambda_{\max}(S_{ff})$ using the Laplacian matrix.

Proposition 7.2.5 *Let L be the Laplacian matrix of the underlying weighted graph $(\mathcal{V}, K)$ defined in* (2.5)*. Let L_{ff} be the submatrix of L consisting of the rows and columns that correspond to the followers. Then $\lambda_1(S_{ff}) \leq \lambda_1(L_{ff})/2$ and $\lambda_{\max}(S_{ff}) \geq \lambda_{\max}(L_{ff})/2$.*

Proof As each $P_{ij} \in \mathbb{R}^{2\times 2}$ is a projection matrix, we have $P_{ij} + QP_{ij}Q^{-1} = I_2$ where Q is the 2-by-2 orthogonal matrix corresponding to the 90° counterclockwise rotation. Hence, the following holds according to (2.4) and (2.5),

$$S_{ff} + (I_{|\mathcal{F}|} \otimes Q) S_{ff} (I_{|\mathcal{F}|} \otimes Q)^{-1} = L_{ff} \otimes I_2. \tag{7.6}$$

Note that $L_{ff} \otimes I_2$ has twice the dimension as that of L_{ff} and its spectrum is exactly that of L_{ff} repeated twice. Since $(I_{|\mathcal{F}|} \otimes Q) S_{ff} (I_{|\mathcal{F}|} \otimes Q)^{-1}$ is similar to S_{ff}, using the Rayleigh quotients argument on (7.6), we deduce that

$$2\lambda_1(S_{ff}) \leq \lambda_1(L_{ff}), \quad 2\lambda_{\max}(S_{ff}) \geq \lambda_{\max}(L_{ff}),$$

which yield the desired conclusion. ■

Proposition 7.2.5 states that both the convergence rate and the delay tolerance of the AOA localization algorithm are upper bounded by the corresponding performance metrics (after proper scaling) of the leader-follower consensus algorithm running on the same formation graph. This provides a connection between the studies of the AOA localization problem and the consensus problem. On the other hands, the bounds in Proposition 7.2.5 are in general not tight.

7.2.4 Parameter Optimization

Assume that the underlying graph topology $\mathcal{E} = \{(i,j) \,|\, k_{ij} > 0\}$ is fixed, while the values of $k_{ij} > 0$ can be varied through network resource re-allocation, e.g., moving more accurate sensors to strategically more important positions, increasing the transmission power at certain vertices, etc. A natural question is how to choose k_{ij} to maximize the convergence rate $\lambda_1(S_{ff})$ and the delay tolerance margin $\pi/2\lambda_{\max}(S_{ff})$ simultaneously. One way to formulate this is by solving the following condition number minimization problem:

$$\underset{K \in \mathcal{K}(\mathcal{E})}{\text{minimize}} \quad \frac{\lambda_{\max}(S_{ff}(K))}{\lambda_1(S_{ff}(K))}, \tag{7.7}$$

Here, $\mathcal{K}(\mathcal{E})$ denotes the set of all feasible K consistent with the given topology $\mathcal{E}$. Problem (7.7) is equivalent to either of the following two problems: 1) maximize the convergence rate while keeping the delay margin at a certain value; 2) maximize the delay margin while keeping the convergence rate at a given value.

Using the relation (2.8) and the fact that both the numerator and denominator in (7.7) are linear in K, Problem (7.7) can be cast as the following semidefinite program,

$$\begin{array}{ll} \underset{K \in \mathcal{K}(\mathcal{E})}{\text{minimize}} & \mu \\ \text{subject to} & \begin{bmatrix} R_f^\top \Lambda_K R_f - I & \\ & \mu I - R_f^\top \Lambda_K R_f \end{bmatrix} \succeq 0, \end{array} \tag{7.8}$$

which can be solved very efficiently.

Remark 7.2.2 *In the above optimization, the vertex positions as encoded in R_f are assumed to be known* a priori*, which is not the case for localization problems in practice.*

Nevertheless, the optimization problem discussed here is still of potential use in several scenarios. Firstly, if the positions of the vertices can be roughly estimated in advance, then the solution of the problem (7.8) using the rough guess may still identify the bottleneck links in the formation that need to strengthen the most, thus providing at least qualitative directions for topology design and link resource allocation [50]. Secondly, in the scenario where the agents/sensors are mobile and require localization continually, a one-shot optimization of the link connectivity coefficients could improve the performance of the dynamic localization process.

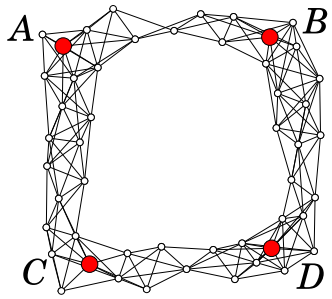

Fig. 7.4.: Sample leader-follower formation graph (ground truth)

As a numerical example, we implement the distributed algorithm (7.5) with uniform communication delay τ on the formation in Fig. 7.4. Two cases with different connectivity matrices K are tested. In the first case, all edges have the same connectivity coefficient 2, and the resulting S_{ff} has the smallest and largest eigenvalues $\lambda_1 \approx 0.072$ and $\lambda_{\max} \approx 18.71$, respectively. For comparison purpose, the bounds in Proposition 7.2.4 yields $14.39 \leq \lambda_{\max} \leq 31.12$. The corresponding delay margin τ^* is hence $\pi/2\lambda_{\max} \approx 84$ ms. By solving the optimization problem (7.8), the optimal K^* is obtained and adopted in the second case study. Calculation shows that while $\lambda_{\max}$ remains the same as in the first case, λ_1 is increased to $\lambda_1 = 0.14$, essentially doubling the convergence rate compared to the uniform K case. Alternatively, we can scale K^* so that the resulting S_{ff} has the same λ_1, hence the convergence rate, as in the first case, but with $\lambda_{\max} = 9.62$, which implies that the delay margin has been increased to 163 ms.

Simulation results of the two test cases (uniform K and optimal K^*, with the same $\lambda_{\max}$ values) are illustrated in Fig. 7.5, which plots the localization errors as a function of time (in seconds) for three different delays. As can be seen, the delay margins for both cases lie between 80 ms and 90 ms. When both dynamics are stable, as expected, the second case using the optimized connectivity matrix K^* converges to the true configuration faster in the long run.

7.2.5 Switching Topologies

We next consider the case where the graph topology $\mathcal{E}$ may vary with time. In practical applications, this could be due to obstructions between vertices, sensor sleeping/wakeup, etc. For ease of analysis, suppose that the connectivity matrix K can only switch among the m matrices in $\mathcal{J} = \left\{K^{(1)}, \ldots, K^{(m)}\right\}$. The AOA localization algorithm (7.3) in Section 7.3 then becomes

$$\dot{\mathbf{x}}_i(t) = -\sum_{j\in\mathcal{V}} k_{ij}^{(\sigma_t)} P_{ij}(\mathbf{x}_j(t) - \mathbf{x}_i(t)), \quad \forall\, i \in \mathcal{F}, \tag{7.9}$$

where σ_t is the *mode sequence* that takes values in the mode set $\mathcal{M} = \{1, \ldots, m\}$ for $t \geq 0$. We assume that σ_t is right-continuous and has a dwell time $\delta > 0$, i.e., consecutive switches are at least δ time apart.

Again let $\boldsymbol{\varepsilon}(t) = \mathbf{x}_f(t) - \mathbf{p}_f^{\perp}$ be the localization error of the followers. The error dynamics for the algorithm (7.9) is

$$\dot{\boldsymbol{\varepsilon}}(t) = -S_{ff}^{(\sigma_t)} \boldsymbol{\varepsilon}(t). \tag{7.10}$$

Here, $S_{ff}^{(\sigma_t)} = R_f^{\top} \Lambda_{K^{(\sigma_t)}} R_f$. The algorithm (7.9) will converge to the true solution $\mathbf{p}_f^{\top}$ if and only if the system (7.10) is asymptotically stable under any valid mode sequence.

Definition 7.2.1 *The set of* recurrent modes *for a given mode sequence σ_t is defined as those modes that appear infinitely often in σ_t:*

$$\mathcal{M}_\infty = \bigcap_{t\geq 0} \bigcup_{s\geq t} \{\sigma_s\} \subset \mathcal{M}.$$

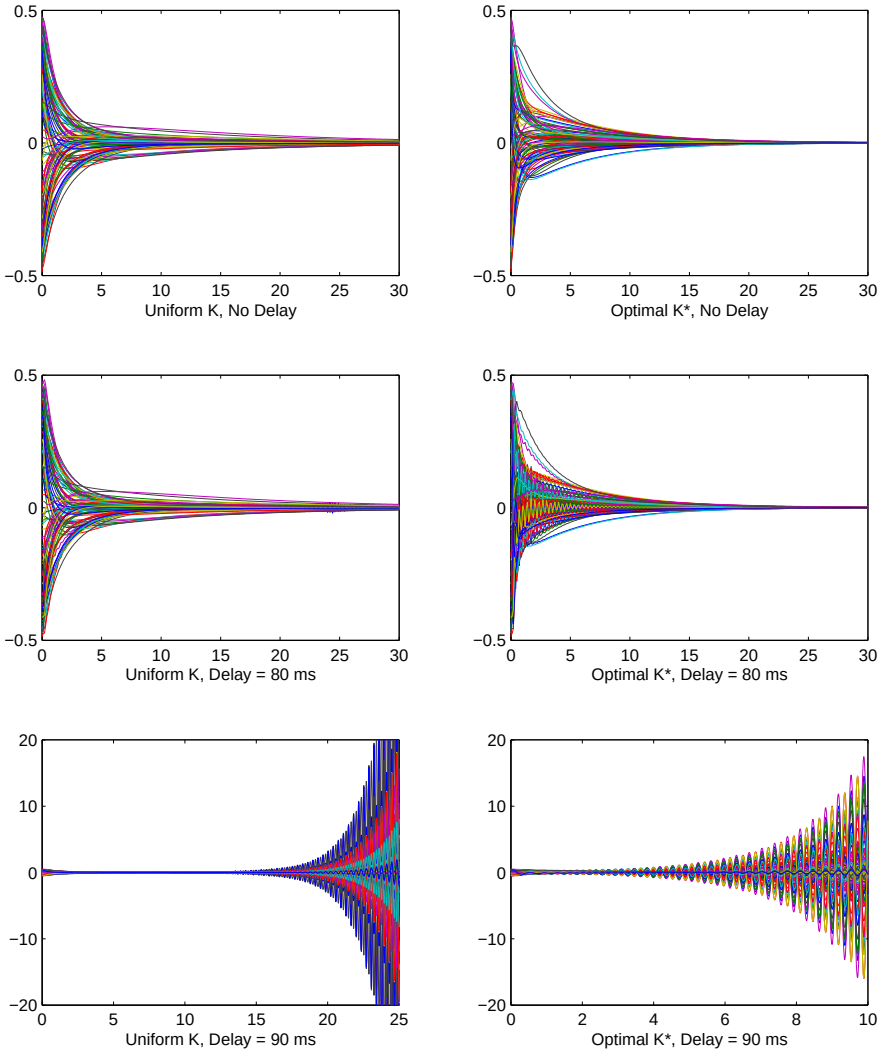

Fig. 7.5.: Comparison of convergence speed and delay performance between uniform connectivity and optimal connectivity.

We now give the necessary and sufficient conditions for the convergence of the algorithm (7.9).

Theorem 7.2.1 *Given the set of vertices $\mathcal{V}$, the position configuration $\mathbf{p}$ and the anchor set $\mathcal{A}$. Suppose the connectivity matrix K switches among the set $\mathcal{J} = \left\{K^{(1)}, \ldots, K^{(m)}\right\}$ and the mode sequence σ_t has a strictly positive dwell time $\tau > 0$. Then the distributed AOA localization algorithm as described in* (7.9) *will always converge to the unique true solution $\mathbf{p}_f$ if and only if the anchored formation $(\mathcal{V}, \mathbf{p}, K, \mathcal{L})$ is fixable, where $K = \sum_{\sigma \in \mathcal{M}_\infty} K^{(\sigma)}$.*

Theorem 7.2.1 can be proven using tools in Lyapunov stability theory, which will be introduced as follows. A *Lyapunov function* for the autonomous system:

$$\dot{\mathbf{x}} = f(\mathbf{x}),\ \mathbf{x} \in \mathbb{R}^n$$

is a continuous function $V : \mathbb{R}^n \to \mathbb{R}$ satisfying: (i) $V(0) = 0$; (ii) $V(\mathbf{x}) > 0,\ \forall\, \mathbf{x} \in \mathbb{R}^n \setminus \{\mathbf{0}\}$; (iii) $\dot{V}(\mathbf{x}) \leq 0,\ \forall\, \mathbf{x} \in \mathbb{R}^n$.

Lemma 7.2.1 (Lyapunov Stability Criterion [79]) *If an autonomous system given by*

$$\dot{\mathbf{x}} = f(\mathbf{x}),\ \mathbf{x} \in \mathbb{R}^n$$

admits a Lyapunov function $V : \mathbb{R}^n \to \mathbb{R}$ which in addition satisfies

1. $\dot{V}(\mathbf{x}) < 0,\ \forall\, \mathbf{x} \in \mathbb{R}^n \setminus \{\mathbf{0}\}$;
2. $\|\mathbf{x}\| \to \infty \Rightarrow V(\mathbf{x}) \to \infty$,

then the autonomous system is globally asymptotically stable at the origin.

We now prove Theorem 7.2.1 using the above lemma.

Proof First assume that $(\mathcal{V}, \mathbf{p}, K, \mathcal{L})$ is not fixable, i.e., its stiffness matrix S_{ff} is singular: $S_{ff}^{(\sigma)}\mathbf{u} = \mathbf{0}$ for some $\mathbf{u} \neq 0$. Note that $S_{ff} = \sum_{\sigma \in \mathcal{M}_\infty} S_{ff}^{(\sigma)}$ with each $S_{ff}^{(\sigma)} \succeq 0$. Therefore, $S_{ff}\mathbf{u} = \mathbf{0}$ implies $\mathbf{u}^\top S_{ff}\mathbf{u} = \sum_{\sigma \in \mathcal{M}_\infty} \mathbf{u}^\top S_{ff}^{(\sigma)}\mathbf{u} = 0$ and hence $S_{ff}^{(\sigma)}\mathbf{u} = \mathbf{0}$ for each

$\sigma \in \mathcal{M}_\infty$. In other words, $\mathbf{u}$ is a common equilibrium point of the error dynamics (7.10) for all the recurrent modes. As a result, localization error does not always converge to zero for all initial conditions.

Conversely, assume that $(\mathcal{V}, \mathbf{p}, K, \mathcal{L})$ is fixable. Define

$$V(\boldsymbol{\varepsilon}(t)) = \frac{1}{2}\|\boldsymbol{\varepsilon}(t)\|^2.$$

Then it is easily verified that $V(\cdot)$ is a common Lyapunov function for the error dynamics (7.10) of all the modes. In fact,

$$\dot{V}(\boldsymbol{\varepsilon}(t)) = \boldsymbol{\varepsilon}(t)^\top \dot{\boldsymbol{\varepsilon}}(t) = -\boldsymbol{\varepsilon}(t)^\top S_{ff}^{(\sigma_t)} \boldsymbol{\varepsilon}(t) \leq 0.$$

Starting from the initial error $\boldsymbol{\varepsilon}(t_0) = \boldsymbol{\varepsilon}_0$, we use the following procedures to recursively find intervals $[s_k, t_k)$, $k = 1, 2, \ldots$, in which the trajectory of $\boldsymbol{\varepsilon}$ is not constant:[2]

$$s_k = \inf\left\{s : s > t_{k-1}, \boldsymbol{\varepsilon}(t)^\top S_{ff}^{(\sigma_t)} \boldsymbol{\varepsilon}(t) > 0\right\}, \tag{7.11}$$

$$t_k = \inf\left\{t : t > s_k, \sigma_t \neq \sigma_{s_k}\right\}. \tag{7.12}$$

with the definition $\inf \emptyset = +\infty$. Since S_{ff} is nonsingular, for every $\mathbf{u} \in \mathbb{R}^{2|\mathcal{F}|} \setminus \{\mathbf{0}\}$ there exists $\sigma \in \mathcal{M}_\infty$ such that $\mathbf{u}^\top S_{ff}^{(\sigma)} \mathbf{u} > 0$. Therefore, it is guaranteed that $s_k < +\infty$ whenever $t_{k-1} < +\infty$. Furthermore, we have $\sum_{i=1}^{k}(t_k - s_k) \to +\infty$ as $k \to \infty$. Define $\omega : [t_0, +\infty) \to [t_0, +\infty)$ as

$$\omega(t) = \begin{cases} \sum_{0<i<k}(t_i - s_i) + (t - s_k) & \text{if } s_k \leq t < t_k \\ \sum_{0<i<k}(t_i - s_i) & \text{if } t_{k-1} \leq t < s_k. \end{cases}$$

and let $\hat{\boldsymbol{\varepsilon}}(t) \triangleq \boldsymbol{\varepsilon}(\omega(t))$. Note that $\hat{\boldsymbol{\varepsilon}}(t)$ is continuous, piecewise differentiable,

$$\lim_{t \to +\infty} \hat{\boldsymbol{\varepsilon}}(t) = \lim_{t \to +\infty} \boldsymbol{\varepsilon}(t),$$

and

$$\begin{aligned} \dot{V}(\hat{\boldsymbol{\varepsilon}}(t)) &= \boldsymbol{\varepsilon}(\omega(t))^\top \dot{\boldsymbol{\varepsilon}}(\omega(t)) \\ &= -\boldsymbol{\varepsilon}(\omega(t))^\top S_{ff}^{\left(\sigma_{\omega(t)}\right)} \boldsymbol{\varepsilon}(\omega(t)) < 0, \ \forall\, t \geq t_0, \end{aligned}$$

[2] In fact, s_k, t_k $(k > 0)$ are functions of $\boldsymbol{\varepsilon}_0$, which we omit for simplicity of notations.

where the strict inequality follows from the definition in (7.11). According to Lemma 7.2.1, $\lim_{t\to+\infty} \hat{\boldsymbol{\varepsilon}}(t) = 0$. Therefore, the error dynamics of the distributed AOA localization algorithm as described in (7.10) is globally asymptotically stable. ■

7.3 Discrete-Time AOA Localization

According to Theorem 7.1.1, Equation (7.1) provides a feasible and reliable method of solving the AOA Localization Problem. However, computing S_{ff}^{-1} is time-costly and technically difficult to carry out in a distributed fashion. To overcome this limitation, we decompose S_{ff} into $D_{ff} - F_{ff}$, where D_{ff} is composed of the 2×2 diagonal blocks in S_{ff} and F_{ff} the negated off-diagonal blocks. We first need to verify the invertibility of matrix D_{ff}.

Proposition 7.3.1 *If a leader-follower formation is fixable, then all* 2*-by-*2 *diagonal blocks of the matrix* S_{ff} *are invertible.*

Proof We prove by contraposition. Suppose a 2-by-2 diagonal block of S_{ff}, say S_{ii}, is singular. Recall from (2.4) that S_{ii} is the sum of the projection matrices. In the two-dimensional case, S_{ii} is singular if and only if all the projection matrices share the same null space. This implies that the null space shared by all the 2-by-2 blocks in the i-th block column and row is nontrivial. Therefore, S_{ff} must also be singular. ■

We assume that the leader-follower formation is fixable. By Proposition 7.3.1, D_{ff} is invertible. Therefore, (7.1) can be manipulated into the following iterative form,

$$\mathbf{p}_f^{\perp} = D_{ff}^{-1} F_{ff} \mathbf{p}_f^{\perp} - D_{ff}^{-1} S_{f\ell} \mathbf{p}_{\ell}^{\perp}. \tag{7.13}$$

We propose as follows a damped version of (7.13) which gives the same solution,

$$\mathbf{p}_f^{\perp} = (D_{ff} + \Lambda)^{-1} (F_{ff} + \Lambda) \mathbf{p}_f^{\perp} - (D_{ff} + \Lambda)^{-1} S_{f\ell} \mathbf{p}_{\ell}^{\perp}, \tag{7.14}$$

where Λ is assumed to be 2-by-2 block diagonal , i.e., $\Lambda = \mathrm{diag}(\Lambda_{ii})$ where $\Lambda_{ii} \in \mathbb{R}^{2\times 2}$. According to (2.4), we can write (7.14) in the decentralized form as below,

$$\mathbf{p}_i^{\perp} = \left(\Lambda_{ii} + \sum_{j \in \mathcal{V}\setminus\{i\}} k_{ij} P_{ij} \right)^{-1} \left(\Lambda_{ii} \mathbf{p}_i^{\perp} + \sum_{j \in \mathcal{V}\setminus\{i\}} k_{ij} P_{ij} \mathbf{p}_j^{\perp} \right), \ \forall\, i \in \mathcal{F}.$$

The above expression can be viewed as the weighted average of the vectors $\mathbf{p}_i$ and $\mathbf{p}_j$ with matrix-valued weights Λ_{ii} and $k_{ij}P_{ij}$. Now we can design the following algorithm to solve (7.14) distributedly.

Algorithm 1 Distributed AOA Localization Algorithm for agent i at time step k

Input: $\Lambda_{ii} \in \mathbb{R}^{2\times 2},\ \hat{\mathbf{p}}_i^{\perp}[k],\ \hat{\mathbf{p}}_j^{\perp}[k],\ \theta_{ij} \in [0, 2\pi), \quad (j \in \mathcal{N}_i)$

Output: $\hat{\mathbf{p}}_i^{\perp}[k+1]$

$A \leftarrow \Lambda_{ii}$

$\mathbf{u} \leftarrow \Lambda_{ii}\hat{\mathbf{p}}_i[k]$

for all $j \in \mathcal{N}_i$ **do**

$\mathbf{e} \leftarrow [\cos\theta_{ij}, \sin\theta_{ij}]^\top$

$\mathbf{u} \leftarrow \mathbf{u} + \mathbf{e}\mathbf{e}^\top\hat{\mathbf{p}}_j^{\perp}[k]$

$A \leftarrow A + \mathbf{e}\mathbf{e}^\top$

end for

$\hat{\mathbf{p}}_i^{\perp}[k+1] \leftarrow A^{-1}\mathbf{u}$

Remark 7.3.1 *Algorithm 1 is essentially similar to a consensus process over the network. The subtle difference is that each node will converge to its respective localized position through the execution of the algorithm; whereas in the classical notion of consensus, all nodes converge to the same value over the network.*

7.3.1 Stability and Convergence Rate

Let $\hat{\mathbf{p}}_f[k]$ in Algorithm 1 denote the estimated positions of the followers at step k. Note that the discrete-time dynamics of $\hat{\mathbf{p}}_f[k]$ can be expressed as below,

$$\hat{\mathbf{p}}_f^{\perp}[k+1] = (D_{ff} + \Lambda)^{-1}(F_{ff} + \Lambda)\,\hat{\mathbf{p}}_f^{\perp}[k] - (D_{ff} + \Lambda)^{-1} S_{f\ell}\mathbf{p}_\ell^{\perp}. \tag{7.15}$$

We hereby define the convergence of the dynamics (7.15), thus equivalently, the convergence of the algorithm (that is, Algorithm 1).

Definition 7.3.1 (Convergence) *Given a leader-follower formation $(\mathcal{V}, \mathbf{p}, K, \mathcal{L})$, if for any initial guess $\hat{\mathbf{p}}_f^{\perp}[0] \in \mathbb{R}^{2n}$, the dynamics* (7.15) *always converges to the true configuration $\mathbf{p}_f$, then the algorithm is said to be* convergent.

It can be readily inferred from Theorem 7.1.1 that the fixability of the underlying formation graph is necessary for convergence. The following theorem gives a sufficient condition for convergence.

Theorem 7.3.1 (Sufficient Condition of Convergence) *The proposed algorithm is convergent if $(\mathcal{V}, \mathbf{p}, K, \mathcal{L})$ is fixable and Λ is symmetric positive definite.*

Proof Since $(\mathcal{V}, \mathbf{p}, K, \mathcal{L})$ is fixable, the convergence of the algorithm is implied by the stability of the discrete time-invariant affine system (7.15), which is given by

$$\rho\left(\left(D_{ff}+\Lambda\right)^{-1}\left(F_{ff}+\Lambda\right)\right) < 1,$$

where $\rho(\cdot)$ denotes the spectral radius. Since the following matrix,

$$\left(D_{ff}+\Lambda\right)^{-\frac{1}{2}}\left(F_{ff}+\Lambda\right)\left(D_{ff}+\Lambda\right)^{-\frac{1}{2}},$$

is symmetric and similar to $\left(D_{ff}+\Lambda\right)^{-1}\left(F_{ff}+\Lambda\right)$, we can alternatively show that

$$I \succ \left(D_{ff}+\Lambda\right)^{-\frac{1}{2}}\left(F_{ff}+\Lambda\right)\left(D_{ff}+\Lambda\right)^{-\frac{1}{2}} \succ -I.$$

The first part of the inequality is easily seen given the positive definiteness of $\left(D_{ff}+\Lambda\right)^{-\frac{1}{2}}$ and $D_{ff}-F_{ff}$ (which is equal to S_{ff} and positive definite, by the assumption that the formation is fixable).

For the second part, it suffices to show that $D_{ff}+F_{ff}+2\Lambda \succ 0$. We observe that $D_{ff}+F_{ff}$ is the matrix whose off-diagonal blocks are negated compared to S_{ff}. Inspired by the following relation,

$$D_{ff}-F_{ff} = S_{ff} = R_f^{+\top}\Lambda_K R_f^{+},$$

we can see that $D_{ff}+F_{ff}$ can be similarly decomposed as follows,

$$D_{ff}+F_{ff} = \tilde{R}_f^{+\top}\Lambda_K \tilde{R}_f^{+}, \tag{7.16}$$

where the matrix $\tilde{R}_f^+$ consists of rows in the following form

$$\tilde{\mathbf{r}}^{(ij)} = \big[\mathbf{0} \ \cdots \ \mathbf{0} \ \underbrace{\mathbf{e}_{ij}^\top}_{i\text{-th block}} \ \cdots \ \underbrace{\mathbf{e}_{ij}^\top}_{\substack{j\text{-th block} \\ \textit{(negated)}}} \ \mathbf{0} \ \cdots \ \mathbf{0}\big]^\top.$$

The decomposition in (7.16) certifies that $D_{ff} + F_{ff} \succeq 0$. Consequently, we have $D_{ff} + F_{ff} + 2\Lambda \succ 0$. ■

We test our distributed AOA localization algorithm on a multi-agent network consisting of 50 agents as shown in Fig. 7.4. Four agents at the corners of the formation (marked by red dots and labeled A, B, C and D) serve as leaders (i.e., their positions are *a priori* known). Fig. 7.6 shows the simulation result. As is theoretically proven, the localization result converges to the ground truth as the number of iterations increases. Fig. 7.7 illustrates the localization error with respect to the number of iterations. The solid line denotes the convergence performance for the case shown in Fig. 7.6, while the two dashed lines denote the performance for the same formation but starting from different random initial guesses. We see that after a large number of iterations, the convergence rate, depicted by the slope of logarithmic line, converge to the same value. This value is essentially determined by the largest eigenvalue of the matrix $(D_{ff} + \Lambda)^{-1}(F_{ff} + \Lambda)$. We make some comments toward the end of the paper on the potential improvements that can be made in future works.

7.4 Steady-State Error Analysis

In the study of AOA localization problem so far, the leaders' positions and the angle measurements are assumed to be precisely known. In practice these are often subject to errors. In this case, the algorithm (7.3) will still converge, though to a result that deviates from the ground truth. In this section, through perturbational analyses, we will study how these measurement errors affect the localization results.

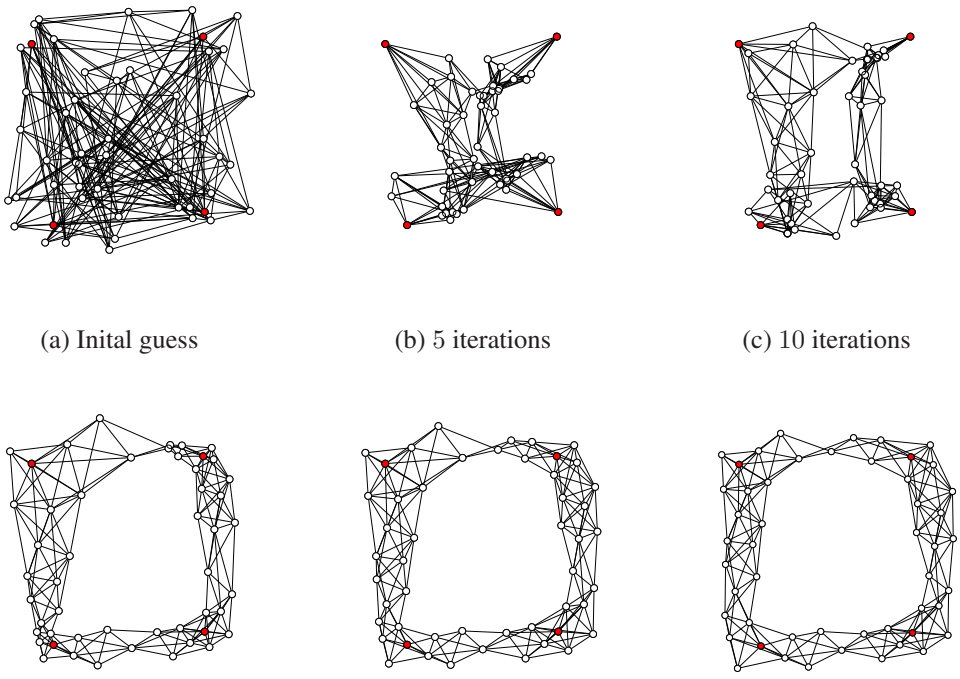

(a) Inital guess (b) 5 iterations (c) 10 iterations

(d) 50 iterations (e) 100 iterations (f) Ground truth

Fig. 7.6.: Simulation result of the algorithm

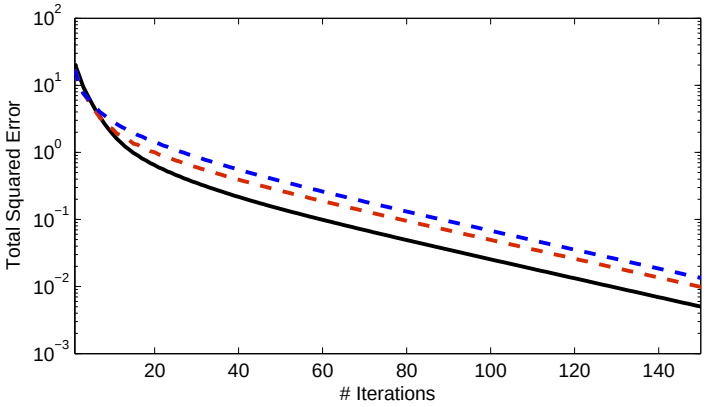

Fig. 7.7.: Convergence performance of localization algorithm

7.4.1 Inaccurate Leader Positions

Consider the scenario where the measurements of the absolute leader positions differ from their true values by $\delta\mathbf{p}_\ell$. From (7.1) the resulting steady-state localization error is

$$\delta\mathbf{p}_f(\delta\mathbf{p}_\ell) = (I_{|\mathcal{F}|} \otimes Q) S_{ff}^{-1} S_{f\ell} (\delta\mathbf{p}_\ell)^\perp. \tag{7.17}$$

We propose two metrics to quantify how much the errors in leader positions affect the localization results.

Definition 7.4.1 *The* worst-case error propagation coefficient *of leader positions, denoted by $\varepsilon_\ell^{\mathrm{w}}$, is defined as*

$$\varepsilon_\ell^{\mathrm{w}} \triangleq \max_{\delta\mathbf{p}_\ell \neq \mathbf{0}} \frac{\|\delta\mathbf{p}_f(\delta\mathbf{p}_\ell)\|}{\|\delta\mathbf{p}_\ell\|}.$$

It can be readily seen from (7.17) that $\varepsilon_\ell^{\mathrm{w}} = \left\|S_{ff}^{-1} S_{f\ell}\right\|_2$, i.e., the largest singular value of $S_{ff}^{-1} S_{f\ell}$.

Definition 7.4.2 *The* mean error propagation coefficient *of leader positions, denoted by $\varepsilon_\ell^{\mathrm{m}}$, is defined as*

$$\varepsilon_\ell^{\mathrm{m}} \triangleq \sqrt{\mathbb{E}\left[\frac{\|\delta\mathbf{p}_f(\delta\mathbf{p}_\ell)\|^2}{\|\delta\mathbf{p}_\ell\|^2}\right]},$$

where $\delta\mathbf{p}_\ell$ is random and $\mathbb{E}$ is the expectation operator.

Proposition 7.4.1 *Suppose $\delta\mathbf{p}_\ell$ has an isotropic probability distribution (i.e., equally likely in all directions) and $P(\delta\mathbf{p}_\ell = \mathbf{0}) = 0$, then*

$$\varepsilon_\ell^{\mathrm{m}} = \frac{1}{\sqrt{2|\mathcal{L}|}} \left\|S_{ff}^{-1} S_{f\ell}\right\|_F,$$

where $\|\cdot\|_F$ denotes the Frobenius norm of a matrix.

Proof We compute

$$\begin{aligned}\sqrt{\mathbb{E}\left[\frac{\|\delta\mathbf{p}_f\|^2}{\|\delta\mathbf{p}_\ell\|^2}\right]} &= \sqrt{\mathbb{E}\left[\frac{(\delta\mathbf{p}_\ell)^{\perp\top} S_{f\ell}^\top S_{ff}^{-1} S_{ff}^{-1} S_{f\ell} (\delta\mathbf{p}_\ell)^\perp}{\|\delta\mathbf{p}_\ell\|^2}\right]} \\ &= \sqrt{\mathrm{tr}\left(S_{ff}^{-1} S_{f\ell} \underbrace{\mathbb{E}\left[\frac{(\delta\mathbf{p}_\ell)^\perp (\delta\mathbf{p}_\ell)^{\perp\top}}{(\delta\mathbf{p}_\ell)^{\perp\top}(\delta\mathbf{p}_\ell)^\perp}\right]}_{\triangleq P} S_{f\ell}^\top S_{ff}^{-1}\right)}.\end{aligned} \tag{7.18}$$

Since $\delta\mathbf{p}_\ell$ is isotropic by assumption, the symmetric matrix P define above must satisfy $T^{-1}PT = P$ for all $T \in \mathbb{SO}_{2|\mathcal{L}|}$, which implies that $P = \alpha I_{2|\mathcal{L}|}$ for some $\alpha \in \mathbb{R}$. Matching the traces of P and $\alpha I_{2|\mathcal{L}|}$ yields $\alpha = \frac{1}{2|\mathcal{L}|}$. The desired expression can be obtained by plugging $P = \frac{1}{2|\mathcal{L}|} I_{2|\mathcal{L}|}$ into (7.18). ■

It is noteworthy that the values of $(\varepsilon_\ell^{\mathrm{w}})^2$ and $(\varepsilon_\ell^{\mathrm{m}})^2$ are precisely the maximum manipulability index $m_{\max}$ and the mean manipulability index $\bar{m}$, respectively, as defined in Definition 4.1.1.

7.4.2 Inaccurate Angle Measurements

We next take the AOA measurement errors $\delta\theta_{ij}$ into account and carry out a perturbational analysis of (7.1). Denote by $\delta\boldsymbol{\theta}$ the vector composed of all $\delta\theta_{ij}$ and let $\delta\mathbf{p}_f = \delta\mathbf{p}_f(\delta\boldsymbol{\theta})$ be the resulting AOA localization error. Since the map $\delta\mathbf{p}_f(\cdot)$ is nonlinear, the error propagation coefficients are defined locally as below.

Definition 7.4.3 *The* worst-case error propagation coefficient *of AOA measurements, denoted by $\varepsilon_\theta^{\mathrm{w}}$, is defined as*

$$\varepsilon_\theta^{\mathrm{w}} \triangleq \max_{\delta\boldsymbol{\theta}\neq\mathbf{0}} \lim_{\epsilon\downarrow 0} \frac{\|\delta\mathbf{p}_f(\epsilon\cdot\delta\boldsymbol{\theta})\|}{\|\epsilon\cdot\delta\boldsymbol{\theta}\|}.$$

Definition 7.4.4 *The* mean error propagation coefficient *of AOA measurements, denoted by $\varepsilon_\theta^{\mathrm{m}}$, is defined as*

$$\varepsilon_\theta^{\mathrm{m}} \triangleq \sqrt{\mathbb{E}\left[\lim_{\epsilon\downarrow 0} \frac{\|\delta\mathbf{p}_f(\epsilon\cdot\delta\boldsymbol{\theta})\|^2}{\|\epsilon\cdot\delta\boldsymbol{\theta}\|^2}\right]},$$

where $\delta\boldsymbol{\theta}$ is assumed to be random.

Lemma 7.4.1 *The Taylor expansion of $\delta\mathbf{p}_f(\delta\boldsymbol{\theta})$ at $\delta\boldsymbol{\theta} = \mathbf{0}$ is*

$$\delta\mathbf{p}_f(\delta\boldsymbol{\theta}) = (I_{|\mathcal{F}|}\otimes Q)^{-1} S_{ff}^{-1} W \Lambda_K \delta\boldsymbol{\theta} + o(\delta\boldsymbol{\theta}). \tag{7.19}$$

where W is a matrix whose columns are $\mathbf{w}_{ij}$ defined as

$$\mathbf{w}_{ij} \triangleq \begin{bmatrix} | \\ \mathbf{p}_i - \mathbf{p}_j \\ | \end{bmatrix} \leftarrow i\text{-th block row.}$$

The notation "$|$" here means that all components except the one specifically indicated are zero.

Proof Let θ_{ij} denote the orientation angle of vertex j w.r.t. vertex i for $i \in \mathcal{F}$ and $(i,j) \in \mathcal{E}$. If there is no measurement error, then $|\theta_{ij} - \theta_{ji}| = \pi$. Consequently,

$$P_{ij} = \begin{bmatrix} \cos\theta_{ij} \\ \sin\theta_{ij} \end{bmatrix} \begin{bmatrix} \cos\theta_{ij} \\ \sin\theta_{ij} \end{bmatrix}^\top = P_{ji}.$$

If both i and j are followers, then

$$\frac{\partial(\delta\mathbf{p}_f)^\perp}{\partial\theta_{ij}} = \frac{\partial(-S_{ff}^{-1})}{\partial\theta_{ij}} S_{f\ell}\mathbf{p}_\ell^\perp = -S_{ff}^{-1}\frac{\partial S_{ff}}{\partial\theta_{ij}}\left(-S_{ff}^{-1}S_{f\ell}\mathbf{p}_\ell^\perp\right) = -S_{ff}^{-1}\frac{\partial S_{ff}}{\partial\theta_{ij}}\mathbf{p}_f^\perp. \tag{7.20}$$

Note that the matrix derivative $\frac{\partial S_{ff}}{\partial\theta_{ij}}$ has only two nonzero blocks: $k_{ij}\frac{\partial P_{ij}}{\partial\theta_{ij}}$ at (i,i) and $-k_{ij}\frac{\partial P_{ij}}{\partial\theta_{ij}}$ at (i,j), where

$$\frac{\partial P_{ij}}{\partial\theta_{ij}} = \begin{bmatrix} -\sin\theta_{ij} \\ \cos\theta_{ij} \end{bmatrix} \begin{bmatrix} \cos\theta_{ij} \\ \sin\theta_{ij} \end{bmatrix}^\top + \begin{bmatrix} \cos\theta_{ij} \\ \sin\theta_{ij} \end{bmatrix} \begin{bmatrix} -\sin\theta_{ij} \\ \cos\theta_{ij} \end{bmatrix}^\top = QP_{ij} + P_{ij}Q^{-1}.$$

Plugging these into (7.20) and recalling that $P_{ij}(\mathbf{p}_i - \mathbf{p}_j)^\perp = \mathbf{0}$, we have

$$\begin{aligned} \frac{\partial(\delta\mathbf{p}_f)^\perp}{\partial\theta_{ij}} &= -S_{ff}^{-1}\begin{bmatrix} | \\ k_{ij}(QP_{ij} + P_{ij}Q^{-1})(\mathbf{p}_i - \mathbf{p}_j)^\perp \\ | \end{bmatrix} \\ &= -k_{ij}S_{ff}^{-1}\begin{bmatrix} | \\ P_{ij}Q^{-1}(\mathbf{p}_i - \mathbf{p}_j)^\perp \\ | \end{bmatrix} = -k_{ij}S_{ff}^{-1}\mathbf{w}_{ij}. \end{aligned} \tag{7.21}$$

Next, we consider the case when j is a leader. In this case both S_{ff} and $S_{f\ell}$ depend on θ_{ij}. Hence,

$$\begin{aligned}
\frac{\partial(\delta \mathbf{p}_f)^\perp}{\partial \theta_{ij}} &= \frac{\partial(-S_{ff}^{-1})}{\partial \theta_{ij}} S_{f\ell} \mathbf{p}_\ell^\perp - S_{ff}^{-1} \frac{\partial S_{f\ell}}{\partial \theta_{ij}} \mathbf{p}_\ell^\perp \\
&= -S_{ff}^{-1} \left(\frac{\partial S_{ff}}{\partial \theta_{ij}} \mathbf{p}_f^\perp + \frac{\partial S_{f\ell}}{\partial \theta_{ij}} \mathbf{p}_\ell^\perp \right) \\
&= -S_{ff}^{-1} \begin{bmatrix} | \\ k_{ij}(QP_{ij} + P_{ij}Q^{-1})(\mathbf{p}_i - \mathbf{p}_j)^\perp \\ | \end{bmatrix} \\
&= -k_{ij} S_{ff}^{-1} \mathbf{w}_{ij}, \qquad (7.22)
\end{aligned}$$

which turns out to be identical to the case when i, j are both followers. The expression (7.19) can be obtained from (7.21) and (7.22) by stacking the $\mathbf{w}_{ij}$ horizontally to form W. ■

Proposition 7.4.2 *The error propagation coefficients of AOA measurements in the worst case and in the mean case (with isotropic distribution of $\delta\theta$) are respectively*

$$\varepsilon_\theta^{\mathrm{w}} = \left\| S_{ff}^{-1} W \Lambda_K \right\|_2, \qquad \varepsilon_\theta^{\mathrm{m}} = \frac{1}{\sqrt{|\mathcal{E}|}} \left\| S_{ff}^{-1} W \Lambda_K \right\|_F,$$

where W is the matrix stacking the corresponding $\mathbf{w}_{ij}$ horizontally.

The derivation of the above expressions is entirely similar to that of Proposition 7.4.1; hence the proof is omitted.

7.4.3 Numerical Examples

To illustrate the results in the previous sections numerically, we computed the error propagation coefficients for the formation shown in Fig. 7.4 with different leader sets. The four candidates for leaders are labeled A, B, C and D. The numerical results of the error propagation coefficients are listed in Table 7.1. The random measurement errors for the mean case are assumed to be isotropic.

Table 7.1: Error propagation coefficients for Fig. 7.4

Leader Set	$\varepsilon_\ell^{\mathrm{w}}$	$\varepsilon_\ell^{\mathrm{m}}$	$\varepsilon_\theta^{\mathrm{w}}$	$\varepsilon_\theta^{\mathrm{m}}$
A, B, C, D	5.8885	3.8852	6.5043	0.6061
A, B, C	5.4307	3.9999	15.1156	1.2606
A, B	9.2271	5.8950	184.1435	13.7199
A, D	5.0222	4.5624	24.1448	1.9578

From the numbers in Table 7.1, several observations can be made. Firstly, the values of mean error propagation coefficients are always smaller than their worst-case counterparts, consistent with their definitions. Secondly, the mean error propagation coefficients for the AOA measurement errors are significantly smaller than that of the worst cases. Therefore, one may effectively suppress the worst-case localization errors by averaging the results of multiple measurements. Thirdly, in general the more leaders the network possesses, the smaller $\varepsilon_\theta^{\mathrm{w}}$ and $\varepsilon_\theta^{\mathrm{m}}$ becomes. This complies with our intuition that the more leaders help suppress the uncertainty caused by measurement errors. In the particular case of A, B being the leaders, the localization errors caused by inaccurate AOA measurements could potentially be huge. This is because the bottom part, hardly "pinned down" by the leaders A and B, can be easily deformed without causing large AOA measurement errors on any edge.

The numerical results regarding the error propagation coefficients for the leader position errors do not have as easy an interpretation. It can be seen from the first, second and fourth cases in Table 7.1 that adding more leaders may not decrease the error propagation coefficients. On the other hand, a small but poorly chosen leader set, such as the third case, could still potentially lead to much larger error propagation coefficients. We will investigate further these observations in our future work.

7.5 Summary

In this chapter, the angle-of-arrival (AOA) localization problem is studied using the concepts of formation rigidity. Specifically, we characterize the AOA localizability using the fixability of the underlying anchored formation. Moreover, we propose a distributed algorithm that can localize the followers whenever the formation is fixable, and derive its convergence speed and robustness to communication delay. We formulate and solve an optimization problem whose solution can maximize the convergence speed and delay tolerance of the algorithm at the same time. We also study the sensitivity of the localization results to inaccuracy in anchor positions and AOA measurements. Some simulation results are provided to demonstrate the effectiveness of the proposed algorithm and its performance.

Many interesting research problems arising from the setup of this paper deserve further investigation. Examples include finding the best formation topology and/or anchor selection under resource constraints for fast and robust AOA localization; incorporating distance information into angle-based localization algorithms; devising methods that can blunt the destabilizing effect caused by communication delay. Solution of these problems will not only reveal new properties of formation graphs, but also have practical implications in the many applications of multi-agent systems.

8. CONCLUSION

Formations, more specifically, the geographic configurations of agents together with their interconnection topologies, play a significant role in the collaborative performance of multi-agent systems involving formation control, localization, and other geo-sensitive applications. This dissertation proposed a general theory toward the quantitative analysis of formations, and demonstrated its applications in formation control and network localization.

In Chapter 2 an algebraic formation theory was developed which served as a fundamental tool for the study of formations in the later chapters. Two basic quantities associated with a formation, namely the *rigidity matrix* and the *stiffness matrix*, were derived from a spring-mass mechanical analogy of multi-agent formations. From these two quantities, the definitions of formation *rigidity*, *fixability* and *looseness/tightness* were proposed and their interesting relations reported through chains of propositions and theorems. Moreover, it was shown that a unique decomposition into *rigid components* exists for any given formation. Based on this decomposition, the concept of *skeleton graphs* was introduced so that the analysis of formations with complicated structures can be better visualized and vastly simplified. It is also interesting to see that many concepts in the framework of algebraic formation theory have corresponding counterparts in the classic graph theory, and a list of such correspondence was provided to bring a deeper understanding of these concepts.

Chapter 3 introduced two novel quantitative measures of formation rigidity, namely the *worst-case rigidity index* and the *mean rigidity index*, via inspecting the spectrum of the stiffness matrix associated with the formation. Many properties shared by both indexes were reported, indicating that the proposed measures conform well to our intuitive conception of formation rigidity. It was also shown that the performance of a class of formation control and localization algorithms was precisely characterized by these indexes, rendering them useful in evaluating the general "goodness" of a given formation and thus helping in the process of multi-agent system design.

In Chapter 4, the *manipulability matrix* were formulated, followed by the definitions of *manipulability indexes*, quantitative measures derived from the spectrum of the manipulability matrix. The manipulability indexes quantifies the amplification effect on the dynamics of followers from leaders' movements, hence are indicative of the effectiveness of leader-follower formations. It also shown that for single-leader rigid formations and trailers, the special formation structures may be taken advantage of to significantly reduce the computational cost of evaluating the manipulability indexes.

With a handful of quantities related to formations proposed in the previous chapters, multi-agent formation optimization problems were proposed in Chapter 5 and 6, where both problem formulations solution algorithms of the optimization with respect to rigidity indexes and manipulability indexes were provided. Specifically, problems including link resource allocation, configuration optimization, topology optimization, leaders' selection and position optimization were covered in the discussion of the two chapters, with each type of optimization demonstrated through some numerical examples.

Lastly in Chapter 7, the network localization problem, as an instance of systematic application of the proposed quantitative analysis framework, was investigated with the assumption that relative orientational information is available through signal angle-of-arrival measurements. It was proven that the solvability of the problem necessarily depends on the rigidity of formation. Considering the fact that the rigidity property was previous derived from a *distance*-preserving, this result is an intriguing one which bridges the distance-based and direction-based network localization schemas. Distributed localization algorithms based on AOA measurements of neighbors was proposed and proven to converge to the true configuration under scenarios with limited amount of uniform communication delay and switching topologies. A discrete version of such algorithm was also shown to converge exponentially fast. Other analyses such as convergence rate, delay tolerance, topology switching paradigms and steady-state error due to inaccurate measurements, were also conducted and illustrated through numerical simulation.

8.1 Future Work

Many of the algorithms proposed in this thesis are centralized, hence are not effectively deployable in multi-agent systems where there is often no central node or station. The decentralized versions of our algorithms can potentially be obtained by solving the corresponding optimization problems in the dual space. In such a way, the constraints in the optimization problems are converted to the minimization of Lagrangians, which can often be decomposed such that each agent can process a local minimization involving the states of a limited set of neighboring agents. However, more work is demanded for an algorithm for computing the rigidity indexes in a decentralized fashion.

In our current model, all connections among agents are symmetric. It is natural to extend the model to accommodate asymmetric connections, in which case the connectivity matrices K will be asymmetric; as a result, complex values in rigidity indexes may occur. It is interesting to study the behaviors of such formations and generalize our existing work to these cases.

LIST OF REFERENCES

LIST OF REFERENCES

[1] B. Anderson, B. Fidan, C. Yu, and D. Walle, "UAV formation control: theory and application," in *Recent Advances in Learning and Control* (V. Blondel, S. Boyd, and H. Kimura, eds.), vol. 371 of *Lecture Notes in Control and Information Sciences*, pp. 15–33, Springer Berlin / Heidelberg, 2008.

[2] P. Bhatta, E. Fiorelli, F. Lekien, N. Leonard, D. Paley, F. Zhang, R. Bachmayer, R. Davis, D. Fratantoni, and R. Sepulchre, "Coordination of an underwater glider fleet for adaptive sampling," in *International Workshop on Underwater Robotics*, pp. 61–69, 2005.

[3] N. Leonard, D. Paley, F. Lekien, R. Sepulchre, D. Fratantoni, and R. Davis, "Collective motion, sensor networks, and ocean sampling," *Proceedings of the IEEE*, vol. 95, pp. 48–74, January 2007.

[4] D. Vail and M. Veloso, "Dynamic multi-robot coordination," in *Multi-Robot Systems: From Swarms to Intelligent Automata* (A. Schultz, L. Parker, and F. Schneider, eds.), vol. 2, pp. 87–100, Kluwer Academic Publishers, 2003.

[5] D. Mellinger, M. Shomin, N. Michael, and V. Kumar, "Cooperative grasping and transport using multiple quadrotors," in *Distributed Autonomous Robotic Systems*, vol. 83, pp. 545–558, Springer Berlin / Heidelberg, 2013.

[6] J. Yick, B. Mukherjee, and D. Ghosal, "Wireless sensor network survey," *Computer Networks*, vol. 52, no. 12, pp. 2292–2330, 2008.

[7] I. Akyildiz, W. Su, Y. Sankarasubramaniam, and E. Cayirci, "A survey on sensor networks," *IEEE Communications Magazine*, vol. 40, pp. 102–114, August 2002.

[8] L. Bodrozic, D. Stipanicev, and M. Stula, "Agent based data collecting in a forest fire monitoring system," in *International Conference on Software in Telecommunications and Computer Networks (SoftCOM)*, pp. 326–330, October 2006.

[9] D. Helbing, I. Farkas, and T. Vicsek, "Simulating dynamical features of escape panic," *Nature*, vol. 407, pp. 487–490, September 2000.

[10] H. Van Dyke Parunak, ""Go to the ant": Engineering principles from natural multi-agent systems," *Annals of Operations Research*, vol. 75, pp. 69–101, 1997.

[11] B. Fidan, C. Yu, and B. D. Anderson, "Acquiring and maintaining persistence of autonomous multi-vehicle formations," *IET Control Theory & Applications*, vol. 1, pp. 452–460, March 2007.

[12] R. Olfati-saber and R. M. Murray, "Distributed cooperative control of multiple vehicle formations using structural potential functions," in *Proceedings of the 15th IFAC World Congress*, (Barcelona, Spain), 2002.

[13] M. Ji, A. Muhammad, and M. Egerstedt, "Leader-based multi-agent coordination: controllability and optimal control," in *American Control Conference*, pp. 1358–1363, IEEE, June 2006.

[14] T. Eren, O. Goldenberg, W. Whiteley, Y. Yang, A. Morse, B. Anderson, and P. Belhumeur, "Rigidity, computation, and randomization in network localization," in *INFOCOM*, vol. 4, pp. 2673–2684, March 2004.

[15] M. Hermary, *Rigidity of graphs*. PhD thesis, Simon Fraser University, 1986.

[16] B. Roth, "Rigid and flexible frameworks," *American Mathematical Monthly*, vol. 88, pp. 6–21, January 1981.

[17] L. Asimow and B. Roth, "The rigidity of graphs," *Transactions of the American Mathematical Society*, vol. 245, pp. 279–289, November 1978.

[18] M. Laurent, "Cuts, matrix completions and graph rigidity," *Mathematical Programming*, vol. 79, pp. 255–283, October 1997.

[19] R. Connelly, *Handbook of Convex Geometry*, ch. Rigidity, pp. 223–271. Amsterdam: North-Holland, 1993.

[20] G. Laman, "On graphs and rigidity of plane skeletal structures," *Journal of Engineering mathematics*, vol. 4, no. 4, pp. 331–340, 1970.

[21] T. Tay and W. Whiteley, "Generating isostatic frameworks," *Structural Topology*, vol. 11, pp. 21–69, 1985.

[22] W. Whiteley, "Some matroids from discrete applied geometry," in *AMS-IMS-SIAM Joint Summer Research Conference on Matroid Theory*, vol. 197, (University of Washington, Seattle), pp. 171–311, American Mathematical Society, July 1995.

[23] L. Lovasz and Y. Yemini, "On generic rigidity in the plane," *SIAM Journal on Algebraic Discrete Methods*, vol. 3, no. 1, pp. 91–98, 1982.

[24] J. E. Graver, B. Servatius, and H. Servatius, *Combinatorial rigidity*, vol. 2. American Mathematical Society, 1993.

[25] T. Eren, B. D. O. Anderson, A. S. Morse, W. Whiteley, and P. N. Belhumeur, "Operations on rigid formations of autonomous agents," in *Communications in Information and Systems*, pp. 223–258, 2004.

[26] B. D. Anderson, C. Yu, B. Fidan, and J. Hendrickx, "Rigid graph control architectures for autonomous formations," *IEEE Control System Magazine*, vol. 28, pp. 48–63, December 2008.

[27] W. Ong, C. Yu, and B. D. Anderson, "Splitting rigid formations," in *Proceedings of the 48th IEEE Conference on Decision and Control, held jointly with 28th Chinese Control Conference*, pp. 859–864, December 2009.

[28] R. Olfati-Saber and R. Murray, "Graph rigidity and distributed formation stabilization of multi-vehicle systems," in *Proceedings of the 41st IEEE Conference on Decision and Control*, vol. 3, pp. 2965–2971, December 2002.

[29] T. Eren, B. Anderson, A. Morse, W. Whiteley, and P. Belhumeur, "Information structures to control formation splitting and merging," in *American Control Conference*, vol. 6, pp. 4951–4956, July 2004.

[30] H. Kawashima and M. Egerstedt, "Approximate manipulability of leader-follower networks," in *Proceedings of the 50th IEEE Conference on Decision and Control and European Control Conference*, (Orlando, Florida), pp. 6618–6623, December 2011.

[31] H. Kawashima, G. Zhu, J. Hu, and M. Egerstedt, "Responsiveness and manipulability of formations of multi-robot networks," in *Proceedings of the 51st IEEE Conference on Decision and Control*, pp. 4622–4628, December 2012.

[32] Y. Kim and M. Mesbahi, "On maximizing the second smallest eigenvalue of a state-dependent graph laplacian," *IEEE Transactions on Automatic Control*, vol. 51, pp. 116–120, January 2006.

[33] R. Olfati-Saber and R. M. Murray, "Consensus problems in networks of agents with switching topology and time-delays," *IEEE Transactions on Automatic Control*, vol. 49, pp. 1520–1533, September 2004.

[34] A. Rahmani, M. Ji, M. Mesbahi, and M. Egerstedt, "Controllability of multi-agent systems from a graph-theoretic perspective," *SIAM Journal on Control and Optimization*, vol. 48, no. 1, pp. 162–186, 2009.

[35] N. M. Maia and de Abreu, "Old and new results on algebraic connectivity of graphs," *Linear Algebra and its Applications*, vol. 423, no. 1, pp. 53–73, 2007.

[36] G. Zhu and J. Hu, "Stiffness matrix and quantitative measure of formation rigidity," in *Proceedings of the 48th IEEE Conference on Decision and Control, held jointly with 28th Chinese Control Conference*, pp. 3057–3062, December 2009.

[37] C. Del Carpio M, E. Ichiishi, M. Koyama, M. Kubo, and A. Miyamoto, "A flexibility index for analysis of bio-molecular complexes," in *International Joint Conference on Neural Networks*, pp. 2337–2344, 0-0 2006.

[38] M. Egerstedt and X. Hu, "Formation constrained multi-agent control," *Robotics and Automation, IEEE Transactions on*, vol. 17, pp. 947 –951, dec 2001.

[39] J. Aspnes, T. Eren, D. Goldenberg, A. Morse, W. Whiteley, Y. Yang, B. Anderson, and P. Belhumeur, "A theory of network localization," *IEEE Transactions on Mobile Computing*, vol. 5, pp. 1663–1678, December 2006.

[40] J. E. Graver, "Rigidity matroids," *SIAM Journal on Discrete Mathematics*, vol. 4, no. 3, pp. 355–368, 1991.

[41] B. Jackson and T. Jordán, "Connected rigidity matroids and unique realizations of graphs," *Journal of Combinatorial Theory, Series B*, vol. 94, no. 1, pp. 1–29, 2005.

[42] D. West, *Introduction to graph theory*, vol. 1. Prentice Hall, New Jersey, 2001.

[43] C. Godsil and G. F. Royle, *Algebraic Graph Theory*. New York: Spring, 2001.

[44] I. Shames, B. Fidan, and B. D. Anderson, "Minimization of the effect of noisy measurements on localization of multi-agent autonomous formations," *Automatica*, vol. 45, no. 4, pp. 1058–1065, 2009.

[45] R. Horn and C. Johnson, *Matrix analysis*. Cambridge University Press, 1990.

[46] P. Bullen, *Handbook of means and their inequalities*. Springer Netherlands, 2003.

[47] C. Chang and A. Sahai, "Estimation bounds for localization," in *First Annual IEEE Communications Society Conference on Sensor and Ad Hoc Communications and Networks*, pp. 415–424, October 2004.

[48] A. V. Oppenheim, A. S. Willsky, and S. H. Nawab, *Signals & systems (2nd ed.)*. Upper Saddle River, NJ, USA: Prentice-Hall, 1996.

[49] A. Ben-Israel and T. Greville, *Generalized inverses: theory and applications*, vol. 15. Springer Verlag, 2003.

[50] G. Zhu and J. Hu, "Link resource allocation for maximizing the rigidity of multi-agent formations," in *Proceedings of the 50th IEEE Conference on Decision and Control and European Control Conference*, pp. 2920–2925, December 2011.

[51] Y. Kim, G. Zhu, and J. Hu, "Optimizing formation rigidity under connectivity constraints," in *Proceedings of the 49th IEEE Conference on Decision and Control*, pp. 6590–6595, December 2010.

[52] A. Dersan and Y. Tanik, "Passive radar localization by time difference of arrival," in *MILCOM*, vol. 2, pp. 1251–1257, October 2002.

[53] M. Grant, S. Boyd, and Y. Ye, "CVX: Matlab software for disciplined convex programming," February 2011.

[54] R. Nelson, "Simplified calculation of eigenvector derivatives," *AIAA journal*, vol. 14, pp. 1201–1205, 1976.

[55] J. Mangus and H. Neudecker, *Matrix differential calculus with applications in statistics and econometrics (revised edition)*. New York: John Wiley & Sons, 1999.

[56] E. Chong and S. Żak, *An introduction to optimization (third edition)*. John Wiley & Sons, New Jersey, 2008.

[57] S. Boyd and L. Vandenberghe, *Convex optimization*. Cambridge University Press, 2004.

[58] J. Bunch, C. Nielsen, and D. Sorensen, "Rank-one modification of the symmetric eigenproblem," *Numerische Mathematik*, vol. 31, pp. 31–48, 1978.

[59] Y. Kim, "Bisection algorithm of increasing algebraic connectivity by adding an edge," *IEEE Transactions on Automatic Control*, vol. 55, pp. 170–174, January 2010.

[60] G. W. Stewart, "On the perturbation of pseudo-inverses, projections and linear least squares problems," *SIAM Review*, vol. 19, no. 4, pp. 634–662, 1977.

[61] B. Hofmann-Wellenhof, H. Lichtenegger, and J. Collins, *Global positioning system: theory and practice*. New York: Springer, 5th ed., 2001.

[62] N. Patwari, J. Ash, S. Kyperountas, I. Hero, A.O., R. Moses, and N. Correal, "Locating the nodes: cooperative localization in wireless sensor networks," *IEEE Signal Processing Magazine*, vol. 22, pp. 54–69, July 2005.

[63] C. Savarese, J. Rabaey, and J. Beutel, "Location in distributed ad-hoc wireless sensor networks," in *Proceedings of IEEE International Conference on Acoustics, Speech, and Signal Processing (ICASSP)*, vol. 4, pp. 2037–2040, 2001.

[64] A. Savvides, C.-C. Han, and M. B. Strivastava, "Dynamic fine-grained localization in ad-hoc networks of sensors," in *Proceedings of the 7th Annual International Conference on Mobile Computing and Networking*, (New York, NY, USA), pp. 166–179, 2001.

[65] N. B. Priyantha, A. Chakraborty, and H. Balakrishnan, "The Cricket location-support system," in *Proceedings of the 6th Annual International Conference on Mobile Computing and Networking*, (New York, NY, USA), pp. 32–43, ACM, 2000.

[66] N. B. Priyantha, H. Balakrishnan, E. Demaine, and S. Teller, "Anchor-free distributed localization in sensor networks," Tech. Rep. 892, LCS, 2003.

[67] J. Saxe, "Embeddability of weighted graphs in k-space is strongly NP-hard," in *Proceedings of the 17th Allerton Conference in Communications, Control and Computing*, pp. 480–489, 1979.

[68] Y. Dieudonne, O. Labbani-Igbida, and F. Petit, "Deterministic robot-network localization is hard," *IEEE Transactions on Robotics*, vol. 26, pp. 331–339, April 2010.

[69] D. Moore, J. Leonard, D. Rus, and S. Teller, "Robust distributed network localization with noisy range measurements," in *Proceedings of the 2nd International Conference on Embedded Networked Sensor Systems*, (New York, NY), pp. 50–61, 2004.

[70] J. Bruck, J. Gao, and A. A. Jiang, "Localization and routing in sensor networks by local angle information," *ACM Transactions on Sensor Networks*, vol. 5, pp. 1–31, February 2009.

[71] J. N. Ash and L. C. Potter, "Robust system multiangulation using subspace methods," in *Proceedings of the 6th International Conference on Information Processing in Sensor Networks*, IPSN '07, (New York, NY, USA), pp. 61–68, ACM, 2007.

[72] T. Eren, W. Whiteley, and P. Belhumeur, "Using angle of arrival (bearing) information in network localization," in *Proceedings of the 45th IEEE Conference on Decision and Control*, pp. 4676–4681, Dec. 2006.

[73] J. Chen, K. Yao, and R. Hudson, "Source localization and beamforming," *IEEE Signal Processing Magazine*, vol. 19, pp. 30–39, March 2002.

[74] G. Zhu and J. Hu, "Distributed continuous-time protocol for network localization using angle-of-arrival information," in *Proceedings of 2013 American Control Conference*, June 2013.

[75] G. Zhu and J. Hu, "Distributed network localization based on angle-of-arrival information: algorithm and error analysis," in *Proceedings of 2013 American Control Conference*, June 2013.

[76] M. Ji and M. Egersted, "A graph-theoretic characterization of controllability for multi-agent systems," in *Proceedings of 2007 American Control Conference*, pp. 4588–4593, IEEE, 2007.

[77] A. N. Bishop, I. Shames, and B. D. Anderson, "Stabilization of rigid formations with direction-only constraints," in *Proceedings of the 50th IEEE Conference on Decision and Control and European Control Conference*, pp. 746–752, December 2011.

[78] D. G. Feingold and R. S. Varga, "Block diagonally dominant matrices and generalizations of the Gerschgorin circle theorem," *Pacific Journal of Mathematics*, vol. 12, pp. 1241–1250, 1962.

[79] S. Sastry, *Nonlinear systems: analysis, stability, and control*, vol. 10. Springer Verlag, 1999.

VITA

VITA

Guangwei Zhu was born and raised in Shanghai, China. He earned his Bachelor of Engineering degree with an Outstanding Bachelor Thesis Award from Tsinghua University (Beijing, China) in 2008. He was then enrolled at Purdue University where he began his Ph.D. study on Automatic Control in the School of Electrical and Computer Engineering, advised by Prof. Jianghai Hu. Meanwhile, he received his M.S. degree in Applied Mathematics from Purdue University in 2012. He was a graduate teaching assistant in the School of Electrical and Computer Engineering from Fall 2008 to Spring 2010 under Prof. Yung-Hsiang Lu, and received Magoon Award for Excellence in Teaching from College of Engineering in 2009. Since 2010, he is a graduate research assistant under Prof. Hu. During his graduate study, he has published 12 peer-reviewed papers in the proceedings of major conferences in the field of automatic control and engineering education, and won two Finalists for Best Paper awards. His research interests include the modeling and analysis of multi-agent systems, hybrid systems, sensor networks, wireless communication networks, building HVAC control systems and software engineering.